Technical University of Munich
TUM School of Engineering and Design

Numerical Study on Wall Heat Flux in Film Cooling of Methane/Oxygen Rocket Engine Combustion Chamber

Jianing Liu

Complete reprint of the dissertation approved by the TUM School of Engineering and Design of the Technical University of Munich for the award of the

Doktors der Ingenieurwissenschaffen

Chair:

Prof. Dr.-Ing. Florian Holzapfel

Examiners:

1. Prof. Dr.-Ing. Oskar J. Haidn
2. Priv.-Doz. Dr. -Ing. habil Xiangyu Hu

The dissertation was submitted to the Technical University of Munich on 12 August 2024 and accepted by the TUM School of Engineering and Design on 11 November 2024.

Declaration of Authorship

I, Jianing Liu, hereby declare that this dissertation, titled " Methane/Oxygen Rocket Engine Film Cooling Wall Heat Transfer Research", is my own original work, except where otherwise acknowledged. I have acknowledged all the sources used in this work and have cited them accurately. This work has not been previously submitted for any other degree or qualification at any other institution, and all data, figures, and findings presented are authentic and have not been manipulated or fabricated in any way.

Jianing Liu
April 9, 2024

jianing.liu@tum.de

Released April 9, 2024

IV

Life was like a box of chocolates,
you never know what you're going to get.

— *《Forrest Gump》*

All is well

Abstract

Methane/oxygen rocket engines have garnered significant interest within the aerospace propulsion domain owing to their favorable attributes, including facile storage and transportability, inherent stability, elevated combustion efficiency, environmentally benign emissions, and recyclability. Throughout engine operation, the management of wall heat dissipation poses a substantial challenge. Employing film cooling stands out as a pivotal technique for wall protection. Concurrently, within the realm of rocket engine research, numerical simulation emerges as an efficient and cost-effective investigative approach. Reynolds Averaged Navier-Stokes (RANS) simulation, acclaimed for its convenience, rapidity, and economical nature, finds widespread application in engineering endeavors.

However, Observations from numerical simulations reveal significant disparities between predicted and experimental wall heat flux despite consistent distributions of other combustion chamber parameters. These disparities are attributed to the neglect of chemical reactions within the boundary layer when employing general wall functions. To address this, a coupled wall function accounting for near-wall chemical reactions is integrated into the RANS method to improve wall heat flux prediction accuracy in this thesis.

The study initially focuses on establishing and validating the numerical framework, overcoming challenges such as integrating coupled wall functions and processing nonlinear experimental data. The effectiveness of the framework is demonstrated in mitigating overestimated wall heat transfer while maintaining accuracy in flow and combustion calculations. Quantitative analysis highlights the impact of chemical reactions on wall heat transfer, and preliminary investigations into 3D effects reveal influences on temperature boundary layer thickness and flow characteristics.

Subsequent optimization of parameters governing the coupled wall function improves prediction accuracy, as demonstrated in a single-injector rectangular combustion chamber. Practical applications of the framework advocate for using Net Heat Flux Reduction (NHFR) as a metric for assessing film cooling efficiency. Further exploration reveals the interplay between enhanced wall heat flux and cooling efficiency, emphasizing the need for tailored film cooling strategies balancing efficiency with engine performance.

Investigation into multi-injector combustion chambers elucidates the combined effects of flow dynamics and near-wall chemical reactions, highlighting the importance

of tailored film cooling strategies in methane/oxygen rocket engines. Manipulating the velocity ratio between the film and the mainstream through various methods reveals that the disparity in velocities exerts diverse influences on the flow and combustion dynamics. Concurrently, its interaction with chemical reactions within the boundary layer further coupling modulates the wall heat flux. Additionally, distinct approaches to controlling the film velocity yield disparate impacts on the aforementioned parameters. Findings underscore the necessity of optimizing film cooling inlet spacing and mass flow rates to achieve desired cooling efficiency while considering engine performance implications.

Acknowledgment

Firstly, I would like to express my heartfelt gratitude to my supervisor, Prof. Oskar J. Haidn, who has been an incredibly supportive, knowledgeable, and creative researcher. He introduced me to the fascinating field of aerospace propulsion, and I remain deeply passionate about it to this day. Secondly, I want to thank my mentor, Prof. Silong Zhang, who provided invaluable guidance throughout my doctoral thesis, imparting a wealth of knowledge in numerical simulation and offering numerous ideas while generously assisting me during challenging times. Lastly, I am grateful to Prof. Chiara Manfletti for her encouragement and support during my doctoral studies.

Moreover, reflecting on my time at the Institute of Aerospace Propulsion at the Technical University of Munich fills me with warmth. Although the Ph.D. journey is often challenging, my colleagues Dr. Meng Luo, Dr. Nikolaos Perakis, Dr. Zijie Li, Andrej Sternin, Dr. Hao Ma, Dr. Ye Hong, Dr. Hongxin Wang, Dr. Yang Zhang, Mai Ye, Yongchuan Yu, Zhengdong Yu, Dr. Jingying Zuo, Zhentong Wang, Xiaojing Tang, Dr. Xin Li, Fernanda Winter, Dr. M. P. Celano, Prof. Volker Gümmer, Mattia Straccia have continuously provided encouragement and support, not only academically but also personally. I am especially grateful to Jianfei Wei from the Institute of Advanced Power at Harbin Institute of Technology, as well as PD Dr. Xiangyu Hu and his team member Dr. Chi Zhang from TUM, for their assistance in research.

Furthermore, I deeply appreciate the financial support provided by the Chinese Scholarship Council during my four years of study abroad, enabling me to explore the broader world. I would also like to thank my friends for their unwavering encouragement during my moments of uncertainty, allowing me to persevere through this lengthy period of study abroad. They include Qin Ma, Kunpeng He, Xuesong Bi, Yi Sun, Dr. Yao Xu, and many others.

Last but certainly not least, I want to express my deepest gratitude to my family. My parents have always supported me throughout my academic journey, and without their unwavering support, I would not have been able to navigate through this challenging yet fulfilling path. I am also profoundly grateful to my fiancée, Wenjing Yin, for her constant support and companionship along the way. I look forward to exploring even more enriching experiences with her together in the future.

Finally, I'd like to thank everyone who has helped me along the way, even if I haven't mentioned them individually.

Contents

List of Symbols

Nomenclature	
A	surface area, m^2
C_p	specific heat capacity, J/(kg·K)
E_{ij}	component of rate of deformation
$\boldsymbol{f}$	body force vector, m/s^2
H	total enthalpy of mixed gas, J/kg
H_f^0	standard formation enthalpy of mixed gas, J/kg
H^s	specific sensible enthalpy, J/kg
h	Total enthalpy, J/kg
h_f^0	standard formation enthalpy, J/kg
h^s	specific sensible enthalpy, J/kg
$\dot{m}$	mass flow rate, g/s
Pr	Prandtl number
p	pressure, bar
Q_c	Volume heat release rate, $W/(m^3 \cdot s)$
q	heat flux, W/m^2
$\boldsymbol{q}$	heat flux vector, W/m^2
R	radius, m
Re	Reynolds number
R_F	film-fuel ratio
ROF	oxidizer-fuel ratio
Sc	Schmidt number
T	temperature, K
t	time, s
u	velocity, m/s
u_i	velocity component in corresponding direction, m/s
$\boldsymbol{V}$	velocity vector, m/s
$\boldsymbol{V_D}$	diffusion velocity vector, m/s
Y	mass fraction
y^+	dimensionless wall distance
λ	thermal conductivity, W/(m·K)

μ_t	$=\rho C_\mu \frac{k^2}{\varepsilon}$, eddy viscosity, Pa·s
ρ	density, kg/m^3
$\tilde{\boldsymbol{\tau}}$	stress tensor, Pa
τ	shear stress, Pa
$\dot{\omega}$	Net production rate, kg/(m^3·s)
Subscripts	
0	case without film cooling
ad	adiabatic
c	the first layer grid center
cc	combustion chamber
CH4	methane
k	component k
O2	oxygen
t	turbulent
th	throat
w	wall
x,y,z,r	coordinate

1. Introduction

1.1 Methane/Oxygen Rocket Engines

Methane/oxygen engines, also known as methane rocket engines, stand at the forefront of propulsion sysytems, leveraging methane as a potent fuel source and oxygen as the oxidizer. This propulsion paradigm has garnered substantial attention owing to its potential applications across various domains, including aerospace and terrestrial transportation[1-6].

In the realm of space exploration, methane/oxygen engines exhibit promising characteristics conducive to future missions. Notably, the adaptability of methane as a propellant aligns with the objectives of long-duration missions, such as crewed missions to Mars and beyond. The versatility of methane as a fuel offers advantages in terms of production, storage, and sustainability compared to traditional propellants. Furthermore, methane/oxygen engines demonstrate enhanced efficiency and performance metrics, contributing to cost-effectiveness and mission feasibility [7-11]. Moreover, the environmental benefits associated with methane combustion, notably reduced emissions of greenhouse gases and pollutants, position methane/oxygen engines as promising candidates for sustainable transportation solutions[12-16].

When designing and manufacturing methane rocket engines, several advantages come into play. Firstly, methane as a fuel boasts a high energy density and low molecular weight, rendering methane rocket engines highly efficient within propulsion systems. Secondly, compared to traditional liquid hydrogen fuels, methane offers higher density and wider availability, thereby reducing the costs associated with fuel transportation and storage[17]. Additionally, the methane/oxygen rocket engines take advantages from its sustainability and recyclability[18, 19]. Moreover, the lower combustion temperatures of methane rocket engines facilitate easier material selection and manufacturing processes[20-22]. In summary, the advantages of methane rocket engine design and manufacturing encompass high energy density, cost-effectiveness, environmental friendliness, and simplified manufacturing processes[23-25].

However, challenges persist in realizing the full potential of methane/oxygen engines. Technical hurdles related to combustion dynamics, engine efficiency, and materials compatibility necessitate ongoing research and development efforts[24, 26]. Nevertheless, methane/oxygen engines represent a pivotal advancement in propulsion

technology with significant implications for space exploration[27]. While progress has been made in harnessing the capabilities of methane as a fuel source, continued innovation and strategic investments are imperative to address existing challenges and unlock the full potential of methane/oxygen engines in the contemporary landscape.

1.2 Film Cooling

Film cooling is a widely employed technique in the field of thermal engineering, particularly in the design of liquid rocket engines and gas turbine components subjected to high-temperature environments. This method involves the injection of a thin layer of coolant fluid through a series of discrete orifices onto the surface of a hot component, forming a protective film that shields it from excessive thermal loads. The coolant film acts as a barrier, reducing the convective heat transfer between the hot gas and the solid surface, thus helping to maintain component integrity and prolong operational lifespan[28, 29].

Film cooling in liquid rocket engines confers several notable advantages pertinent to their operation. Firstly, in the extreme thermal environment of liquid rocket engines, characterized by combustion temperatures exceeding several thousand degrees Celsius, film cooling serves as a vital thermal management strategy. By establishing a thin, protective coolant layer along the interior surfaces of critical components such as combustion chambers and nozzles, film cooling effectively mitigates thermal stresses and prevents material degradation, thereby enhancing engine durability and reliability[30-33].

Secondly, in this study, methane is used as both fuel and coolant in the combustion chamber. Thus, film cooling enables liquid rocket engines to operate at higher performance levels by facilitating the implementation of advanced propulsion cycles and materials. Through efficient heat transfer management, film cooling enables the integration of regenerative cooling systems, wherein coolant fluid absorbs heat from the combustion chamber walls before being recirculated into the engine cycle. This capability allows for the utilization of elevated chamber pressures and combustion temperatures, resulting in improved thrust and efficiency[32, 34, 35].

Moreover, film cooling contributes significantly to the safety and stability of rocket engines by minimizing the risk of thermal-induced failures and catastrophic events. By maintaining critical engine components within safe temperature thresholds, film cooling mitigates thermal-induced instabilities such as combustion chamber wall overheating or nozzle erosion, thereby reducing the likelihood of engine malfunction or loss of control.

Currently, the predominant research emphasis concerning film cooling in rocket

engines pertains to the investigation of geometric parameters, including the angle of incidence of the coolant film and the configuration of the film entrance port[36-41]. Nonetheless, it is imperative to acknowledge that the implementation of film cooling may engender aerodynamic losses and induce a pressure drop within the flow system, thereby exerting a discernible influence on the overall efficiency of the engine. Moreover, the design and optimization of film cooling configurations necessitate meticulous consideration of multiple factors, such as the rate of coolant flow, the size of injection orifices, and the extent of film coverage. The objective of this investigation is to elucidate the interplay between these parameters and ascertain their collective impact on cooling effectiveness while concurrently mitigating any deleterious ramifications on aerodynamic performance.

In summary, film cooling provides significant advantages in liquid rocket engine design by enhancing durability, enabling higher performance levels, and improving safety and reliability. Thus, the optimization of film cooling performance is able to effectively manage thermal loads within the engine contributes to the overall efficiency and success of liquid propulsion systems in demanding aerospace applications.

1.3 Numerical Simulations of Methane/Oxygen Rocket Engines

Ever since the initial proposal of liquid rocket engines by Russian educator Konstanty Ciołkowski in 1903[42], substantial research efforts have been dedicated to this field, encompassing both experimental[43-48] and numerical methodologies[46, 49-51]. In light of advancements in computer technology, numerical simulations have emerged as pivotal instruments within methane rocket engine research, affording unparalleled capabilities in comprehending, refining, and propelling propulsion technology forward. The inherent versatility, computational efficiency, and capacity to offer intricate insights into multifaceted phenomena render numerical simulations indispensable assets in the pursuit of innovative and efficacious rocket propulsion and thermal management systems.

In numerical simulations, the most concerned issue is to solve the Navier-Stokes (N-S) equations, and three primary models are commonly employed: Direct Numerical Simulation (DNS), Large Eddy Simulation (LES) and Reynolds-Averaged Navier-Stokes (RANS) models. DNS is a high-resolution numerical simulation method that involves the explicit resolution of the NS equations at every time and spatial point. DNS can capture all scales of turbulent structures and behaviors without any statistical averaging. LES is an intermediate turbulence simulation method between DNS and RANS. In LES, the flow

field is decomposed into large-scale turbulent structures and small-scale turbulent structures. Only the large-scale turbulence is explicitly resolved, while the small-scale turbulence is modeled.

Scholars have conducted numerous numerical simulations utilizing DNS[52-54] and LES[55-58] methods in the context of methane rocket engines. These investigations have revealed that DNS and LES methodologies excel in capturing turbulent phenomena, particularly small- to medium-scale turbulent flows, but they frequently necessitate substantial computational resources and are typically confined to scenarios involving relatively limited spatial or temporal scales. Conversely, in engineering practice, where expeditious acquisition of approximate characteristic flow distributions and wall heat fluxes in rocket engines is paramount, the precise depiction of small-scale vortex structures within the flow field is often of secondary concern. Consequently, RANS-based simulations, which employ time-averaged modeling of the Navier-Stokes equations, enjoy greater prominence in engineering applications.

RANS models entail time-averaging the flow filed and solving the resultant averaged governing equations to simulate turbulent flow. Despite the inherent neglect of spatiotemporal fluctuations in turbulence, RANS models adeptly predict flow field behaviors, rendering them highly applicable and efficient in practical scenarios. Correspondingly, numerous investigations have utilized the RANS method to explore combustion and heat transfer characteristics within the methane combustion chamber[59-64]. These studies consistently demonstrate the RANS method's capability to accurately predict flow dynamics, combustion processes, chemical reactions, and other pertinent characteristics within methane/oxygen engine combustion chambers while demanding minimal computational resources.

In summary, RANS models, as economically efficient turbulence simulation methods, have found widespread application in methane/oxygen rocket engine simulations, offering advantages such as high computational efficiency, broad applicability and the ability to predict the flow and combustion behaviors precisely.

1.4 Wall Heat Transfer of Combustion Chamber

While RANS-based models demonstrate effectiveness in simulating methane combustion flows, challenges arise due to the presence of a viscous boundary layer near the wall, particularly in high Reynolds number (*Re*) models. To address the low Reynolds number region induced by viscosity near the wall, wall functions are commonly employed to circumvent direct solution of the boundary layer. Instead, the entire computational

domain is configured as a fully turbulent zone[65]. This approach significantly reduces computational costs and enhances computational efficiency and stability.

The wall function acts as an intermediary between the wall and the computational domain. On one side, it facilitates the transmission of characteristics such as heat flux and shear stress to the wall, while on the other side, it furnishes boundary conditions for the turbulence calculation domain. Subsequently, the calculation of the low Reynolds number region can be circumvented by employing empirically derived distributions of variables within the boundary layer, as informed by experimental or simulation data, such as the simplest linear distribution.

However, when using the RANS method equipped with traditional wall functions to simulate a methane/oxygen combustion chamber, some problems occurred in the engineering of calculating wall heat transfer. In the numerical simulation of a multi-injector methane/oxygen rocket combustion chamber, J. Wei et al. [66] observed that while the pressure distribution obtained from the simulation closely matched experimental results, the computed wall heat flux consistently exceeded experimental values by approximately 30%, irrespective of the chosen wall treatment method. This phenomenon is illustrated in Figure 1. A similar phenomenon manifests in the methane combustion chamber incorporating film cooling, In the investigation of single-injector combustion chamber, it is observed by A. Sternin et al. that RANS-based simulations consistently overestimate the wall heat flux, as depicted in Figure 2[67]. Similar heat flux overestimation is evident in the study conducted by D. Muto et al.[68] and F. Di Matteo et al.[69].

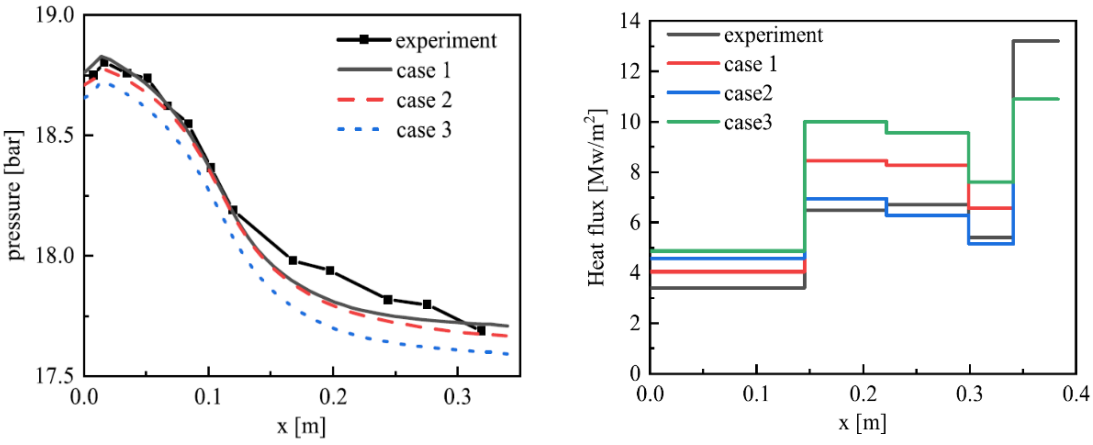

Pressure distribution Heat flux distribution

Figure 1 Pressure and wall heat flux distribution in a seven-element chamber (case 1: Enhanced wall treatment with y^+=1; case 2: Coupled wall treatment with y^+=30; case 3: Enhanced wall treatment with y^+=30)

According to the research, the overestimation of wall heat flux may stem from the derivation process of general wall functions. Typically, wall functions are derived based on single-component, non-reacting flow scenarios, thereby completely disregarding chemical reactions within the boundary layer. However, numerous studies have indicated that chemical reactions occurring in the boundary layer can significantly influence wall heat flux[70-75]. This effect becomes particularly pronounced when reactants are utilized as wall coolants, underscoring at the importance of considering chemical effects near the wall.

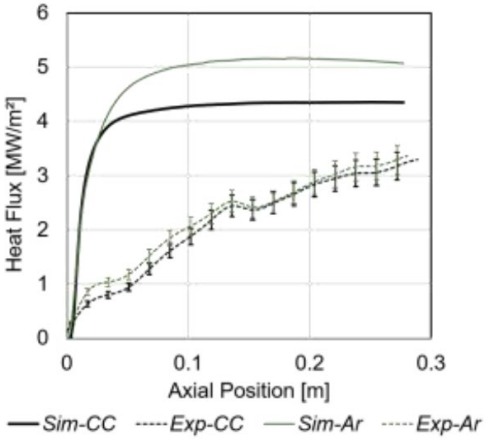

Figure 2 wall heat flux distribution of experiments and simulations in a single-element chamber with film cooling

In summary, to address the challenge of RANS-based overestimation in predicting wall heat flux, this study implemented a coupled wall function proposed by O. Cabrit and F. Nicoud[76]. This approach accounted for the impact of chemical reactions in the boundary layer, thereby mitigating the over-prediction of wall heat flux. A numerical framework based on the coupled wall function was proposed and subsequently experimentally validated. Utilizing the proposed framework, this study further investigated and predicted combustion and wall heat transfer characteristics in methane/oxygen rocket engines.

1.5 Outline

This thesis presents a comprehensive summary as follows: Chapter 2 details the methodologies utilized in this research, encompassing the establishment of numerical framework, derivation and embed of couple wall function, reference and comparative experiments, as well as the delineation of parameters and boundary conditions. Chapter 3 delves into the verification and application of the constructed numerical framework[77]. Investigations into parameter optimization aimed at enhancing predictions of wall heat

flux in single-injector methane/oxygen combustion chamber[78], as well as research into improving film cooling efficiency. Research on wall heat transfer and cooling efficiency in multi-injector methane/oxygen engines subjected to velocity drive. Along with scholarly contributions based on these endeavors. Chapter 4 provides a discussion on existing research findings and offers insights into future of the field.

2. Methodology

This chapter serves primarily as an introduction to the methodology, outlining various approaches employed to obtain the research outcomes presented in Chapter 3. It comprises two main parts: reference experiment part and numerical framework part. The reference experiment part provides an overview of the experimental geometric characteristics utilized to validate the numerical framework, it includes descriptions of operating parameters, typical experimental results, and the modeling of the discrete experimental data. In addition, the numerical framework part delineates the diverse numerical models utilized, reaction mechanisms, model construction and mesh establishment, derivation and embedding of coupled wall function, stipulated boundary conditions and verification of grid independence, among other aspects.

2.1 Reference Experiments

The comparative assessment of the numerical model in this investigation draws upon experimental data conducted at the Technical University of Munich (TUM) Aerospace Propulsion Institute. These experiments encompassed two distinct configurations: one featuring a methane/oxygen combustion chamber with a single injector characterized by a rectangular cross-section incorporating film cooling, and the other comprising a methane/oxygen combustion chamber equipped with a circular cross-section housing seven injectors. These experiments were both conducted within the controlled environment of a laboratory test bench.

To investigate the efficacy of the numerical framework presented in this thesis within a combustion chamber incorporating film cooling, experimental findings from methane/oxygen combustion with film cooling are employed as a benchmark. Concurrently, to mitigate deviations arising from intricate flow dynamics, the optimal outcomes from a simplified single-injector rectangular combustion chamber conducted by Maria P. Celano et al[47]. are utilized for comparation. The primary geometric parameters of this testbench are detailed in Table 1.

Figure 3 illustrates a schematic depiction of the test bench. As depicted, the combustion chamber comprises two distinct segments, namely front and rear. Positioned along the exterior of the upper wall of the chamber are multiple orifices, each possessing a diameter of 0.5 mm, spaced uniformly. These orifices accommodate T-type thermocouples within the combustion chamber, and in the front segment of the chamber,

grouped thermocouples situated at distances of 1, 2 and 3 mm from the chamber wall surface, facilitating enhanced acquisition of wall temperature distribution and heat transfer. Additionally, a series of pressure sensors are correspondingly arranged along the side wall of the combustion chamber to capture the pressure distribution within the chamber.

Table 1 Main geometrical parameters of single-element testbench

Geometry	Unit	Value
Chamber length	(mm)	290
Chamber width	(mm)	12
Chamber height	(mm)	12
Throat height	(mm)	4.8
Contraction ratio A_{cc}/A_{th}	(-)	2.5

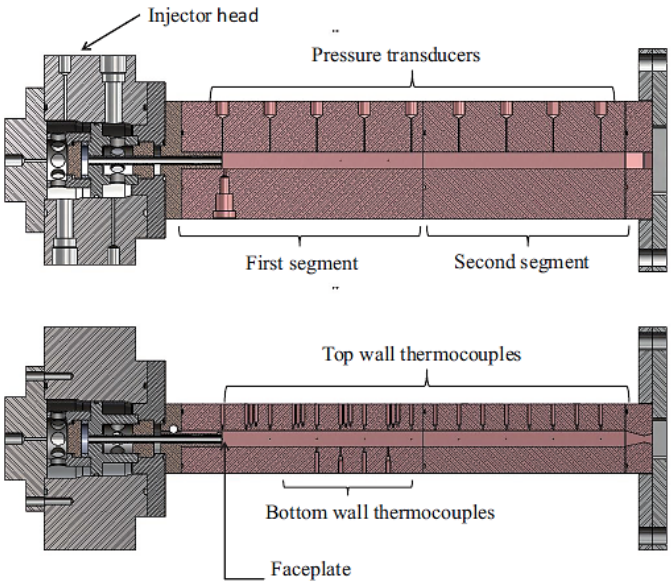

Figure 3 Side view and top view of the single element chamber section

Table 2 presents the fundamental operational parameters of the test bench during its functioning. Regarding the film cooling injection, Figure 4 shows a schematic cross-sectional view of the inlet section. Notably, the film is expelled through an inlet with a height of merely 0.25mm attach the upper wall surface, while the width of the film inlet spans 11mm. A more comprehensive elucidation of the test bench parameters can be found in Reference [47] and [48].

Table 2 Operating conditions of combustion chamber

p [bar]	$\dot{m}_{CH_4}$ [g/s]	$\dot{m}_{O_2}$ [g/s]	ROF [-]	$\dot{m}_{Film}$ [g/s]	R_F [%]
0.968	7.7	24.1	3.13	2.2	22.2

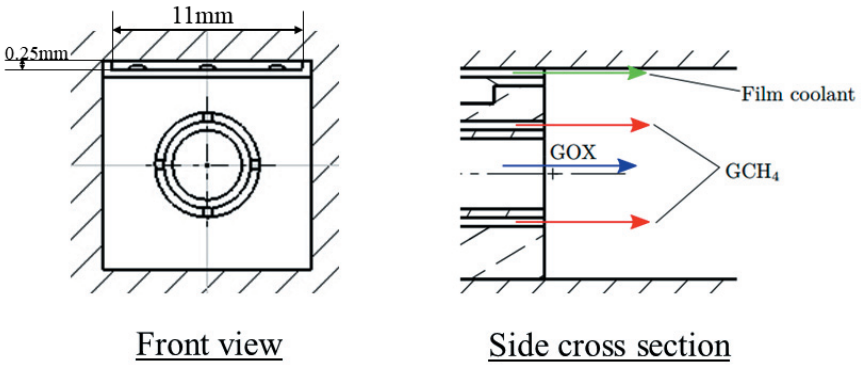

Figure 4 Cross section of single element combustion chamber and film injector

Figure 5 illustrates typical output curves of experimental pressure and temperature during combustion process. Considering the constraints associated with a heat-sink combustion chamber, a duration of approximately 3 seconds is selected for steady-state combustion to measure the heat load. Moreover, to mitigate the influence of the ignition process on temperature measurement, the ignition duration is limited to 300 milliseconds. Given the transient nature of combustion, three specific time points are identified: the initiation time t_0, the evaluation time t_1, and the cessation time t_2. Parameters of the chamber at the commencement of the experiment are determined at t_0, while those at the conclusion are established at t_2. Additionally, since the primary focus lies on attaining a steady-state equilibrium, t_1 is designated as the time point when equilibrium is achieved.

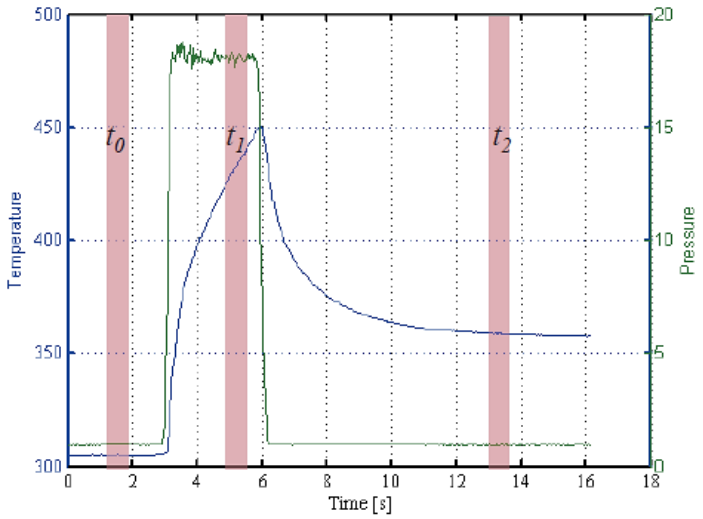

Figure 5 Example of pressure-temperature output curve and time points for combustion experiments

Figure 6 depicts the typical temporal evolution of pressure and temperature distributions from experiments. Notably, the pressure exhibits a gradual decrease as the sensor approaches the chamber exit, while conversely, the temperature exhibits a gradual increase. This observed trend aligns with the expected combustion pattern within the rocket combustion chamber. Furthermore, an experimental duration spanning from 4.2 seconds to 5.9 seconds is selected as the evaluation time as discussed. At this juncture, combustion attains equilibrium, and the experimental parameters acquired during this interval are chosen for validating the numerical model.

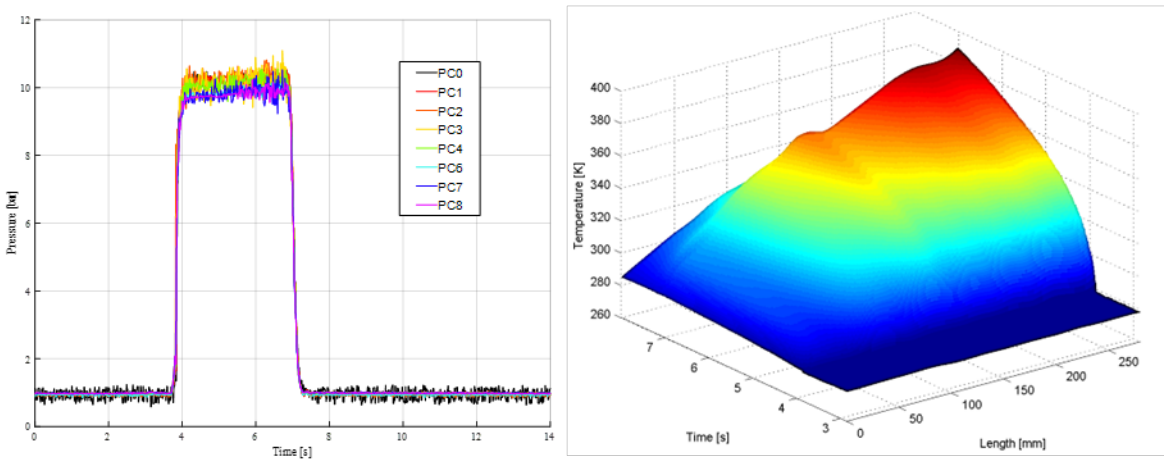

Figure 6 Typical single element combustion chamber pressure and temperature output curves

Subsequently, to investigate the intricate flow conditions within the combustion chamber of a more realistic rocket engine, the experimental outcomes from a multi-injector combustion chamber are employed to assess the three-dimensional effect within the chamber[59]. The schematic diagram of the test bench is presented in Figure 7. The combustion chamber boasts a circular cross-section with a diameter measuring 30 mm. Seven coaxial nozzles are meticulously arranged in an annular configuration. The spacing between the centers of these injectors amounts to 9 mm, and the contraction ration stands at 2.5 with a chamber pressure of approximately 20 bar. Similar to the single-injector test bench, it adopts a comparable methodology for thermocouples and pressure sensors arrangement. Additional primary geometric parameters are enumerated in Table 3.

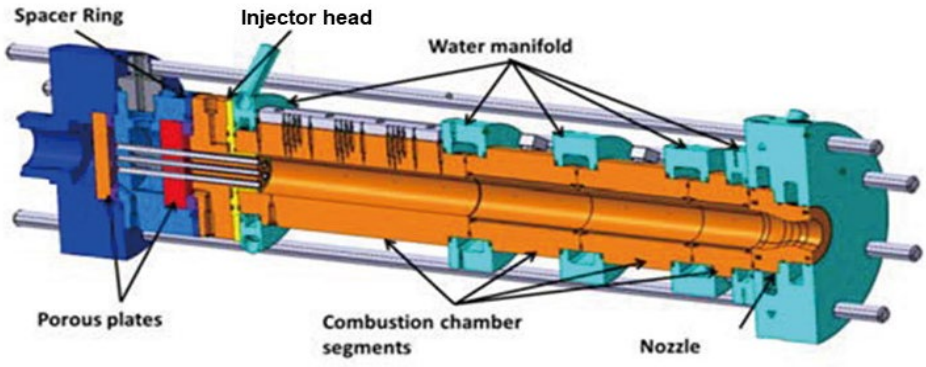

Figure 7 Seven-element combustion chamber schematic

Table 3 Main geometrical parameters of seven-element testbench

Geometry	Unit	Value
Chamber length	(mm)	340
GOX post inner diameter	(mm)	4
GCH4 annulus inner diameter	(mm)	5
GCH4 annulus outer diameter	(mm)	6
Injector area ratio A_{CH4}/A_{OX}	(-)	0.7

2.2 Inverse Heat Transfer Method

As elucidated in the preceding section, the thermocouples are strategically positioned at distances of 1-3 mm from the chamber wall. This arrangement is motivated by the challenging hot gas environment within the combustion chamber, making direct temperature measurements of the hot gas arduous. However, this arrangement may introduce potential inaccuracies in temperature measurements. Unlike other test benches employing external water or other cooling media, where the heat flux can be straightforwardly calculated from the enthalpy difference between the incoming and outcoming coolant, the temperature within a heat-sink combustion chamber is not a static parameter during combustion. Therefore, a transient inverse heat calculation method is applied to compute the transient heat flux profile and distribution on the chamber wall.

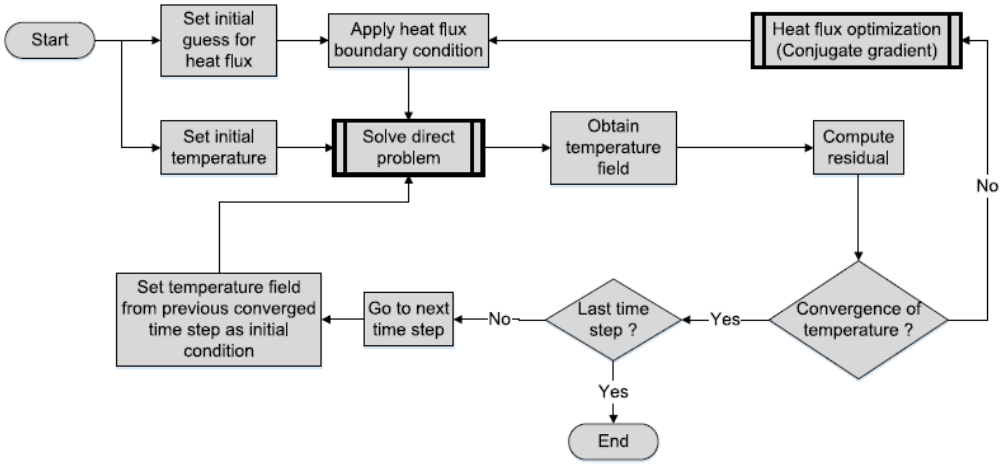

Figure 8 Iterative algorithm for inverse heat transfer method

The inversion algorithm, proposed and validated by N. Perakis et al. as referenced in [79], employs an iterative procedure outlined in Figure 8. Initially, an assumed heat flux is established, and the initial temperature T_0 serves as the starting condition for the temperature field. At this initial stage, the temperature field in the computational domain is known as the ambient temperature. A direct numerical solver, $Ro\dot{q}FITT$, developed using a 3D finite difference (FD) code, is employed for iteration[80, 81] . Residuals are computed by comparing the measured point values with experimentally obtained values in each iteration. Once the residuals converge, a more accurate temperature distribution and wall heat flux are obtained. Figure 9 illustrates the wall heat flux calculated by the inverse method, compared with experimental values, demonstrating noticeable differences that affirm the efficacy of the inverse method. Further details regarding the calculation and validation process of the inverse method are provided in references [79, 82]. The thermodynamic experimental data used to subsequently validate the numerical framework in this paper have been optimally adjusted using the inverse method.

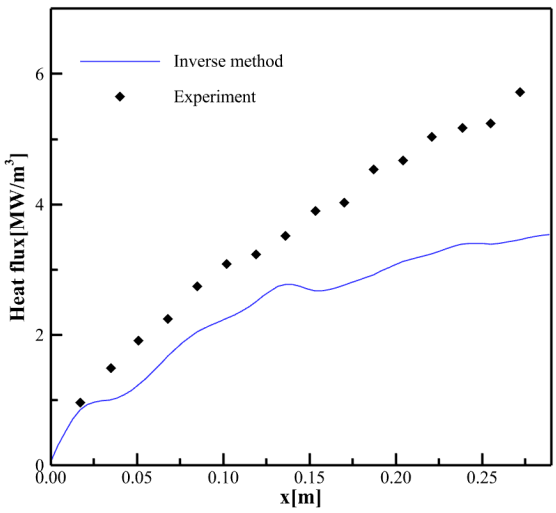

Figure 9 Experimental value and calculated value of wall heat flux

2.3 Numerical Setup

Based on the described experimental setup, the geometric and physical model for simulation is constructed. Given primary focus on combustion and heat transfer characteristics within the chamber, only the chamber and nozzle mesh constitute the calculation domain. Additionally, to ensure the complete development of the fuel and oxygen, specific length of fuel and oxygen injection pipe are retained. The geometrical configuration of the single-element combustion chamber computational domain is illustrated in Figure 10(a), with specific geometrical parameters of the combustion chamber referenced in Table 1. A mesh has also been generated based on this configuration, as depicted in Figure 10(b). To enhance computation efficiency, only one-fourth of the chamber is retained, with symmetric boundary conditions applied for the truncated sections. The mesh is refined in the corresponding shear layer area, and the mesh thickness near the chamber wall is controlled to maintain the wall y^+ at approximately 30.

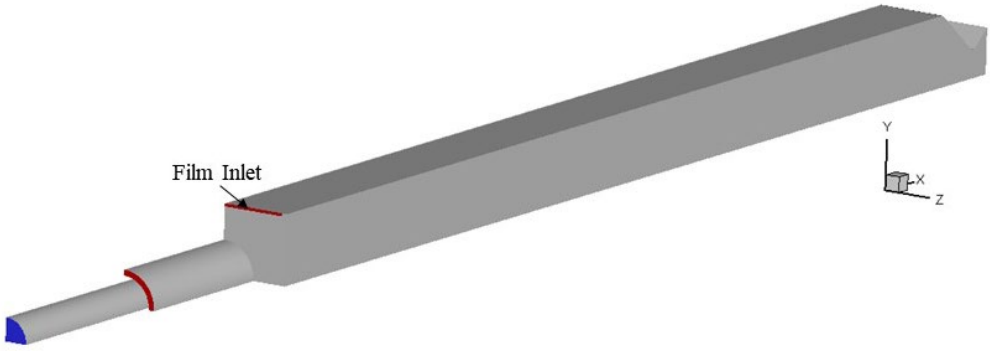

(a) Single element combustion chamber geometry

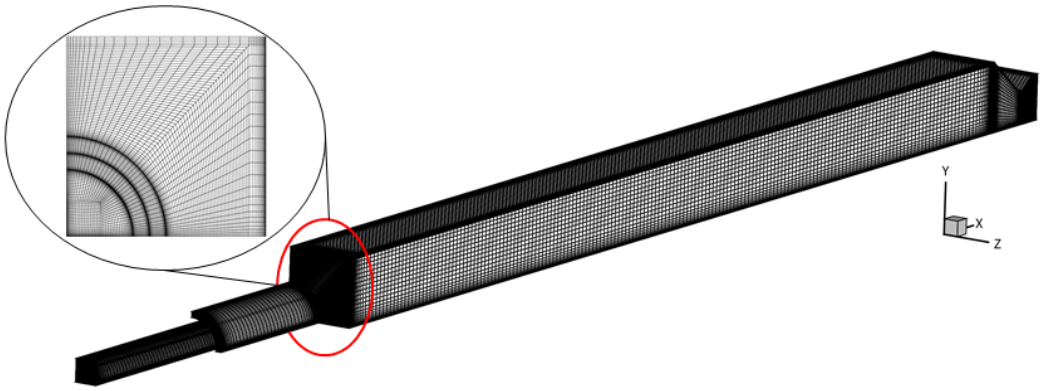

(b) Single element combustion chamber mesh

Figure 10 Geometry and mesh of single element combustion chamber

For the multi-element combustion chamber, the geometric model is established with

reference to the experimental apparatus in Table 3. The original experiment lacks film cooling, thus, in the simulation process, the film injection port is artificially positioned in the injection plate adjacent to the wall. The geometry is depicted in Figure 11(a), with 50 mm of fuel and oxygen injection pipes reserved to ensure fully developed flows. The mesh, constructed based on the geometry of the 7-element chamber, is presented in Figure 11(b), with wall y^+ values controlled around 30 and mesh refinement in the shear layer region similar to the single-element chamber. Correspondingly, to curtail computational costs, only one-sixth of the combustion chamber is retained, with mesh density reduced appropriate at the nozzle, given that the primary focus is on the combustion chamber section.

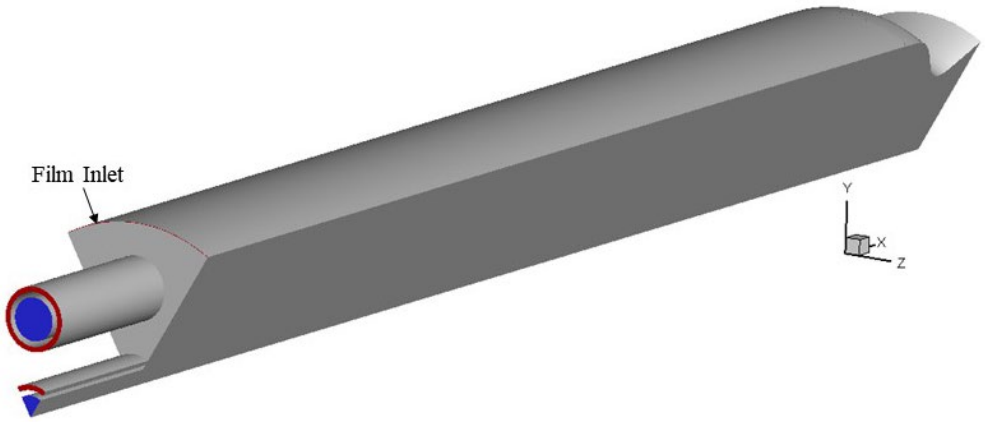

(a) Multiple elements combustion chamber geometry

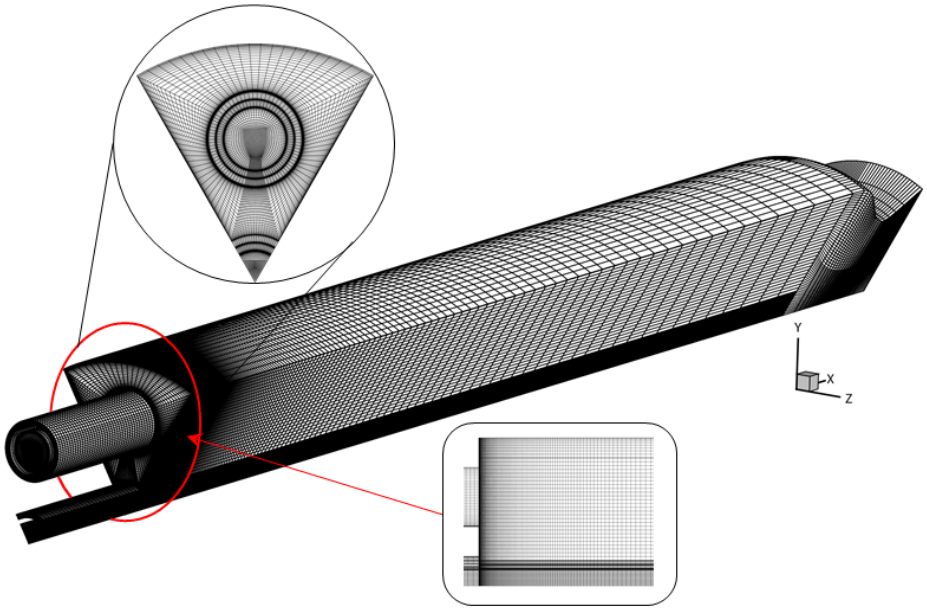

(b) Multiple elements combustion chamber mesh

Figure 11 Geometry and mesh of multiple elements combustion chamber

Concerning the numerical model, the initial consideration is the selection of the turbulence model. As delineated in Chapter 1, RANS-based numerical models are adept at simulating turbulence and combustion chambers, offering significant computational advantages compared to LES and DNS methods[59, 67, 83-85]. Moreover, the standard $k-\varepsilon$ turbulence model is predicated upon the foremost comprehension of pertinent phenomena, there mitigating uncertainties and furnishing a suite of equations amenable to a broad array of turbulent scenarios[86], where *k* is turbulent kinetic energy and can be derived from:

$$\frac{\partial(\rho k)}{\partial t}+\frac{\partial(\rho k u_i)}{\partial x_i}=\frac{\partial}{\partial x_j}\left[\frac{\mu_t}{\sigma_k}\frac{\partial k}{\partial x_j}\right]+2\mu_t E_{ij}E_{ij}-\rho\varepsilon \tag{2-1}$$

and ε is turbulent dissipation and can be obtained from:

$$\frac{\partial(\rho\varepsilon)}{\partial t}+\frac{\partial(\rho\varepsilon u_i)}{\partial x_i}=\frac{\partial}{\partial x_j}\left[\frac{\mu_t}{\sigma_\varepsilon}\frac{\partial\varepsilon}{\partial x_j}\right]+C_{1\varepsilon}\frac{\varepsilon}{k}2\mu_t E_{ij}E_{ij}-C_{2\varepsilon}\rho\frac{\varepsilon^2}{k} \tag{2-2}$$

the equations are comprised of several adjustable constants, which have been determined through extensive iterations of data fitting across a broad spectrum of turbulent flows[87], they are outlined as follows: $C_\mu=0.09, \sigma_k=1, \sigma_\varepsilon=1.3, C_{1\varepsilon}=1.44, C_{2\varepsilon}=1.92$. Research have shown that the standard $k-\varepsilon$ model can effectively predict mixing processes with satisfactory accuracy while maintaining a low computational consumption[88-91].

Additionally, investigations demonstrate the viability of characterizing the methane combustion process within the chamber as finite-rate reactions, warranting the utilization of the eddy dissipation concept (EDC) model as a suitable reaction model[61, 67, 92, 93]. Regarding the chemical reaction mechanism, the mechanism employed in this thesis comprises a formulation of 14 distinct species and 18 reactions, as originally proposed by Dong G et al[94]. Moreover, the validation of the chemical mechanism is further substantiated through a comparative analysis between experimental data and simulation outcomes. As depicted in Figure 12, which illustrates the velocity distribution across the cross-section within the domain characterized by turbulent and chemical interplays, the simulated velocity values closely align with the experimental data. This concordance underscores the appropriateness of the mechanism for facilitating methane combustion calculations.

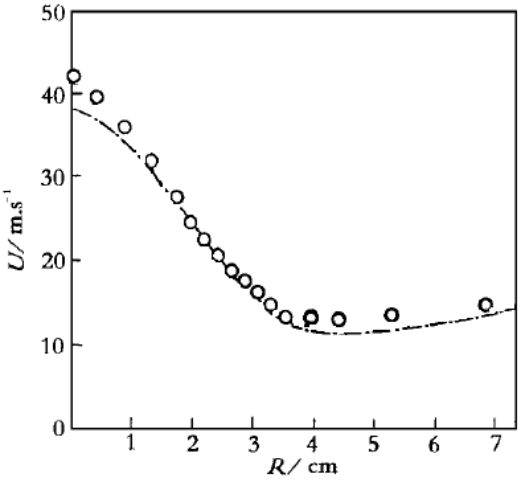

Figure 12 Distribution of velocity field (○- experiment; -·- - simulation)

In the case of the single-element chamber, both the turbulent Prandtl number (Pr_t) and turbulent Schmidt number (Sc_t) are prescribed as 0.7, discussion pertaining to dimensionless numbers will be elaborated upon in following studies[78] of this thesis. Conversely, for the multi-element chamber, these parameters are assigned a value of 0.85, determined through insights gleaned from previous multi-element chamber simulations due to the unavailability of pertinent experimental data. Concerning the approach to wall treatment, the coupled wall function is integrated into the Ansys Fluent software via the User Defined Function (UDF) method, aimed at refining the prediction accuracy of wall heat transfer. The subsequent section will provide a succinct exposition on the derivation and modeling procedures of the coupled wall function. The enhanced wall function is adopted as a reference control in the analysis.

2.4 Wall Treatments

As previously mentioned, to effectively leverage the high Reynolds number model, tailored handling of the boundary layer proximate to the wall is imperative to furnish suitable boundary conditions and reduce computational expenses. This necessitates the adoption of the wall function approach. To delve into the intricacies of the wall function, more discussion and derivation process need to be carried out. The momentum and energy governing equation of general flow can be expressed as:

$$\rho\left(\frac{\partial \boldsymbol{V}}{\partial t}+\boldsymbol{V}\cdot\nabla\boldsymbol{V}\right)=-\nabla p+\nabla\cdot\tilde{\boldsymbol{\tau}}+\rho\boldsymbol{f} \tag{2-3}$$

$$\rho\left(\frac{\partial H}{\partial t}+\boldsymbol{V}\cdot\nabla H\right)=-\nabla\cdot\boldsymbol{q}+\nabla\cdot(\tilde{\boldsymbol{\tau}}\cdot\boldsymbol{V})+\frac{dp}{dt} \tag{2-4}$$

the physical interpretation of the above equations lies in the equivalence between the convection flux on the left-hand side and the diffusion flux on the right-hand side. As the

Reynolds number diminishes, the relative magnitude of the diffusion flux progressively ascends. Leveraging this insight, a statistical average of Equation (2-3) and Equation (2-4) has been conducted. It is observed that the diffusion flux component adjacent to the chamber wall in the vertical direction substantially surpasses that in the other two directions. Consequently, only the *y*-directional component is retained, with the remaining values transferred to the right side of the equations, the final former of these equations convert to:

$$\frac{\partial \tau_w}{\partial y} = F \tag{2-5}$$

$$\frac{\partial q_w}{\partial y} = G \tag{2-6}$$

where *F* and *G* are unknown functions.

At this juncture, provided that the expression of the distribution functions *F* and *G* are attainable, the nexus between wall shear stress and heat flow can be established through the integration of *y* across the boundary layer. These connections defined as the wall distribution laws. Such laws delineate the algebraic linkage between the physical parameters at the wall and the center of the first layer grid, circumventing the discretization of the viscous layer within the boundary. The mathematical underpinning of the wall function lies in furnishing the wall heat flux value directly, thereby obviating the need for discretizing the gradient operator.

Broadly speaking, the widely employed wall functions postulates $F=G=0$. This premise represents the simplest assumption. Nonetheless, in the context of methane/oxygen rocket engines, within combustion chambers employing methane as the film coolant, this assumption implies that the chemical reaction in the boundary layer is insignificant, rendering it evidently unsuitable. Consequently, to address this issue, coupled wall function devised by O. Cabrit and F. Nicoud[76], grounded on multicomponent reaction flow, are employed to forecast intense temperature gradients and chemical reactions within the boundary layer of the combustion chamber. Subsequent to this, a succinct introduction to the derivation and modelling of coupled wall functions for the combustion cases investigated in this thesis is presented.

In turbulent flows entailing chemical reactions, the momentum and energy equations retain their forms as Equation (2-3) and Equation (2-4). Given that chemical reactions still presume complete elastic collisions among molecules, the influence of reactions on Equation (2-3) can be neglected, implying that the coupled wall function exerts no impact on flow characteristics. However, the energy equation incorporates a chemical enthalpy term. Since the rocket engine combustion chamber represents a standard low Mach

number flow, the unsteady pressure term and viscous dissipation term in Equation (2-4) can be disregarder, thereby permitting a rewritten form as follows:

$$\rho \frac{dH}{dt} = -\nabla \cdot \boldsymbol{q} \tag{2-7}$$

In the absence of considering the Soret thermal diffusion and Dufour effect[95] stemming from the thermodynamic non-equilibrium, the total enthalpy H and heat flux vector $\boldsymbol{q}$ in the aforementioned equation can be articulated as:

$$H = \sum_{k=1}^{N} Y_k \left(h_{f,k}^0 + h_k^s\right) = H^s + H_f^0 \tag{2-8}$$

$$\boldsymbol{q} = -\lambda \nabla T + \rho \sum_{k=1}^{N} Y_k V_{k,D} h_k \tag{2-9}$$

By reintegrating Equation (2-8) and Equation (2-9) back into Equation (2-7), and amalgamating with the component transport equation, the Equation (2-7) can be streamlined to:

$$\rho \frac{dH^s}{dt} = -\nabla \cdot \left(-\lambda \nabla T + \rho \sum Y_k V_{k,D} h_k^s\right) - \sum h_{f,k}^0 \dot{\omega}_k \tag{2-10}$$

Equation (2-10) can be further simplified within the boundary layer. Since this research focuses on the steady-state combustion investigation, the partial derivative term with respect to time can be neglected. Additionally, the convection term near the wall and the x-direction and z-direction component are disregarded. Consequently, the diffusion flux wall distribution law considering chemical reactions is derived as:

$$\frac{\partial q_w^*}{\partial y} = \sum h_{f,k}^0 \dot{\omega}_k \tag{2-11}$$

where q_w^* represents wall heat flux in specific sensible enthalpy form. It is noteworthy that when chemical reactions are taken into account, the unknown function G in Equation (2-6) of the wall distribution law is $\sum h_{f,k}^0 \dot{\omega}_k$. The meaning of this term lies in its representation of the conversion rate of chemical energy to thermal energy. In the event of chemical reaction cessation, wherein the generation rate of each component becomes zero, chemical energy ceases to be converted into heat, causing the function G to approach zero. Consequently, the coupled wall function regresses into a standard wall function with G=0.

Equation (2-11) elucidates the physical significance of the wall heat flux distribution law of the coupled wall function. Nevertheless, due to the absence of an explicit

mathematical expression, its highly nonlinear nature renders its numerical implementation challenging. Hence, to facilitate the application of the coupled wall function within the numerical framework, certain numerical manipulations are warranted. By conducting Favre time averaging on Equation (2-7), and likewise excluding the unsteady terms and divergence components in the x- and z-direction, Equation (2-12) can be derived:

$$\frac{\partial \overline{q_w}}{\partial y} = \frac{\partial}{\partial y}\left(\bar{\rho}\widetilde{v''h_s''} + \bar{\rho}\sum_k \widetilde{v''Y_k''}\, h_{f,k}^0 - \overline{\lambda \frac{dT}{dy}} + \bar{\rho}\sum_k (h_k\, Y_k \widetilde{V_{k,y}}) \right) \tag{2-12}$$

Based on the DNS simulation results by Cabrit and Nicoud[76] regarding the relative significance of terms on the brackets in Equation (2-12), it is evident that the latter two terms $\overline{\lambda \frac{dT}{dy}} + \bar{\rho}\sum_k (h_k\, Y_k \widetilde{V_{k,y}})$ can be disregarded within the logarithmic region of the turbulent boundary layer. Additionally, the first two terms can be approximated using the Boussinesq vortex viscosity assumption[96]. Subsequently, this leads to the derivation of an explicit expression for the coupled wall function employed in computing the wall heat flux:

$$\overline{q_w} = -\mu_t \left(\frac{C_P}{Pr_t} + \frac{1}{Sc_t} \sum_k \frac{d\overline{Y_k}}{d\overline{T}} h_{f,k}^0 \right) \frac{d\overline{T}}{dy} \tag{2-13}$$

The $\sum_k \frac{d\overline{Y_k}}{d\overline{T}} h_{f,k}^0$ term in Equation (2-13) are pivotal for the excellent performance of the coupled wall function in forecasting wall heat flux. It signifies the wall heat flux arising from the equilibrium motion of chemical reactions. Eventually, the coupled wall function can be integrated into the current numerical models.

In the particular embedding procedure, as commonly used numerical simulation software such Ansys Fluent typically lacks direct modification capabilities for wall heat flux, UDF are employed to override the computed wall heat flux values. Given the inability to directly assign wall heat flux, a transformation of Equation (2-13) into a programmatically convenient form becomes necessary. A brief outline of the transformation approach is provided below. Initially, introduce a variable T^+:

$$T^+ = K(Pr) + \frac{\alpha}{B_q} u^+ \tag{2-14}$$

where $K(Pr)$ represents a constant derived through least-squares approximation, contingent upon the Prandtl number (Pr):

$$K(Pr) = \beta(Pr) - Pr_t C + \left(\frac{Pr_t}{\kappa} - 2.12 \right)(1 - 2ln20) \tag{2-15}$$

$$\beta(Pr) = \left(3.85Pr^{\frac{1}{3}} - 1.3\right)^2 + 2.12ln(Pr) \tag{2-16}$$

The coefficient C represents a constant in the logarithmic law of velocity, while κ denotes the von Kármán constant. The influence of their selection on the efficacy of the coupled wall function is addressed in Paper 2 in this thesis. The coefficient before the dimensionless velocity u^+ can be expressed as follows:

$$\frac{\alpha}{B_q} = \frac{C_P}{\frac{C_P}{Pr_t} + \frac{1}{Sc_t}\sum_k \frac{d\bar{Y}_k}{d\bar{T}} h_{f,k}^0} \tag{2-17}$$

and u^+ is dimensionless wall velocity, defined as:

$$u^+ = \frac{u_p}{u_\tau} \tag{2-18}$$

where u_p is velocity component parallel to the wall. $u_\tau = \sqrt{\frac{\tau_w}{\rho}}$ is the friction velocity.

Subsequently, according to the relationship between T^+ and q_w:

$$T^+ = \frac{\rho C_p u^*}{q_w}(T_w - T_c) \tag{2-19}$$

where $u^* = \frac{u_p u_{kt}}{u_\tau^2}$ is the improved dimensionless wall velocity, and $u_{kt} = C_\mu^{1/4} k_t^{1/2}$ is the velocity unit, it can be calculated from the C_μ(=0.09, coefficient for computing eddy viscosity in turbulent model) and turbulent kinetic energy k_t. The wall heat flux q_w can be explicitly express as:

$$q_w = -\frac{\rho C_P u^*}{T^+}(T_c - T_w) \tag{2-20}$$

This formulation can be effectively incorporated into the numerical framework using the UDF method, below a concise overview of the incorporating process will be provide.

The Ansys Fluent offers an extensive array of macro commands, enabling users to customize functions as needed. In this research, the DEFINE_ADJUST macro is predominantly utilized to compute the coefficient $-\frac{\rho C_P u^*}{T^+}$ in Equation (2-20), and store it in a user-defined memory (UDM). Afterwards, the obtained coefficients are invoked by DEFINE_HEAT_FLUX macro to calculate the wall heat flux value and assign it to the Fluent solver. The DEFINE_EXECUTE_AT_END macro is employed to monitor key parameters.

2.5 Boundary Conditions

The boundary conditions for both the single- and seven-element combustion chambers are detailed in Tables 4 and 5 correspondingly. The film coolant utilized

maintains a methane composition, consistent with that of the fuel. Regarding the upper wall of the chamber, the temperature distribution is established as the initial boundary condition, derived through the process of fitting and discretizing experimental data. Additionally, it is pertinent to highlight that a constant wall temperature is prescribed for the nozzle section. This decision stems from the absence of a thermocouple in that region during the experimental procedure. However, given our primary focus on the wall heat flux within the chamber section, maintaining a constant temperature at the nozzle is deemed acceptable. The specific value for this temperature is determined to ensure continuity with the wall temperature of the chamber section.

Table 4 Boundary conditions of single-element chamber

Boundary	Type	Specific	Temperature
GOX inlet	Mass flow inlet	0.006025 kg/s	268K
GCH4 inlet	Mass flow inlet	0.001925 kg/s	275K
Film inlet	Mass flow inlet	0.0011 kg/s	266K
Outlet	Pressure outlet	0.968 bar	300K
Injector wall & faceplate	Non-slip wall	-	Adiabatic
Chamber wall	Non-slip wall	-	Polynomial fitting
Nozzle wall	Non-slip wall	-	400K
Symmetric face	Symmetry	-	-

Table 5 Boundary conditions of multi-element chamber

Boundary	Type	Specific	Temperature
GOX inlet	Mass flow inlet	0.0301 kg/s	259.4K
GCH4 inlet	Mass flow inlet	0.001143 kg/s	237.6K
Film inlet	Mass flow inlet	0.001333 kg/s	237.6K
Outlet	Pressure outlet	1.01325 bar	300K
Injector wall & faceplate	Non-slip wall	-	Adiabatic
Chamber wall	Non-slip wall	-	Polynomial fitting
Nozzle wall	Non-slip wall	-	412K
Symmetric face	Symmetry	-	-

At this juncture, the numerical framework aimed at enhancing heat transfer prediction precision on the combustion chamber wall of the methane/oxygen rocket engine has been largely established. Concurrently, to facilitate a comprehensive assessment of the influence of chemical reactions occurring in the boundary layer on wall

heat flux, simulations employing enhanced wall function but with the same numerical setup and boundary conditions are conducted as a control group for comparative analysis.

2.6 Free Shear Layer Velocity Discrepancy

Finally, it is imperative to extend an assumption, positing that the fluid proximate to the wall resides in a state of chemical equilibrium. This assumption constitutes a necessary concession aimed at facilitating the computation of Equation (2-17), given that the derivative term hinges not solely on temperature but also on pressure and mixture composition, variables that prove exceedingly arduous to incorporate into the UDF within a non-equilibrium fluid framework. Consequently, it becomes imperative to deliberate upon the mechanism and applicability of the coupled wall function within the confines of the specific GCH4/GO2 combustion chamber featuring film cooling, as scrutinized in this study.

As the investigation conducted by J. Wei concerning a multi-element combustion chamber devoid of film[66], it has been observed that the heat flow values derived from the coupled wall function surpass those generated by general wall functions when evaluated at a circumferential angle of 0°. This phenomenon contradicts the anticipated outcome wherein the coupled wall function is anticipated to mitigate the predicted heat flux; this discrepancy arises due to the study's confinement to a two-dimensional scenario, disregarding the substantial impact of three-dimensional effects on component distribution.

In the simplified two-dimensional scenario, as the hot gas converges towards the cooler wall, its chemical equilibrium shifts towards a lower total chemical enthalpy, thereby instigating additional exothermic reactions within the gas, consequently yielding a negative chemical enthalpy gradient along the y-direction. This phenomenon engenders an augmentation in the calculated heat flux as Equation (2-13). Conversely, when film cooling is incorporated, the temperature of the film coolant decreases, leading to a reduction in the gas temperature proximate to the wall. Moreover, the coolant substance, methane, possesses the potential to partake in exothermic chemical reactions, thereby influencing the alteration in chemical enthalpy resulting from shifts in chemical equilibrium. This disparity constitutes one of the ramifications of film cooling on the anticipated wall heat flux predicted through the coupled wall function.

In the context of the three-dimensional scenario, akin to the actual combustion chamber, provided that the density of the gas mixture adjacent to the wall remains constant, it is feasible to express Equation (2-20) in terms of column coordinates:

$$\sum_k \frac{d\overline{Y_k}}{dy} h_{f,k}^0 = \frac{1}{\bar{\rho}} \sum_k \frac{d\bar{\rho}\overline{Y_k}}{dr} h_{f,k}^0 = \frac{1}{\bar{\rho}} \sum_k \frac{d\overline{\rho_k}}{dt} \frac{dt}{dr} h_{f,k}^0 = \frac{\sum_k h_{f,k}^0 \, \dot{\omega}_k}{\bar{\rho} V_r} = \frac{Q_C}{\bar{\rho} V_r} \qquad (2\text{-}21)$$

Examination of Equation (2-21) reveals that alteration in the direction of radial velocity V_r result in changes in the polarity of the equation, subsequently affecting the orientation of the enthalpy term. Consequently, from a three-dimensional standpoint, the sign of the radial velocity proximal to the wall significantly influences the prognostication of wall heat flux. Moreover, the introduction of film injection along the wall modifies flow dynamics, leading to divergent radial velocity patterns, thereby culminating in varying orientations of the chemical enthalpy term and, consequently, exerting a discernible impact on the prediction of wall heat flux.

In addition to the impact on flow characteristics, examination should extend beyond the localized heat flux at specific angles or regions to encompass the cumulative influence of the enthalpy term across the entirety of the chamber wall. The introduction of film injection alters the mass fraction gradient of each component in the near-wall region compared to conditions sans film cooling, thereby modifying the inner product of enthalpy and mass fraction gradient. Consequently, this alteration results in scenarios where the action direction of chemical enthalpy aligns or opposes the temperature gradient, thereby engendering varied effects of the chemical enthalpy term on the predicted heat flux value. The precise ramifications of this influence and the underlying causes thereof will be expounded upon in Paper 1 of this thesis.

Furthermore, extending beyond mere consideration of the coupled influence of the 3D effect and film injection on wall heat flow. Due to the influence of viscosity, the velocity disparity engenders shear stresses from distinct orientations within the mixing zone of the shear layer, arising from the interaction between two turbulent flows, as illustrated in Figure 13. Consequently, the turbulence within the mixing zone attains greater complexity, affecting species distribution, heat transfer, and the associated chemical reaction processes. Hence, it is imperative to scrutinize the influence of the velocity differential between the film and the main flow within the combustion chamber of the rocket engine, with a specific emphasis on its implications for combustion dynamics and heat transfer phenomena. Base on this view, this study delves into investigating the ramifications of the disparity between the film injection velocity and the mainstream velocity in Paper 3.

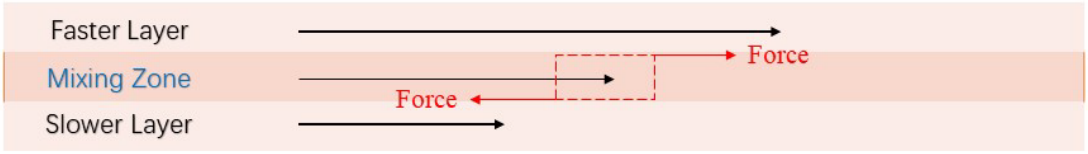

Figure 13 Shear force diagram of the fluid mixing zone

A dimensionless quantity, denoted as R_V, is introduced to quantify the relationship between the velocity of the main flow and that of the film. R_V is defined as follows:

$$R_V = \frac{V_{film}}{V_{mainflow}} \tag{2-22}$$

where V_{film} is the velocity of film and $V_{mainflow}$ is the velocity of the main flow. In the endeavor to uphold the oxygen-fuel ratio, the mass flow rate at the methane and oxygen inlets is deliberately maintained at a constant level throughout the velocity investigation, while the film inlet velocity is varied to achieve different R_V values. As depicted in Figure 14, the average velocity distribution of the near wall injector illustrates a marginal increase in fluid velocity as combustion progresses downstream in the chamber, reaching the speed of sound at the nozzle throat before experiencing a further augmentation upon traversing through the nozzle. Notably, minimal changes in velocity are observed in the frontal section of the combustion chamber, where the reactions have yet to commence significantly, precisely corresponding to the area where the film predominantly performs. Consequently, the average velocity of the main flow within the initial 0.1 meters of the chamber (highlighted in red in Figure 14), denoted as $V_{mainflow}$ in Equation (2-22), is intercepted and calculated, yielding a value of $V_{mainflow}$=92.578 m/s.

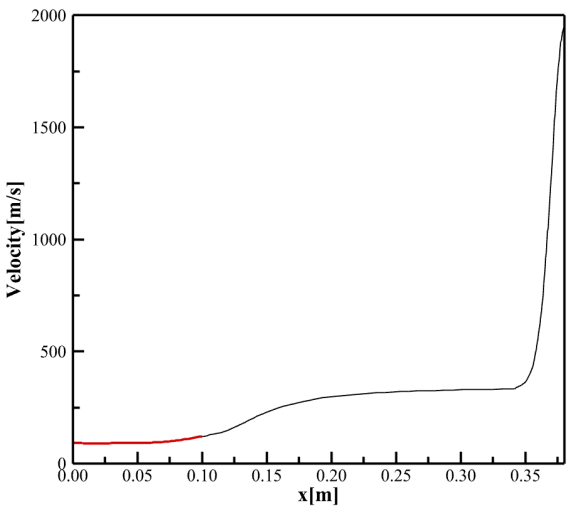

Figure 14 Velocity distribution of the main flow

Consequently, it becomes evident that there exist two distinct methodologies for regulating the injection velocity of the film: one entails manipulation of the film inlet mass flow rate, while the other involves adjustment of the film inlet size (inlet height in this study). In this thesis, these two strategies are separately employed to attain different R_V values, and a series of simulation cases are systematically devised to analyze their impacts. The specifics of these cases are concisely outlined in Table 6.

Table 6 Case summary list

Gr. / No.	Group A		Group B		R_V
	$\dot{m}\ (kg/s)$	$h_{film}(mm)$	$\dot{m}\ (kg/s)$	$h_{film}(mm)$	
0	0.001333	0.05	0.001333	0.05	1.276
1	0.000446	0.05	0.001333	0.15	0.427
2	0.000668	0.05	0.001333	0.10	0.639
3	0.000834	0.05	0.001333	0.08	0.798
4	0.001026	0.05	0.001333	0.065	0.982
5	0.001903	0.05	0.001333	0.035	1.822

2.7 Mesh Independence Verification

To assess the sensitivity of the calculation results to changes in mesh density and save computational resource, mesh independence investigations are examined for both single- and multi-element combustion chambers using five meshes with varying degrees of sparsity. The number of grids for the single-element chamber ranges from 378,952 for the coarsest mesh to 5,832,214 for the finest mesh, while for the multi-element chamber, the range is from 483,630 to 6,122,580 grids. Additionally, to ensure the validity of the wall functions, the wall y^+ values are adjusted to remain at around 30 after each mesh refinement.

Figures 15 and 16 depict the average temperature and flow velocity along the centerline of the combustion chamber, as well as the average heat flux distribution on the upper wall, for different numbers of grids. It is evident from Figure 15 that for the single-element chamber, the parameters within the combustion chamber stabilize after the grid

number reaches approximately 1.73 million, indicating mesh independence. Conversely, for the multi-element chamber, this stabilization occurs at around 2.46 million grids, as shown in Figure 16. In summary, to balance computational efficiency and numerical accuracy, grid numbers of 1.73 million and 2.46 million are selected for the single- and multi-element chamber simulations, respectively, in this study.

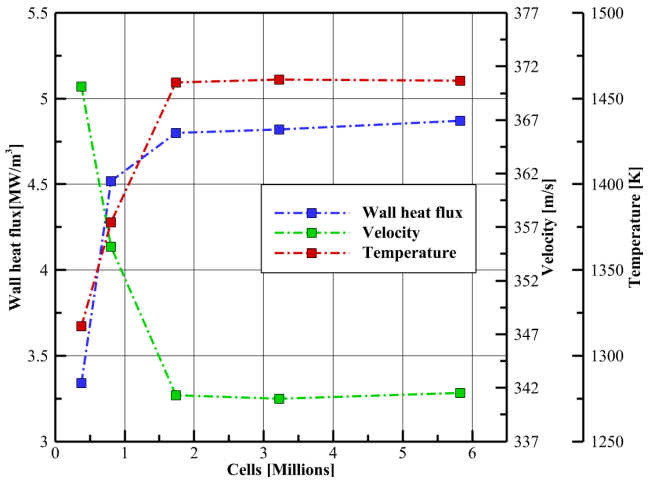

Figure 15 Variation of parameters of single element chamber with the number of grids

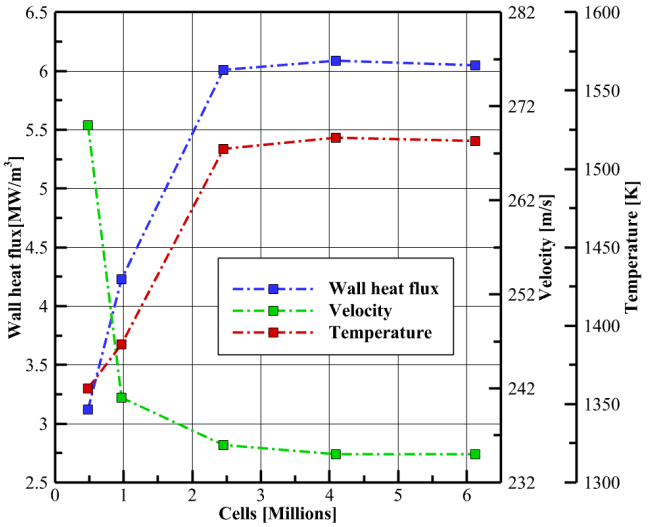

Figure 16 Variation of parameters of multiple elements chamber with the number of grids

2.8 Film Cooling Efficiency

By constructing the aforementioned numerical model, the chemical reactions within the boundary layer are incorporated, thereby enhancing the accuracy of wall heat flux prediction. It is noteworthy as well that in the investigation of film cooling, the cooling efficiency stands as a highly significant parameter. The primary objective of improving

the prediction of wall heat flux lies in achieving more precise determination of film cooling efficiency. Typically, the film cooling efficiency is expressed by the following formula[28, 97-99]:

$$\eta = \frac{T_{ad} - T_{CC}}{T_{film} - T_{CC}} \tag{2-23}$$

However, despite the widespread use of this cooling efficiency calculation method in cooling research, in actual rocket engines, achieving adiabatic conditions at the chamber wall proves challenging. Besides, this study adopts temperature as a boundary condition at the wall and utilizes wall functions to enhance the estimation of wall heat flux accuracy. Consequently, employing Equation (2-23) to quantify may not be appropriate. Instead, employing Net Heat Flux Reduction (NHFR) would be more suitable in this scenario, as indicated by numerous pertinent studies[100-103]. The NHFR can be defined as follows:

$$NHFR = 1 - \frac{\dot{q_{film}}}{\dot{q_0}} \cdot \left(\frac{P_{CC,0}}{P_{CC,film}}\right)^{0.8} \tag{2-24}$$

where $\dot{q_0}$ represents the heat flux without film, and the expression $\left(\frac{P_{CC,0}}{P_{CC,film}}\right)^{0.8}$ constitutes a correction factor introduced by D.R. Bartz [104] to account for the influence of film injection in the combustion chamber pressure.

2.9 Summary

In this chapter, a concise overview of the reference experiments and typical experimental data pertinent to this study is provided. Concurrently, the inverse method is introduced to address measurement errors arising from the distance between the measurement point and the wall in the experiment. Subsequently, the setup and boundary conditions of the numerical framework are briefly elucidated, along with the derivation and incorporation method of the coupled wall function. The energy equation is reformulated in terms of total enthalpy to tackle the nonlinearity inherent in the original coupled wall function, and the derived expression for wall heat flux is programmatically adjustable. Furthermore, grid independence verification is conducted, revealing that 1.73 million grids are optimal for single-nozzle combustion chambers, while 2.46 million grids are preferable for multi-nozzle combustion chambers. Finally, the impact of the coupling between complex flow and film cooling in the combustion chamber on wall heat transfer is deliberated, and velocity-related research methodologies and measurement standards

for film cooling efficiency are elucidated.

3. Summaries of Publications

3.1 Summary of Paper 1

《RANS Based Numerical Simulation of a GCH4/GO2 Rocket Engine Combustion Chamber with Film Cooling and Improvement of Wall Heat Flux Prediction》

Jianing Liu, Silong Zhang, Jianfei Wei, Oskar J. Haidn

The methane/oxygen rocket engine has emerged as one of the most promising propulsion systems today, owing to its cost-effectiveness and reusability. In the intricate design process of rocket engines, the cooling system plays a pivotal role, with film cooling emerging as a cornerstone method. Accurate prediction of heat transfer characteristics is paramount for the design and development of rocket engines employing film cooling. In this study, a comprehensive numerical framework based on the RANS method and the EDC reaction model is established, rigorously verified, and applied to simulate single- and multi-injector combustion chambers with film cooling. Additionally, a single injector combustion experiment with film cooling is conducted to validate the numerical framework.

The investigation reveals that coupled flow and chemical reactions near the wall significantly influence the wall heat load. Consequently, a coupled wall function, derived from Direct Numerical Simulation (DNS), is formulated and integrated into the numerical framework to account for these coupling effects. Results from the single injector chamber investigation demonstrate that considering chemical reactions near the wall reduces the wall heat flux by 50%, aligning more closely with experimental data. This underscores the superior predictive capability of the coupled wall function compared to general wall functions in chambers equipped with film cooling. Moreover, it is observed that the coupled wall function primarily affects the near-wall region and exerts minimal influence on the main flow. Subsequently, following validation in the single injector combustion chamber experiment, the numerical framework is applied to a multiple-injector scenario. The findings reveal that the wall heat flux in multi-injector combustion chambers is 75% lower than that predicted by general wall functions. Furthermore, the study delves into the influence of the film on the chemical enthalpy term near the wall, along with the coupling effects of turbulent flow and temperature gradient near the wall. Lastly, the analysis of vorticity in the multi-injector chamber indicates that the film attenuates vorticity in the front section of the combustion chamber, thereby impacting the flame expansion process.

The main purpose of this paper is to introduce the numerical framework developed for the first time and experimentally validates it using a methane/oxygen combustion chamber equipped with a single nozzle featuring film cooling, thus affirming the efficacy of the coupled wall function in film cooling investigations. Furthermore, the application of the coupled wall function to a multi-nozzle combustion chamber is also demonstrated. Lastly, a quantitative analysis is conducted to elucidate how the coupled wall function enhances the accuracy of wall heat flow calculations.

Individual Contributions:

This paper[77] has been published in the international peer-reviewed journal *Applied Thermal Engineering*. My primary contributions encompass the numerical processing of experimental data, the establishment of the numerical framework employed in this study, the composition and refinement of the UDF file for the coupled wall function, the execution of numerical simulations, the comprehensive analysis and discussion of the simulation outcomes and the writing and proofreading of the manuscript.

3.2 Summary of Paper 2

《Numerical Study of Film Cooling in Single-Element Injector Gaseous CH4/O2 Rocket Engine with Coupled Wall Function》

Jianing Liu, Silong Zhang, Jianfei Wei, Oskar J. Haidn

A coupled wall function is integrated into the framework based on the Ansys Fluent platform to enhance the accuracy of wall heat flux prediction. Furthermore, simulation results are corroborated and parameters optimized through corresponding experiments. Upon parameter study, it is observed that the wall heat flux diminishes while the wall y-plus escalates below 30, subsequently plateauing once the y-plus surpasses 30. Furthermore, the parameters κ and C_{mod} exhibit negligible influence on the film cooling acting area. Meanwhile, an increase in turbulent Prandtl number and Schmidt number within the range of 0.7 to 0.9 correlates with elevated wall heat flux. Following a comparison of various parameter configurations with experimental results, a final parameter setup is determined: $y^+ = 30$, $\kappa = 0.41$, $C_{mod} = 5.5$, and $Pr_t = Sc_t = 0.7$.

Several single-element combustion chamber simulations are conducted based on appropriate parameterization. These simulations reveal that employing coupled wall functions insignificantly alters main flow characteristics, including pressure, heat release rate, and temperature. However, film injection leads to an overall pressure increase and attenuation of the high-temperature zone near the wall. Additionally, film injection results in a higher peak in heat release rate in the front chamber section, followed by progressively decreasing values towards the end due to reactant decay. Analysis of wall heat flux indicates a parabolic distribution along the horizontal direction of the wall, with peak values situated on the midline of the chamber wall. Subsequent examination of downstream wall heat flux suggests that film cooling can mitigate wall heat flux, albeit with general wall functions tending to overestimate it. However, the coupled wall function substantially reduces this overestimation, aligning calculated wall heat flux values more closely with experimental data.

Furthermore, this study employs the NHFR method to investigate film cooling efficiency, rather than the traditional approach based on adiabatic wall temperature. This decision stems from the challenges associated with achieving adiabatic conditions in real rocket combustion chambers. Moreover, the primary focus of this paper is to refine the precision of wall heat flux predictions. Based on the findings, cooling efficiency distribution appears nearly uniform in the horizontal direction. Additionally, the impact of the coupled wall function on the NHFR distribution is found to be negligible, yet results

in higher calculated cooling efficiency compared to cases with general wall functions, suggesting reduced methane consumption as a coolant to achieve equivalent cooling performance. Furthermore, cooling efficiency rapidly diminishes at a distance of 70-80mm from the injection port, suggesting the feasibility of setting injection ports every 70-80mm along the chamber wall to sustain high cooling efficiency and safeguard the chamber wall.

In summary, this paper introduces and employs a numerical framework to accurately simulate the combustion chamber of a single-element GCH4/GO2 rocket engine with low computational cost. An optimized parameter setup and integration of coupled wall functions significantly enhance wall heat flux prediction, critical for research on rocket engine wall protection. Additionally, the study of film cooling efficiency yields more precise results and suggests appropriate film injection arrangements. Application of these findings can enhance the design of rocket propulsion systems and mitigate excessive rocket engine temperatures.

Individual Contributions:

This paper[78] has been published in the international peer-reviewed journal *AIP Advances*. My primary contributions include the processing of experimental data, the modification and optimization of the numerical framework proposed in Paper 1[77], the execution of numerical simulations, the data analysis and discussion of the simulation results, and the writing and proofreading of the manuscript.

3.3 Summary of Paper 3

《Velocity-Driven Optimization of Film Cooling in Methane/Oxygen Rocket Engines Using Coupled Wall Function》

Jianing Liu, Silong Zhang, Jianfei Wei, Oskar J. Haidn

This paper delves into the utilization of coupled wall functions in the examination of film cooling within multi-element methane/oxygen rocket engine combustion chambers. By manipulating parameters such as film mass flow rate and inlet size, the investigation explores the impact of varied film-mainstream velocity ratios on flow dynamics, combustion phenomena, wall heat transfer, and cooling efficiency within the combustion chamber. Findings reveal a nuanced relationship between the ratio of film velocity to mainstream velocity (R_V) and key chamber parameters. Specifically, an increase in R_V initially correlates with a decrease in combustion chamber pressure, followed by a subsequent rise, accompanied by a corresponding trend in vortex intensity at the inlet section.

Comparative analysis demonstrates that, while maintaining a constant mass flow rate, reductions in the film inlet height yield lower pressures and weaker swirl strength. Additionally, wall heat transfer exhibits a gradual decrease with increasing R_V, particularly notable in cases involving supplementary low-temperature methane injection. Notably, the introduction of coupled wall functions has minimal discernible impact on mainstream flow and combustion dynamics.

Evaluation of NHFR reveals a notable decline in cooling efficiency within the front half of the combustion chamber, underscoring the feasibility of employing film cooling inlets at regular intervals, such as every one-fifth section, in methane/oxygen engines. Furthermore, augmenting the mass flow rate enhances cooling efficiency with increasing R_V, while adjustments to the inlet size result in relatively consistent cooling efficiency. Consequently, maximizing film mass flow rate emerges as a preferred approach for optimizing film cooling arrangements within a given rocket engine. Nonetheless, comparative analyses indicate a gradual reduction in engine-specific impulse with escalating mass flow rates, emphasizing the imperative for engine-specific considerations in design determinations.

The primary objective of this paper is to investigate the impact of the velocity differential between the film and the main flow on wall heat flux. This exploration entails considering the coupling effect of complex flow dynamics within the combustion chamber and the chemical reactions occurring near the wall. Furthermore, the paper

delves into discussions surrounding related research on film cooling efficiency, proposing a more rational arrangement for film cooling. Finally, the study on the overall specific impulse of the engine underscores the importance of avoiding a simplistic approach that solely focuses on increasing air film mass flow rate, advocating instead for a holistic evaluation of various parameters to optimize engine performance.

Individual Contributions:

This paper has been submitted to the international peer-reviewed journal *Thermal Science and Engineering Progress*. My principal contributions encompass the proposition of novel velocity research methodologies, the refinement of the aforementioned numerical framework, the execution of numerical simulations, the meticulous analysis and discussion of findings, and the composition and validation of manuscripts.

4. Discussions and Outlooks

4.1 Discussions

This research primarily establishes a numerical framework centered around the coupled wall function to simulate film cooling wall heat transfer within the combustion chamber of a methane/oxygen rocket engine. The primary objective is to address the challenge of excessive wall heat flux calculated using the RANS model. The genesis of this topic stems from observations during the numerical simulations on methane/oxygen combustion chambers, wherein despite achieving distributions of combustion chamber pressure, temperature, and other parameters highly consistent with experimental results, significant disparities in the prediction accuracy of wall heat flux are frequently encountered.

Through investigation, it is discerned that this disparity could be attributed to the omission of chemical reactions within the boundary layer when employing wall functions. However, within research, particularly in engineering disciplines, there exists a compelling need to swiftly and economically predict flow combustion characteristics within the combustion chamber by using the RANS method. Consequently, the integration of a coupled wall function, accounting for chemical reactions near the wall, is employed to refine the RANS method's treatment of wall heat transfer prediction.

The initial focus of this research revolves around the establishment and validation of a numerical framework. Key challenges encountered at this juncture include the integration of coupled wall functions and the processing of nonlinear experimental data. Given that most contemporary numerical simulation software does not inherently support the direct modification of physical quantities, and certain parameters involved in the calculation process are not readily accessible. Besides, the incorporation of coupled wall functions presents formidable nonlinearities. Consequently, appropriate transformations and processing are imperative to facilitate their embedding into Fluent via UDF. Furthermore, this study also addresses errors stemming from measurement points not being proximate to the wall in the reference experimental data through inverse method.

The research outcomes of Paper 1 demonstrate that the numerical framework equipped with coupled wall functions effectively ameliorates the issue of overestimated wall heat transfer, while preserving the accuracy of mainstream flow and combustion characteristics calculations. This finding underscores the significance of accounting for chemical reactions within the boundary layer, pinpointing it as the root cause of wall heat

flow overprediction. Additionally, the magnitude of this discrepancy is quantitatively analyzed in the paper through comparisons of area averages of gradients of each substance with their chemical enthalpy inner product. Furthermore, this article conducts a preliminary analysis of the 3D effect on wall heat transfer in a multi-nozzle circular combustion chamber. The findings indicate that chemical reactions within the boundary layer also influence the thickness of the temperature boundary layer to a certain extent, subsequently impacting temperature gradients near the wall and other flow characteristics such as vortex behavior. In summary, this paper primarily establishes a foundational numerical framework, validates its efficacy, and explores its practical application.

During the verification process of the numerical framework and the discussion of its applicability, it is found that the performance of the coupled wall function is influenced by certain parameters during the numerical calculation process. As a natural progression of the research, the subsequent phase focuses on optimizing these parameters to identify the configuration that most accurately predicts wall heat flux. In Paper 2, centered around a relatively straightforward single-injector rectangular cross-section combustion chamber, all parameters potentially affecting the results are introduced, and their operational principles are elucidated. The paper conducts comparisons between results obtained with different parameter configurations and experimental data, ultimately identifying the optimal parameter combination conducive to the numerical framework incorporating the coupled wall function.

Additionally, Paper 2 delves into a more comprehensive discussion on the practical application of numerical frameworks. Given the substantial challenges associated with measuring film cooling efficiency through conventional means, the paper advocates for employing Net Heat Flux Reduction (NHFR) as a standardized metric for assessing air film cooling efficiency. Finally, the study investigates the impact of enhanced wall heat flux on cooling efficiency, providing valuable insights into the interplay between these factors.

Ultimately, investigation revealed the substantial influence of the coupling between complex flow dynamics and film injection in multi-nozzle combustion chambers on wall heat transfer. Paper 3 delves into a comprehensive exploration of the combined effects of complex flow dynamics and near-wall chemical reactions. This exploration is facilitated through the manipulation of film injection velocity using two distinct methodologies, subsequently controlling the velocity ratio between the film and the mainstream. Findings of Paper 3 indicate that increasing R_V initially decreases combustion chamber pressure before a subsequent rise, alongside similar trends observed in vorticity at the inlet.

Furthermore, contrasting methods of manipulating film velocity reveal that reducing film inlet height leads to lower pressures and weaker swirl strength. Analysis of swirl strength and temperature distribution reveals a gradual thickening of the temperature boundary layer with increasing R_V, affecting wall heat transfer differently when using general versus coupled wall functions. Paper 3 also identifies a decrease in wall heat flux with increasing R_V, particularly notable with additional low-temperature methane injection. Investigation into NHFR suggests optimal film cooling inlet spacing, favoring higher mass flow rates for improved cooling efficiency, albeit with a trade-off in engine specific impulse. These findings emphasize the importance of tailored film cooling strategies in methane/oxygen rocket engines, balancing cooling efficiency with engine performance considerations.

4.2 Outlooks

This study rigorously validates and refines the numerical framework featuring coupled wall functions for accurate prediction of wall heat transfer. Consequently, its demonstrated efficacy warrants its broader application across diverse engineering and research scenarios in future research endeavors. At the end of this thesis, some possible application scenarios of this research in future engineering practice and academic research are introduced, such as:

- It is pertinent to acknowledge the significance of the cooling system, particularly in components like the rocket engine nozzle, where operational conditions may involve supersonic flow. Therefore, the prospective adaptation and integration of the numerical model to address supersonic flow dynamics and the efficacy of wall functions in such contexts warrant careful consideration and further investigation.
- The study underscores the impact of complex flow and near wall reaction interactions on wall heat transfer prediction in the combustion chamber. Consequently, exploring additional combustion chamber conditions, such as coaxial horizontal setups and configurations with more multiple injectors, is promising for further studies.
- The consideration of diverse reaction mechanisms is interesting, as varying mechanisms lead to distinct chemical reaction processes that inherently influence the performance of coupled wall functions. Thus, investigating the impact of different reaction mechanisms on wall function efficacy is highly anticipated.
- In the domain of chemical reactions, it is pertinent to discuss the utilization of coupling functions in alternative fuel/oxidizer components. Given the diverse fuel compositions employed in rocket propulsion, the relevance of numerical models extends to various engine types, such as those powered by hydrogen/oxygen or kerosen

References

[1] J.S. Kim, H. Jung, J.H. Kim, State of the art in the development of methane/oxygen liquid-bipropellant rocket engine, Journal of the Korean Society of Propulsion Engineers, 17 (2013) 120-130.
[2] T. Neill, D. Judd, E. Veith, D. Rousar, Practical uses of liquid methane in rocket engine applications, Acta Astronautica, 65 (2009) 696-705.
[3] S.H. Bae, H. Jung, J.S. Kim, A Preliminary Configuration Design of Methane/Oxygen Bipropellant Small-rocket-engine through Theoretical Performance Analysis, Journal of the Korean Society of Propulsion Engineers, 19 (2015) 47-53.
[4] A. Preuss, D. Preclik, C. Mading, J. Gorgen, S. Soller, O. Haidn, M. Oschwald, W. Clauss, R. Arnold, J. Sender, LOx/Methane technology efforts for future liquid rocket engines, 5th international spacecraft propulsion conference & 2nd international symposium on propulsion for space transportation, 2008.
[5] B. Lim, C. Kim, K.-O. Lee, K. Lee, J. Park, K. Ahn, H.-J. Namkoung, Y. Yoon, Development trends of liquid methane rocket engine and implications, Journal of the Korean Society of Propulsion Engineers, 25 (2021) 119-143.
[6] G. Jeong, J. Bae, S. Jeong, C.H. Sohn, Y. Yoon, Development Trend of Perspective Methane Rocket Engines for Space Development, Journal of the Korean Society for Aeronautical & Space Sciences, 45 (2017) 558-565.
[7] H. Trinh, Liquid methane/oxygen injector study for potential future Mars ascent, 36th AIAA/ASME/SAE/ASEE Joint Propulsion Conference and Exhibit, 2000, pp. 3119.
[8] S. Choi, T.Y. Kim, H.K. Kim, I.-S. Jeung, J. Koo, O.C. Kwon, Combustion stability of gaseous CH4/O2 and H2/O2 coaxial jet flames in a single-element combustor, Energy, 132 (2017) 57-64.
[9] H. Burkhardt, M. Sippel, A. Herbertz, J. Klevanski, Kerosene vs. methane: a propellant tradeoff for reusable liquid booster stages, Journal of Spacecraft and Rockets, 41 (2004) 762-769.
[10] Y. Boué, P. Vinet, S. Magniant, T. Motomura, R. Blasi, J.-P. Dutheil, LOX/methane reusable rocket propulsion at reach with large scale demonstrators tested, Acta Astronautica, 152 (2018) 542-556.
[11] J. Applewhite, Energy Systems Divisions, 2011.
[12] A.S. Gohardani, J. Stanojev, A. Demairé, K. Anflo, M. Persson, N. Wingborg, C. Nilsson, Green space propulsion: Opportunities and prospects, Progress in Aerospace Sciences, 71 (2014) 128-149.
[13] S.-J. Kim, Y.-S. Lee, Y.-S. Ko, Research trend and histories of rocket engines using hydrogen peroxide and liquid methane as green propellants, Journal of the Korean Society of Propulsion Engineers, 14 (2010) 46-58.
[14] I. Remissa, H. Jabri, Y. Hairch, K. Toshtay, M. Atamanov, S. Azat, R. Amrousse, Propulsion Systems, Propellants, Green Propulsion Subsystems and their Applications: A Review, Eurasian Chemico-Technological Journal, 25 (2023) 3-19.
[15] R. Aggarwal, I. Patel, P. Sharma, Green propellant: A study, International Journal of

Latest Trends in Engineering and Technology, 6 (2015) 83-87.
[16] H.K. Kim, S. Choi, T.Y. Kim, O.C. Kwon, Studies on Flame Behaviors of GCH4/GO2 Coaxial Jets in a Model Combustor at Elevated Pressure, 52nd AIAA/SAE/ASEE Joint Propulsion Conference, 2016, pp. 4993.
[17] L.J. Coley, Initial design of a methane and oxygen rocket engine, Mississippi State University2010.
[18] R. Saini, S. Prakash, A. De, R. Yadav, Investigation of NOx in piloted stabilized methane-air diffusion flames using finite-rate and infinitely-fast chemistry based combustion models, Thermal Science and Engineering Progress, 5 (2018) 144-157.
[19] A. Iannetti, N. Girard, D. Tchou-Kien, C. Bonhomme, N. Ravier, E. Edeline, Prometheus, a LOX/LCH4 reusable rocket engine, Proceedings of the 7th European Conference for Aeronautics and Space Sciences (EUCASS), Milan, Italy, 2017, pp. 1-6.
[20] G.B. Ariemma, G. Sorrentino, R. Ragucci, M. de Joannon, P. Sabia, Ammonia/Methane combustion: stability and NOx emissions, Combustion and Flame, 241 (2022) 112071.
[21] D. Olson, W. Gardiner Jr, An evaluation of methane combustion mechanisms, The Journal of Physical Chemistry, 81 (1977) 2514-2519.
[22] S.R. Turns, Introduction to combustion, McGraw-Hill Companies New York, NY, USA1996.
[23] N.A. Adams, W. Schröder, R. Radespiel, O.J. Haidn, T. Sattelmayer, C. Stemmer, B. Weigand, Future Space-Transport-System Components Under High Thermal and Mechanical Loads: Results from the DFG Collaborative Research Center TRR40, Springer Nature2021.
[24] J.H. Morehart, A Survey of LNG-fueled Rocket Engine Development Activity-Non US, AIAA Propulsion and Energy 2021 Forum, 2021, pp. 3581.
[25] P. Simontacchi, R. Blasi, E. Edeline, S. Sagnier, N. Ravier, A. Espinosa-Ramos, J. Breteau, P. Altenhoefer, Prometheus: Precursor of new low-cost rocket engine family, 8th European Conference for Aeronautics and Space Sciences, EUCASS2019-FP0743, Madrid, Spain, 2019.
[26] T. Brown, M. Klem, P. McRight, Foundational Methane Propulsion Related Technology Efforts, and Challenges for Applications to Human Exploration Beyond Earth Orbit, 2016.
[27] A.K. JONNALAGADDA, A Methan engine for an improved access to space, (2022).
[28] R.J. Goldstein, Film cooling, Advances in heat transfer, Elsevier1971, pp. 321-379.
[29] J. Zhang, S. Zhang, W. Chunhua, T. Xiaoming, Recent advances in film cooling enhancement: A review, Chinese Journal of Aeronautics, 33 (2020) 1119-1136.
[30] J. Zuo, S. Zhang, D. Wei, L. Meng, J. Qin, W. Bao, O.J. Haidn, Effects of combustion on supersonic film cooling using gaseous hydrocarbon fuel as coolant, Aerospace Science and Technology, 106 (2020) 106202.
[31] P. Concio, S. D'Alessandro, M. Aranda-Rosales, D. Bianchi, F. Nasuti, J. Steelant, Low-order Modeling and Validation of Film Cooling in Liquid Rocket Combustion Chambers, Proceedings of Space Propulsion Conference 2022, 2022.
[32] S. Shine, S.S. Nidhi, Review on film cooling of liquid rocket engines, Propulsion and Power Research, 7 (2018) 1-18.

[33] W.M. Grisson, Liquid film cooling in rocket engines, United states air force, (1991).
[34] T. Kanda, G. Masuya, F. Ono, Y. Wakamatsu, Effect of film cooling/regenerative cooling on scramjet engine performances, Journal of Propulsion and Power, 10 (1994) 618-624.
[35] S. Luo, D. Xu, J. Song, J. Liu, A review of regenerative cooling technologies for scramjets, Applied Thermal Engineering, 190 (2021) 116754.
[36] S. Soller, R. Behr, F. Grauer, K. Claramunt, C. Dinescu, D. Fiorini, L. Peveroni, A. Simonini, S. General, C. Kirchberger, EXPERIMENTAL AND NUMERICAL INVESTIGATION OF LIQUID FILM COOLING IN SMALL ROCKET ENGINES, Proceedings of the 8th European Conference for Aeronautics and Space Sciences, 2019.
[37] X. Ma, B. Sun, T. Wang, D. Liu, Experimental investigation of the gas film cooling efficiency of the cylindrical holes near the injector region, International Journal of Thermal Sciences, 165 (2021) 106928.
[38] J.-X. Wang, W. Guo, K. Xiong, S.-N. Wang, Review of aerospace-oriented spray cooling technology, Progress in Aerospace Sciences, 116 (2020) 100635.
[39] J. Wang, L. Li, J. Li, F. Wu, C. Du, Numerical investigation on flow and heat transfer characteristics of vortex cooling in an actual film-cooled leading edge, Applied Thermal Engineering, 185 (2021) 115942.
[40] N. Cao, X. Li, Z. Wu, X. Luo, Effect of film hole geometry and blowing ratio on film cooling performance, Applied Thermal Engineering, 165 (2020) 114578.
[41] A.J. Banko, M.J. Benson, F.T. Davidson, W. Zia, A. Bordbar, C. Boyce, E.M. Veley, K.A. Thole, Effects of Surface Roughness on Three-Dimensional Flow Structure Within Shaped Film Cooling Holes, Turbo Expo: Power for Land, Sea, and Air, American Society of Mechanical Engineers, 2023, pp. V07AT12A023.
[42] Е. Галкина, С.Ю. Яблонская, ФИЛОСОФИЯ РУССКОГО КОСМИЗМА: ОТ ИДЕИ К ВОПЛОЩЕНИЮ (КЭ ЦИОЛКОВСКИЙ), Материалы Всероссийской (национальной) научно-практической конференции с международным участием, посвящённой дню основания Российского государственного аграрного университета-Московской сельскохозяйственной академии имени КА Тимирязева, 2023, pp. 302-306.
[43] X. Sun, G. Zhao, P. Jiang, W. Peng, J. Wang, Influence of hole geometry on film cooling effectiveness for a constant exit flow area, Applied Thermal Engineering, 130 (2018) 1404-1415.
[44] L. Ye, C.-l. Liu, H.-r. Zhu, J.-x. Luo, Experimental investigation on effect of cross-flow Reynolds number on film cooling effectiveness, AIAA Journal, 57 (2019) 4804-4818.
[45] M. Pizzarelli, F. Battista, Oxygen-methane rocket thrust chambers: Review of heat transfer experimental studies, Acta Astronautica, (2023).
[46] O.J. Haidn, M. Celano, M. Luo, C. Roth, S. Silvestri, N.A. Slavinskaya, On methane/oxygen combustion for rocket applications, Proceedings of the International Symposium on Innovation and Prospects of Liquid Propulsion Technology, Xi'an, China, 2016, pp. 4-6.
[47] M.P. Celano, S. Silvestri, C. Kirchberger, G. Schlieben, D.I. Suslov, O.J. Haidn, Gaseous Film Cooling Investigation in a Model Single Element GCH4-GOX Combustion

Chamber, Transactions of the Japan society for aeronautical and space sciences, aerospace technology Japan, 14 (2016) Pa_129-Pa_137.
[48] M. Celano, C. Kirchberger, Model Assessment for Gaseous Film Cooling in a Subscale Single Element CH4/GOX Combustion Chamber: Steady State Simulation and Validation, Space Propulsion, 2016.
[49] M.A. Keller, M.J. Kloker, H. Olivier, Influence of cooling-gas properties on film-cooling effectiveness in supersonic flow, Journal of Spacecraft and Rockets, 52 (2015) 1443-1455.
[50] A. Chemnitz, T. Sattelmayer, C. Roth, O. Haidn, Y. Daimon, R. Keller, P. Gerlinger, J. Zips, M. Pfitzner, Numerical investigation of reacting flow in a methane rocket combustor: turbulence modeling, Journal of Propulsion and Power, 34 (2018) 864-877.
[51] S. Zurbach, J.-L. Thomas, M. Sion, T. Kachler, L. Vingert, M. Habiballah, Recent advances on LOX/methane combustion for liquid rocket engine injector, 38th AIAA/ASME/SAE/ASEE Joint Propulsion Conference & Exhibit, 2002, pp. 4321.
[52] D. Martinez-Sanchis, A. Sternin, D. Balbuena-Silvestre, O.J. Haidn, Mixture fraction statistics in methane-oxygen turbulent combustion for space propulsion, Aerospace Science and Technology, 139 (2023) 108355.
[53] D. Martinez-Sanchis, A. Sternin, T. Santese, O.J. Haidn, The role of turbulence in the characteristic velocity and length of rocket combustors, Aerospace Science and Technology, 134 (2023) 108158.
[54] D. Martinez-Sanchis, A. Sternin, O. Haidn, A. Jocher, Effects of injection recess in methane turbulent combustion for space propulsion, Physics of Fluids, 36 (2024).
[55] D. Maestro, B. Cuenot, L. Selle, Large eddy simulation of combustion and heat transfer in a single element gch 4/gox rocket combustor, Flow, Turbulence and Combustion, 103 (2019) 699-730.
[56] S. Yu, X. Liu, X. Bai, A.M. Elbaz, W.L. Roberts, LES/PDF modeling of swirl-stabilized non-premixed methane/air flames with local extinction and re-ignition, Combustion and Flame, 219 (2020) 102-119.
[57] H. Zhang, A. Giusti, E. Mastorakos, LES/CMC modelling of ignition and flame propagation in a non-premixed methane jet, Proceedings of the Combustion Institute, 37 (2019) 2125-2132.
[58] P. Pal, S. Demir, P. Kundu, S. Som, Large-eddy simulations of methane-oxygen combustion in a rotating detonation rocket engine, AIAA Propulsion and Energy 2021 Forum, 2021, pp. 3642.
[59] S. Silvestri, C. Kirchberger, G. Schlieben, M.P. Celano, O. Haidn, Experimental and numerical investigation of a multi-injector gox-gch4 combustion chamber, Transactions of the Japan Society for Aeronautical and Space Sciences, Aerospace Technology Japan, 16 (2018) 374-381.
[60] K.A. Verma, K.M. Pandey, M. Ray, K.K. Sharma, The numerical analysis of combustion performance of a wedge shaped strut-based scramjet combustor, Thermal Science and Engineering Progress, 20 (2020) 100714.
[61] J. Wei, M. Ye, S. Zhang, J. Qin, O.J. Haidn, Modeling of a 7-elements GOX/GCH4 combustion chamber using RANS with Eddy-Dissipation Concept model, Aerospace Science and Technology, 99 (2020) 105762.

[62] N. Perakis, O.J. Haidn, D. Eiringhaus, D. Rahn, S. Zhang, Y. Daimon, S. Karl, T. Horchler, Qualitative and quantitative comparison of RANS simulation results for a 7-element GOX/GCH4 rocket combustor, 2018 Joint Propulsion Conference, 2018, pp. 4556.
[63] B. Betti, E. Martelli, F. Nasuti, Heat flux evaluation in oxygen/methane thrust chambers by RANS approach, 46th AIAA/ASME/SAE/ASEE Joint Propulsion Conference & Exhibit, 2010, pp. 6721.
[64] P. Concio, M. Tindaro Migliorino, D. Bianchi, F. Nasuti, Numerical Estimation of Nozzle Throat Heat Flux in Oxygen-Methane Rocket Engines, Journal of Propulsion and Power, 39 (2023) 71-83.
[65] P. Bradshaw, G.P. Huang, The law of the wall in turbulent flow, Proceedings of the Royal Society of London. Series A: Mathematical and Physical Sciences, 451 (1995) 165-188.
[66] J. Wei, S. Zhang, X. Zhou, C. Cheng, J. Qin, O.J. Haidn, Effects of near wall flow and non-equilibrium reaction coupling on heat flux prediction inside a 7-elements GOX/GCH4 combustion chamber, Applied Thermal Engineering, 204 (2022) 118021.
[67] A. Sternin, N. Perakis, M.P. Celano, O. Haidn, CFD-analysis of the effect of a cooling film on flow and heat transfer characteristics in a GCH4/GOX rocket combustion chamber, Space Propulsion 2018, (2018).
[68] D. Muto, Y. Daimon, H. Negishi, T. Shimizu, Wall modeling of turbulent methane/oxygen reacting flows for predicting heat transfer, International Journal of Heat and Fluid Flow, 87 (2021) 108755.
[69] F. Di Matteo, M. Venanzi, M. De Rosa, M. Onofri, Modelling and simulation of film cooling in liquid rocket engine propulsion systems, 48th AIAA/ASME/SAE/ASEE Joint Propulsion Conference & Exhibit, 2012, pp. 3908.
[70] T. Kitano, H. Iida, R. Kurose, Effect of chemical reactions of H2/O2 combustion gas on wall heat flux in a turbulent channel flow, Journal of Heat Transfer, 139 (2017) 044501.
[71] B. Betti, D. Bianchi, F. Nasuti, E. Martelli, Chemical reaction effects on heat loads of CH4/O2 and H2/O2 rockets, AIAA Journal, 54 (2016) 1693-1703.
[72] J. Zuo, S. Zhang, J. Qin, W. Bao, N. Cui, X. Liu, Effects of cracking reaction on supersonic film cooling using gaseous hydrocarbon fuel as coolant, Applied Thermal Engineering, 171 (2020) 115134.
[73] G.A. Marxman, Boundary-layer combustion in propulsion, Symposium (international) on Combustion, Elsevier, 1967, pp. 269-289.
[74] E.R.G. Eckert, Survey of boundary layer heat transfer at high velocities and high temperatures, Wright Air Development Center, Air Research and Development Command, United …1960.
[75] D. Altman, H. Wise, Effect of chemical reactions in the boundary layer on convective heat transfer, Journal of Jet Propulsion, 26 (1956) 256-258.
[76] O. Cabrit, F. Nicoud, Direct simulations for wall modeling of multicomponent reacting compressible turbulent flows, Physics of Fluids, 21 (2009).
[77] J. Liu, S. Zhang, J. Wei, O.J. Haidn, RANS based numerical simulation of a GCH4/GO2 rocket engine combustion chamber with film cooling and improvement of wall heat flux prediction, Applied Thermal Engineering, 219 (2023) 119544.

[78] J. Liu, S. Zhang, J. Wei, O.J. Haidn, Numerical study of film cooling in single-element injector gaseous CH4/O2 rocket engine with coupled wall function, AIP Advances, 14 (2024).
[79] N. Perakis, O.J. Haidn, Inverse heat transfer method applied to capacitively cooled rocket thrust chambers, International Journal of Heat and Mass Transfer, 131 (2019) 150-166.
[80] M.P. Celano, S. Silvestri, J. Pauw, N. Perakis, F. Schily, D. Suslov, O.J. Haidn, Heat flux evaluation methods for a single element heat-sink chamber, 6th European Conference of Aeronautics and Space Science, Krakow, Poland, 2015.
[81] N. Perakis, M.P. Celano, O.J. Haidn, Heat flux and temperature evaluation in a rectangular multi-element GOX/GCH4 combustion chamber using an inverse heat conduction method, 7th European Conference for Aerospace Sciences, 2017.
[82] N. Perakis, J. Strauß, O.J. Haidn, Heat flux evaluation in a multi-element CH4/O2 rocket combustor using an inverse heat transfer method, International Journal of Heat and Mass Transfer, 142 (2019) 118425.
[83] L. Vervisch, R. Hauguel, P. Domingo, M. Rullaud, Three facets of turbulent combustion modelling: DNS of premixed V-flame, LES of lifted nonpremixed flame and RANS of jet-flame, Journal of turbulence, 5 (2004) 004.
[84] F.F. Winter, N. Perakis, O.J. Haidn, Emission imaging and CFD simulation of a coaxial single-element GOX/GCH4 rocket combustor, 2018 Joint Propulsion Conference, 2018, pp. 4764.
[85] C.M. Roth, O.J. Haidn, A. Chemnitz, T. Sattelmayer, G. Frank, H. Müller, J. Zips, R. Keller, P.M. Gerlinger, D. Maestro, Numerical investigation of flow and combustion in a single element GCH4/GOx rocket combustor, 52nd AIAA/SAE/ASEE Joint Propulsion Conference, 2016, pp. 4995.
[86] P. Bradshaw, An introduction to turbulence and its measurement: thermodynamics and fluid mechanics series, Elsevier2013.
[87] N. Ashgriz, J. Mostaghimi, An introduction to computational fluid dynamics, Fluid flow handbook, 1 (2002) 1-49.
[88] A. Sternin, H. Ma, J. Liu, O. Haidn, M. Tajmar, Turbulence and Combustion and Film Prediction in Rocket Application via Parameter Adjustion, Model Variation and Deep Learning Method, Sonderforschungsbereich/Transregio.
[89] Y. Daimon, H. Negishi, S. Silvestri, O.J. Haidn, Conjugated combustion and heat transfer simulation for a 7 element gox/gch4 rocket combustor, 2018 Joint Propulsion Conference, 2018, pp. 4553.
[90] D. He, Y. Yu, Y. Kuang, C. Wang, Model Comparisons of Flow and Chemical Kinetic Mechanisms for Methane–Air Combustion for Engineering Applications, Applied Sciences, 11 (2021) 4107.
[91] H.-J. Kim, Y.-M. Kim, Numerical modeling for combustion processes of hybrid rocket engine, 37th Joint Propulsion Conference and Exhibit, 2001, pp. 4504.
[92] D. He, Y. Yu, Y. Kuang, C. Wang, Analysis of EDC constants for predictions of methane MILD combustion, Fuel, 324 (2022) 124542.
[93] A. Mardani, Optimization of the Eddy Dissipation Concept (EDC) model for turbulence-chemistry interactions under hot diluted combustion of CH4/H2, Fuel, 191

(2017) 114-129.
[94] G. Dong, Y. Huang, Y. Chen, Study of effects of different chemical reaction mechanisms on computation results for methane jet turbulence diffusion flame, Journal of Fuel Chemistry and Technology, 28 (2000) 49-54.
[95] Fluent 2022 R1 User`s Guide, Ansys Inc., USA, 2022.
[96] E.A. Spiegel, G. Veronis, On the Boussinesq approximation for a compressible fluid, Astrophysical Journal, vol. 131, p. 442, 131 (1960) 442.
[97] S. Ludescher, H. Olivier, Film Cooling in Rocket Nozzles, in: N.A. Adams, W. Schröder, R. Radespiel, O.J. Haidn, T. Sattelmayer, C. Stemmer, B. Weigand (Eds.) Future Space-Transport-System Components under High Thermal and Mechanical Loads: Results from the DFG Collaborative Research Center TRR40, Springer International Publishing, Cham, 2021, pp. 65-78.
[98] K. Javadi, Introducing film cooling uniformity coefficient, Heat Transfer Engineering, 39 (2018) 180-193.
[99] Y. Shan, X.-m. Tan, J.-z. Zhang, M.-m. Wang, Numerical study on flow and cooling characteristics for supersonic film cooling, Heat Transfer Engineering, 39 (2018) 1318-1330.
[100] D. Suslov, R. Arnold, O. Haidn, Investigation of film cooling efficiency in a high pressure subscale lox/h2 combustion chamber, 47th AIAA/ASME/SAE/ASEE Joint Propulsion Conference & Exhibit, 2011, pp. 5778.
[101] J.L. Rutledge, P.I. King, R. Rivir, Time Averaged Net Heat Flux Reduction for Unsteady Film Cooling, (2010).
[102] J. McCall, R. Branam, Effects of radial curvature on net heat flux reduction in a film-cooled rocket, 47th AIAA Aerospace Sciences Meeting including The New Horizons Forum and Aerospace Exposition, 2009, pp. 1586.
[103] J.L. Rutledge, P.I. King, R.B. Rivir, Influence of film cooling unsteadiness on turbine blade leading edge heat flux, (2012).
[104] D.R. Bartz, A simple equation for rapid estimation of rocket nozzle convective heat transfer coefficients, Jet Propul., 27 (1957) 49-51.

Appendix A

Original Journal Papers

The original peer-reviewed journal articles are attached here.

A.1 Paper 1

Jianing Liu, Silong Zhang, Jianfei Wei, Oskar J. Haidn

RANS Based Numerical Simulation of a GCH4/GO2 Rocket Engine Combustion Chamber with Film Cooling and Improvement of Wall Heat Flux Prediction

Contribution: My primary contributions encompass the numerical processing of experimental data, the establishment of the numerical framework employed in this study, the composition and refinement of the UDF file for the coupled wall function, the execution of numerical simulations, the comprehensive analysis and discussion of the simulation outcomes and the writing and proofreading of the manuscript.

Applied Thermal Engineering 219 (2023) 119544

Contents lists available at ScienceDirect

Applied Thermal Engineering

journal homepage: www.elsevier.com/locate/apthermeng

Research Paper

RANS based numerical simulation of a GCH4/GO2 rocket engine combustion chamber with film cooling and improvement of wall heat flux prediction

Jianing Liu [a], Silong Zhang [b,*], Jianfei Wei [b], Oskar J. Haidn [a]

[a] School of Engineering and Design, Department Mechanical Engineering, Technical University of Munich, Germany
[b] School of Energy Science and Engineering, Harbin Institute of Technology, PR China

ARTICLE INFO

Keywords:
Rocket engine
RANS
Film cooling
Heat transfer
Coupled wall function

ABSTRACT

Methane/Oxygen rocket engine is becoming one of the most promising rocket engines today due to its cost-effectiveness and reusability. In the design process of rocket engines, cooling system is a crucial part and film cooling is a very important method. The accurate prediction of heat transfer characteristics is crucial for the design and development of rocket engines using film cooling. In this paper, a numerical framework based on the Reynolds Averaged Navier-Stokes (RANS) method and the Eddy Dissipation Concept (EDC) reaction model is established, verified and applied to simulations of single- and multi-injector combustion chamber with film cooling. Besides, a single injector combustion experiment with film cooling is carried out to verify the numerical framework. The investigation indicates that flow and chemistry reactions near the wall coupled influence the wall heat load significantly, and the coupled wall function exploited by Direct Numerical Simulation (DNS) is modelled and embedded on the numerical frame in order to consider these coupling effects. The results of single injector chamber investigation show that by considering the chemical reactions near the wall the wall heat flux reduced 50% and agree much better to the experimental data, which indicates that coupled wall function is more effective at predicting wall heat flux than general wall functions in a chamber with film. In addition, the results also denote that the coupled wall function only acts in the near-wall region and has no effect on the main flow. Furthermore, after being verified in the single injector combustion chamber experiment, the numerical framework is applied to a multiple-injector case. The results indicate that the wall heat flux in multi-injector combustion chamber is 75% lower than the general wall functions, Afterwards, the effect of the film on the chemical enthalpy term near the wall, as well as the coupling effect of the turbulent flow and the temperature gradient near the wall are discussed. Finally, the analysis of the vorticity in the multi-injector chamber shows that the film weakens the vorticity in the front section of the combustion chamber, and subsequently affects the expansion of the flame.

1. Introduction

With the development of space technology, the space propulsion field is focusing on finding easily accessible, reusable, and cost-effective fuels. Using methane as a rocket propellant provides a higher specific impulse than kerosene, has low tendency to coke and has superior cooling capacity [1–3], and methane is easier to store and transport than hydrogen [4]. In addition, the methane rocket engine also has the advantages of simple design, reusability and low production costs [5,6], these advantages make methane becoming a popular propellant in the aerospace propulsion field [7]. In the design process of methane rocket engines, the cooling system is one of the most critical aspects, and the rational organization of the combustion chamber cooling is important to protect the engine walls, improve engine reusability and enhance engine performance. Among the many cooling methods, film cooling is gradually gaining more attention due to its high cooling efficiency, simple structure design and easy storage of coolant [8–11].

Numerous experimental studies have been carried out on the turbulent and heat transfer characteristics of GCH4/GO2 rocket engine combustion chambers [12–14]. Except for experimental studies, numerical simulations are gradually becoming the main method for investigating the turbulence and combustion in combustion chamber. Many numerical simulations based on the Reynolds Averaged Navier-

* Corresponding author at: No. 92, West Da-Zhi Street, Harbin, Heilongjiang 150001, PR China.
E-mail address: zhangsilong@hit.edu.cn (S. Zhang).

https://doi.org/10.1016/j.applthermaleng.2022.119544
Received 4 July 2022; Received in revised form 16 September 2022; Accepted 20 October 2022
Available online 25 October 2022

Nomenclature

A	surface area, m^2
C_p	specific heat capacity, J/(kg·K)
C_μ	turbulent model constant, 0.09
F, G	functions
H	specific enthalpy of the mixture, J/kg
$h^0_{f,k}$	standard formation enthalpy of the species k, J/kg
h^s_k	specific sensible enthalpy of the species k, J/kg
k	turbulent kinetic energy, J/kg
$\dot{m}_{CH_4}$	the mass flow rate of methane, g/s
$\dot{m}_{O_2}$	the mass flow rate of oxygen, g/s
$\dot{m}_{Film}$	the mass flow rate of film, g/s
p	pressure, Pa
Pr	Prandtl number
Pr_t	turbulent Prandtl number
Q_c	Volume heat release rate, $W/(m^3{\cdot}s)$
$\boldsymbol{q}$	molecular heat flux vector, W/m^2
q_w	wall heat flux, W/m^2
ROF	mixture ratio
R_F	film mass flow fraction to total fuel
r	radial coordinate, m
Sc_t	turbulent Schmidt number
T	temperature, K
T^+	dimensionless wall temperature
T_c	temperature at the center of the first layer cells, K
t	time, s
u	velocity, m/s
u^+	dimensionless wall velocity,u/u_τ
u^*	improved dimensionless wall velocity, $u_p u_k/u_\tau^2$
u_p	velocity parallel to the wall, m/s
u_k	velocity unit, $C_\mu^{1/4}k^{1/2}$, m/s
u_τ	friction velocity, $\sqrt{\tau_w/\rho}$, m/s
V_k	diffusion velocity of species k, m/s
V_r	radial velocity, m/s
$\dot{\omega}_k$	Net production rate of species k, $kg/(m^3{\cdot}s)$
x, y, z	Cartesian coordinate, m
Y_k	mass fraction of species k
y^+	dimensionless wall distance
λ	Thermal conductivity, W/(m·K)
μ	molecular viscosity, Pa·s
ρ	density, kg/m^3
τ_w	wall shear stress, Pa

Subscripts

cc	combustion chamber
t	turbulent
th	throat
k	species k
w	wall

Stokes (RANS) method have been carried out [15–18]. The investigations show that while the numerical framework based on the RANS method provides a good prediction of the turbulent flow and chemical reaction process in the combustion chamber, but the simulated value of wall heat flux is difficult to agree with the experimental results [19,20]. In addition to the RANS-based method, several studies chose to operate the combustion chamber simulation based on the Low Reynolds Number models such as the Large Eddy Simulation (LES) method [21–24]. The results show that even though the Low Reynolds Number models are able to capture the flow and heat transfer characteristics near the wall relatively well, the study by S. Kawai and J. Larsson [25] has demonstrated that the viscous length scale of the inner layer of the combustion chamber is only around 1 μm, thus the simulation near the 3D wall using the Low Reynolds Number method requires a very fine mesh, which significantly increases the computational cost. Therefore, the RANS method is still the easiest and most efficient way to simulate the combustion and heat transfer characteristics in a GCH4/GO2 combustion chamber, but only the wall treatment needs to be improved.

In terms of film cooling, many experiments [24,26,27]and numerical simulations [28–30] have also been carried out. However, research on film cooling has mainly focused on the effect of geometry and film inlet parameters, but little attention has been paid to the influence of the film itself on the prediction of chamber wall heat flux. For rocket engine chambers, the wall heat transfer is one of the main factors of researches and design, especially for chambers where film cooling is considered. However, according to current simulation studies of the heat transfer characteristics of GCH4/GO2 chamber walls based on the RANS method, the numerical results of chamber wall heat flux are often higher than the experimental values [31,32].

Numerical simulations of a GCH4/GO2 combustion chamber by J. Wei et al. in the reference [33] and D. Muto et al. in the reference [34] show that the over-prediction of wall heat flow in the simulations based on RANS is caused by that the general used wall model is derived based on unreacted single-component flow, which does not consider the effect of chemical reactions near the wall. And in related studies, it has been concluded that chemical reactions have a significant effect on the wall heat flux, whether or not including film cooling [35–37]. To solve this problem, the coupled wall function is proposed and modelled by O. Cabrit and F. Nicoud in the reference [38] developed by Direct Numerical Simulation(DNS) method which considers the chemical effects near the wall and the computational cost of using coupled wall function is extremely low.

In summary, according to current studies, the RANS-based numerical framework is still the most convenient and least computational expensive method for rocket engine analysis. However, even though it is proved that RANS-based methods are able to simulate the flow and combustion process of the GCH4/GO2 combustion chamber, the wall treatment still requires improved because existing research suggests that RANS-based frameworks with general wall functions are not able to accurately predict the wall heat flux. Although the coupled wall function is found to be able to address this problem in a chamber without film by considering the chemical reactions near the wall, few research attempts to apply it to the combustion chambers with film cooling, or tries to develop a RANS-based numerical framework that can accurately predict the wall heat flux. And in contrast to that, the existence of film has a significant impact on the flow and chemical reactions in the near-wall region, and accurate prediction of the wall heat flux is essential in the chamber with film simulations.

Based on the coupled wall function proposed in reference [38] and the RANS method, this paper aims to establish a numerical framework, which considers the chemical reactions near the wall, in order to predict the turbulent combustion and wall heat transfer characteristics in a GCH4/GO2 combustion chamber with film cooling more accurately. Then, a single injector GCH4/GO2 combustion chamber with film experiment is carried out and its results are used for validating the numerical framework. After being validated, the framework is utilized to a seven coaxial injectors combustion chamber with film simulation, in which turbulence and combustion are more complex but closer to realistic conditions. The results show that the numerical simulation using coupled wall function in a single-injector chamber agrees better with the experimental values than general wall functions, which proves the numerical approach established in this paper can solve the

overestimated heat flux prediction problem in the RANS-based methods. Finally, the combustion and wall heat transfer characteristics in a multi-injector chamber with film are also predicted and the effect of film is analyzed.

2. Reference experiment

2.1. Experiment Setup

In this section, the reference experimental setup for methane/oxygen ignition combustion in a single-element chamber with film cooling is described, along with the correction process of the experimental results by the inverse iterative method proposed and validated by N. Perakis et al. [37]. Experiments in this paper were carried out on a single injector square heat-sink rocket combustion chamber testbench at the Technical University of Munich(TUM) [39]. The experimental combustion chamber was divided into two segments, the main geometrical parameters are shown in Table 1 and shown schematically in Fig. 1. Several 0.5 mm diameter T-type thermocouples were embedded in a series of uniformly distributed axial points at distances of 1 mm, 2 mm and 3 mm respectively from the upper wall surface. And a series of pressure sensors were arranged at corresponding locations on the side-wall surfaces to measure the pressure decay process in the combustion chamber, more details of the experimental setup can be found in the references [39,40].

In terms of film cooling study, a film injector was settled on the top of the injection plate, the schematic diagram is shown in Fig. 2. The film injector has an inlet width of 11 mm and a thickness of approximately 0.25 mm. The coolant injects along the upper surface inside the combustion chamber, covering around 90% of the chamber wall. The experimental operating conditions are referred to Table 2.

Considering the limitations of a heat-sink combustion chamber, a burning time of approximately 3 *s* was chosen at the steady-state combustion to measure the heat load. Also, to weaken the influence of the ignition process on the temperature measurement, the ignition duration was controlled to 300 *ms*. Fig. 3 shows a typical combustion experimental pressure and temperature output curves. As the combustion is a transient process, three time points were extracted, the start time t_0, the evaluation time t_1 and the shutdown time t_2. The parameters of the chamber at the start of the experiment are obtained at t_0 and at the end are obtained at t_2. Furthermore, since we mainly focus on the steady situation when the equilibrium state is reached, so the evaluation time t_1 is chosen as the time point at which the equilibrium state is reached.

2.2. *Inverse heat transfer method*

As described in the previous part, the thermocouples were configured 1–3 mm from the chamber wall, the reason for this arrangement is that the hot gas environment in the combustion chamber is harsh so it is difficult to measure the temperature of the hot gas directly. Hence, this arrangement may result in inaccurate temperature measurements. Unlike other testbenches using external water or other media cooling, in which the heat flux can be simply calculated from the enthalpy difference between the incoming and outgoing coolant, the temperature of a heat-sink combustion chamber is not a static parameter during combustion and therefore a transient inverse heat transfer calculation

Table 1
Main geometrical parameters of testbench.

Geometry	Unit	Value
Chamber length	(mm)	290
Chamber width	(mm)	12
Chamber height	(mm)	12
Throat height	(mm)	4.8
Contraction ratio A_{cc}/A_{th}	(-)	2.5

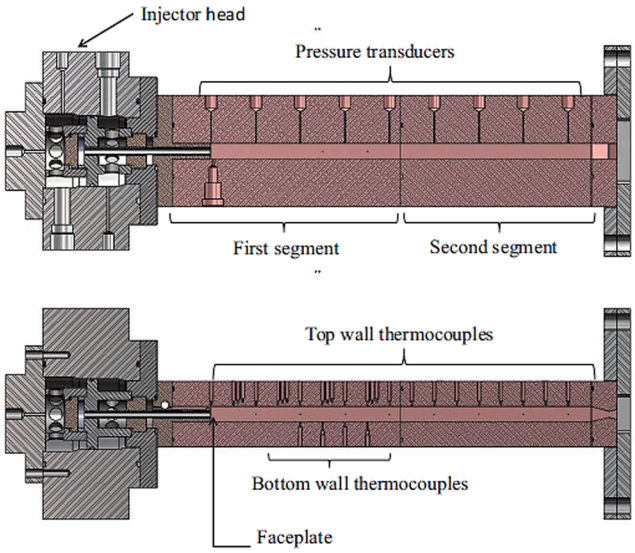

Fig. 1. Side view (top) and top view (bottom) of the single element chamber section.

method is applied to calculate the transient heat flux profile and distribution on the wall of the chamber.

This inversion algorithm was proposed and validated by N. Perakis et al. in the reference [41], and its iterative procedure is shown in Fig. 4. An initial heat flux is firstly assumed and the initial temperature T_0 is used as the initial condition for the temperature field, since the temperature field in the computational domain at this time point is known as the ambient temperature. A direct numerical solver *RoqFITT* developed with a 3D finite difference (FD) code is used to iterate[42,43], and the residuals are calculated by comparing the measured point values with the experimentally obtained values in each iteration, after the residuals converge, a more accurate temperature distribution and wall heat flux are gained. Fig. 5 shows the wall heat flux calculated by inverse method comparing with the experimental values, the difference is obvious, which also proves the effectiveness of inverse method. More details of the calculation and validation process of the inverse method can be found in the references [41,44]. The thermodynamic experimental data used for validating the numerical framework afterwards in this paper have been optimally modified by the inverse method.

3. Numerical setup

This section presents the development process of the numerical simulation framework corresponding to the experiment, including the establishment of mesh, the used physical and mathematical models, the definition of the boundary conditions, and the mesh convergence study.

3.1. Physical model and mesh generation

For the single-element combustion chamber, the physical model used for the simulation is built based on the experimental bench described in section 2. Since we are mainly concerned about the combustion and heat transfer characteristics within the chamber, only the chamber and the nozzle mesh are built as the calculation domain, while a 50 mm long fuel injection pipe and a 100 mm long oxygen injection pipe are also retained to ensure the full development of the fuel and oxygen. The geometrical configuration of the computational domain is shown in Fig. 6(a), and the geometrical parameters of the combustion chamber are referred in Table 3. A mesh has been generated based on the geometrical configuration, as shown in Fig. 6(b). In order to improve the efficiency of the calculation, only 1/4 of the chamber is preserved, and symmetric boundary conditions are applied for the truncated sections. The mesh

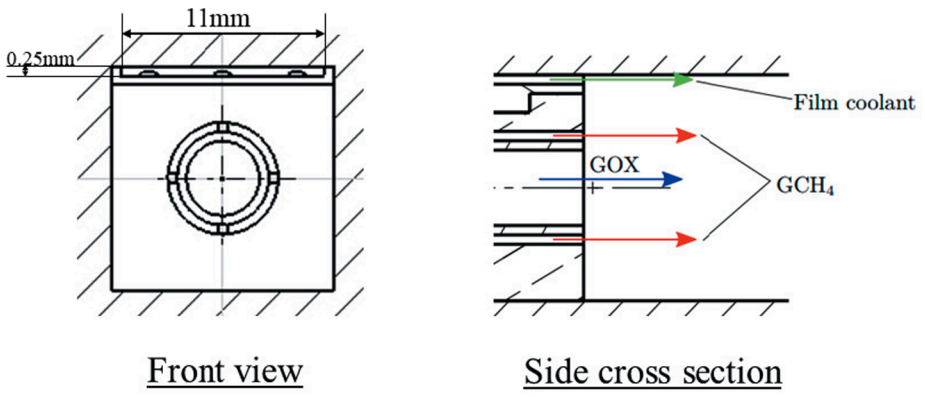

Fig. 2. Cross section of single element combustion chamber and film injector.

Table 2
Operating conditions of combustion chamber.

p [bar]	$\dot{m}_{CH_4}$ [g/s]	$\dot{m}_{O_2}$ [g/s]	ROF[-]	$\dot{m}_{Film}$ [g/s]	R_F [%]
0.968	7.7	24.1	3.13	2.2	22.2

was refined in the corresponding shear layer area, and the thickness of the mesh close to the chamber wall is controlled to keep the wall y^+ at around 30.

For the multi-element combustion chamber, the physical model is built with reference to the experimental equipment of the Institute of

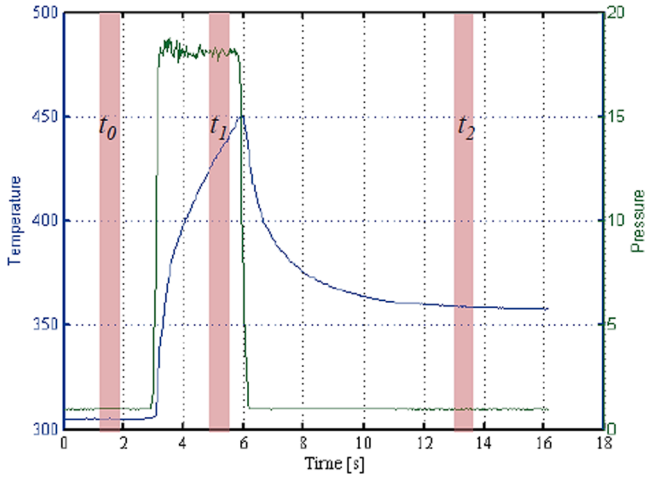

Fig. 3. Example of pressure–temperature output curve and time points for combustion experiments.

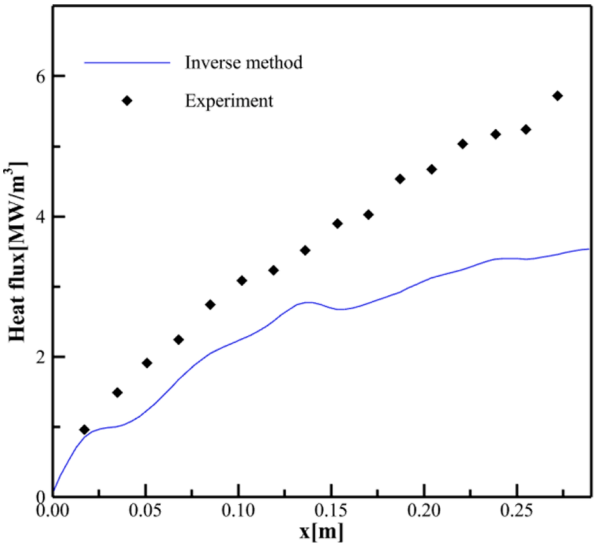

Fig. 5. Experimental value and calculated value of wall heat flux.

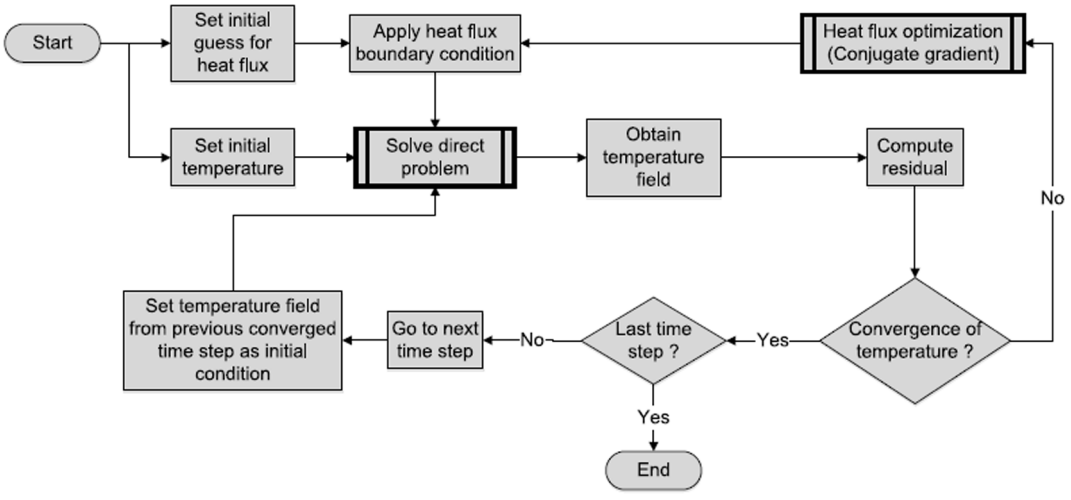

Fig. 4. Iterative algorithm for inverse heat transfer.

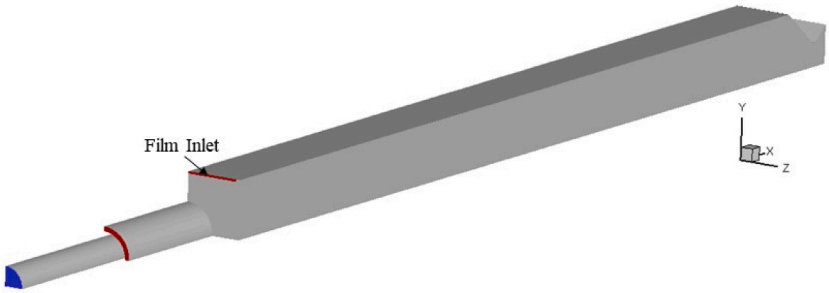

(a) Single element combustion chamber geometry

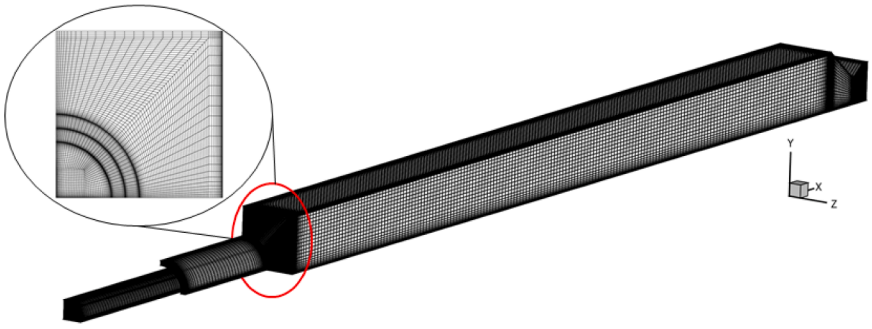

(b) Single element combustion chamber mesh

Fig. 6. Geometry and mesh of single element combustion chamber.

Table 3
Boundary conditions of single element chamber.

Boundary	Type	Specific	Temperature
GOX inlet	Mass flow inlet	0.006025 kg/s	268 K
GCH4 inlet	Mass flow inlet	0.001925 kg/s	275 K
Film inlet	Mass flow inlet	0.0011 kg/s	266 K
Outlet	Pressure outlet	0.968 bar	300 K
Injector wall & faceplate	Non-slip wall	–	Adiabatic
Chamber wall	Non-slip wall	–	Polynomial fitting
Nozzle wall	Non-slip wall	–	400 K
Symmetric face	Symmetry	–	–

Space Propulsion at the TUM [45], the original experiment does not include film cooling, and the film injection port is artificially set in the injection plate adjacent to the wall in the simulation process. The geometry is shown in Fig. 7(a), and again 50 mm of fuel and oxygen injection pipe are reserved to ensure fully developed flows. The mesh constructed on the basis of the 7-element chamber geometry is shown in Fig. 7(b), the wall y^+ values are still being controlled around 30 and mesh in the shear layer region is refined. Finally, in order to reduce the computational cost, only 1/6 of the combustion chamber is retained, and the mesh density at the nozzle was reduced appropriately, as our major focus is on the combustion chamber section.

3.2. *Numerical* ***model and boundary conditions***

Earlier studies have verified that RANS-based numerical models can simulate turbulence and combustion in rocket engine combustion chambers very well at a much lower computational cost than LES and DNS [31,45–47].In addition, researchers have also demonstrated that, the standard $k-\varepsilon$ model can be used to predict mixing processes with acceptable accuracy at a low computational cost[17,30]. Furthermore, studies also reveal that it was reasonable to treat the methane combustion process in the chamber as finite-rate reactions and use the eddy dissipation concept (EDC) model as a reaction model[48]. The chemical reaction mechanism uses in this paper is a 14 species and 18 reactions mechanism proposed by Dong Gang et al. [49]. And in the reference [49], a validation of the chemical mechanism is also given by comparing the experiment data with the PDF simulation results. Fig. 8 shows velocity distribution of the flow of the cross-section in the region with the strongest turbulent and chemical interactions, the simulation velocity values agree well with the experimental data, which indicates that the mechanism is suitable for calculating methane combustion.

For the single-element chamber, both the turbulent Prandtl number and turbulent Schmidt number are set to 0.7, this value is determined by experiment. And for the multi-element chamber, these two numbers are set to 0.85, the value is determined from experience in previous multi-element chamber simulations because of the absence of relevant experiments. Finally, regarding the method of the wall treatment, the coupled wall function is embedded in the Ansys Fluent software through the UDF approach to improve the prediction of wall heat transfer, the derivation and modelling process of the coupled wall function will be presented briefly in the next section, and the enhanced wall function is used as a control group.

The boundary conditions for the single- and seven-element combustion chambers are presented in Table 3 and Table 4, respectively. The composition of the film coolant is methane the same as fuel. For the upper wall of the chamber, the temperature distribution is given as the initial boundary condition, which was obtained by fitting and discretizing the experimental data. It is also to be noted that in the nozzle section, a constant wall temperature is given, this is because there is no thermocouple at the nozzle part in the experiment, but since we mainly focus on the wall heat flux of the chamber section, it is acceptable to set the temperature of nozzle as constant, and the value is determined by the continuity with the wall temperature of the chamber section.

3.3. ***Mesh*** *convergence* ***study***

In order to verify the sensitivity of the calculation results to the change of mesh density, the mesh independence is verified for single- and multi-element combustion chambers using five meshes with different degrees of sparsity respectively. The number of grids for the

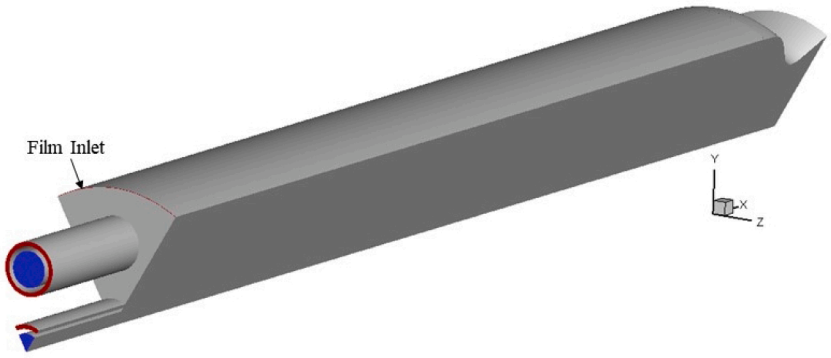

(a) Multiple elements combustion chamber geometry

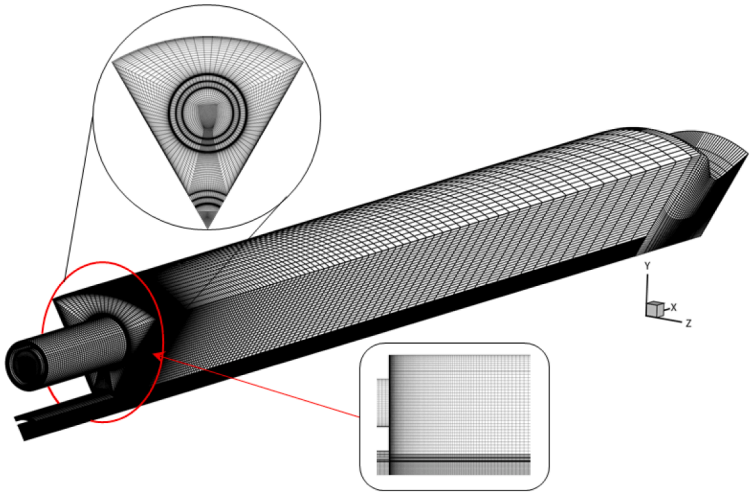

(b) Multiple elements combustion chamber mesh

Fig. 7. Geometry and mesh of multiple elements combustion chamber.

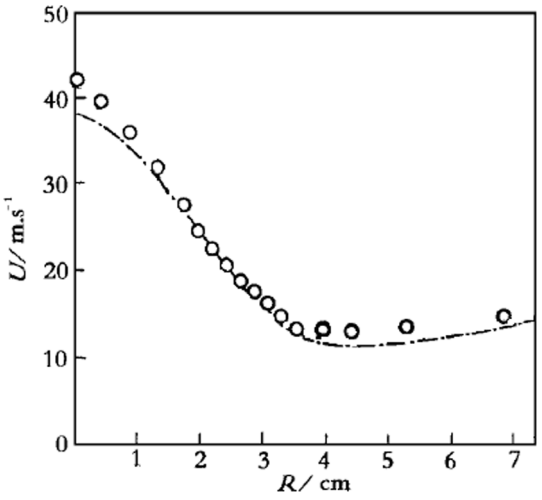

Fig. 8. Distribution of velocity field (○- experiment; — • — –14species, 18 reactions mechanism).

single element chamber has increased from the coarsest 378,952 to the finest 5,832,214, and for multiple elements chamber are from 483,630 to 6,122,580. Also, to ensure the validity of the wall functions, the wall y^+ values are adjusted to remain at around 30 after each mesh refinement.

Table 4
Boundary conditions of multiple elements chamber.

Boundary	Type	Specific	Temperature
GOX inlet	Mass flow inlet	0.0301 kg/s	259.4 K
GCH4 inlet	Mass flow inlet	0.001143 kg/s	237.6 K
Film inlet	Mass flow inlet	0.001333 kg/s	237.6 K
Outlet	Pressure outlet	1.01325 bar	300 K
Injector wall & faceplate	Non-slip wall	–	Adiabatic
Chamber wall	Non-slip wall	–	Polynomial fitting
Nozzle wall	Non-slip wall	–	412 K
Symmetric face	Symmetry	–	–

Fig. 9 and Fig. 10 demonstrate the average temperature and flow velocity at the centerline of the combustion chamber and the average heat flux distribution on the upper wall with different numbers of grid. As can be seen in Fig. 9, for single element chamber, after the grid number reaches approximately 1.73 million, the parameters within the combustion chamber hardly change anymore as the mesh is refined, whereas for multiple elements chamber this number is approximately 2.46 million according to Fig. 10. In summary, considering the efficiency and accuracy of the numerical calculation, a grid number of 1.73 million and 2.46 million are selected respectively for the single- and multi-element chamber simulation in this paper.

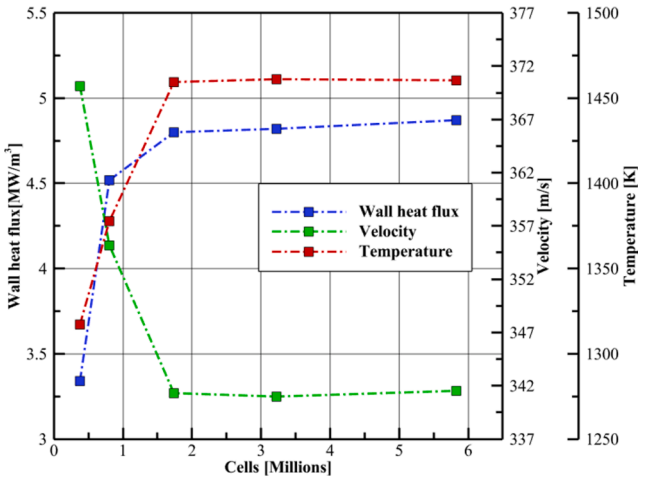

Fig. 9. Variation of parameters of single element chamber with the number of grids.

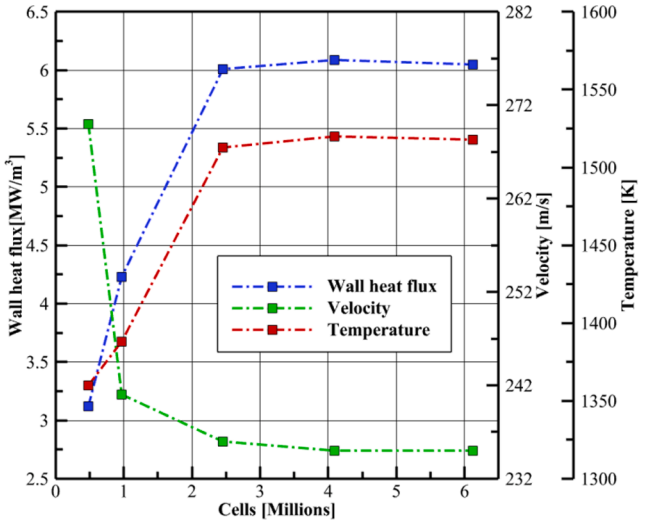

Fig. 10. Variation of parameters of multiple elements chamber with the number of grids.

4. Theory and application of coupled wall function

The coupled wall function has been firstly derived and embedded in a numerical framework based on the RANS method through UDF by J. Wei et al. [33]. This section will briefly describe the modelling process and since this paper mainly focus on the case with film cooling, the possible influence of film cooling on the application of the coupled wall function in a methane/oxygen combustion chamber is discussed.

Cabrit. O and Nicoud. F proposed and modelled the coupled wall function based on numerical experimental results of multicomponent reactive flows [38]. For the viscous layer of general turbulent flows, if we retain the vertical wall component of the diffusive flux only, and Reynolds time average the momentum and energy equations, then moving the remaining terms to the right-hand side of the equation, we have:

$$\frac{\partial \tau_w}{\partial y} = F \tag{4-1}$$

$$\frac{\partial q_w}{\partial y} = G \tag{4-2}$$

Eq. (4–1) and (4–2) are the basis for all wall functions. If the function $F(y)$ and $G(y)$ on the right side of the equations can be known, then the relationship formulas of the wall shear stress τ_w and the wall heat flow q_w can be calculated by integrating y along the path in the boundary layer. These formulas are called wall functions. The general wall functions usually assume that $F = G = 0$, and this assumption is based on a reaction-free flow which does not consider the effects of chemical reactions. For the reaction flows, we still assume the collisions between molecules are inelastic, so the chemical reaction should have no direct influence on the momentum Eq. (4–1), but the energy equation should include an additional term, then the energy equation is reformed as follow:

$$\rho \frac{dH}{dt} = -\nabla \cdot \boldsymbol{q} \tag{4-3}$$

Faver time averaging the Eq. (4–3), while the transient term can be omitted because we are concerned about the steady problem, and since the gradient of the parameter in the vertical direction varies much more than the other two directions within the near wall region, so only the y-direction derivatives are retained, and finally the expression for the wall heat flux is obtained:

$$\frac{\partial \overline{q_w}}{\partial y} = \frac{\partial}{\partial y}\left(\overline{\rho}\widetilde{v''h_s''} + \overline{\rho}\sum_k \widetilde{v''Y_k''}h_{f,k}^0 - \overline{\lambda}\frac{\overline{dT}}{dy} + \overline{\rho}\sum_k (h_k \widetilde{Y_k V_{k,y}})\right) \tag{4-4}$$

According to the DNS simulation results of Cabrit and Nicoud in the reference [38] about the proportion of terms on the right side of Eq. (4–4), the latter two terms can be neglected in the logarithmic region of the turbulent boundary layer. Thus, the first two terms on the right side of Eq. (4–4) can be modelled based on the Boussinesq vortex viscosity assumption, then an explicit expression of coupled wall function used to calculate the wall heat flux is finally obtained:

$$\overline{q_w} = -\mu_t\left(\frac{C_P}{Pr_t} + \frac{1}{Sc_t}\sum_k \frac{d\overline{Y_k}}{d\overline{T}}h_{f,k}^0\right)\frac{d\overline{T}}{dy} \tag{4-5}$$

The second term on the right side of Eq. (4–5) is the chemical enthalpy term, which is the key to the ability of the coupled wall function to improve wall heat flux prediction, it demonstrates the wall heat flux caused by the movement of chemical reaction equilibrium. Although Eq. (4–5) has a compact mathematical form and clear physical meaning, in order to embed it into commercial software such as Ansys Fluent by UDF, further transformation is still needed. Cabrit and Nicoud give a convenient form for implementing the coupled wall function by introducing T^+ [38]:

$$T^+ = K(Pr) + \frac{\alpha}{B_q}u^+ \tag{4-6}$$

where $K(Pr)$ is a constant obtained by least-squares approximation of another equation and depending on the Prandtl number Pr, and the coefficient in front of u^+ can be written as:

$$\frac{\alpha}{B_q} = \frac{C_P}{\frac{C_P}{Pr_t} + \frac{1}{Sc_t}\sum_k \frac{d\overline{Y_k}}{d\overline{T}}h_{f,k}^0} \tag{4-7}$$

The parameters α and B_q are the coefficients in the process of computing the ratio between the wall heat flux q_w and the wall shear stress τ_w, where:

$$\alpha = \frac{C_p B_q}{\frac{C_p}{Pr_t} + \frac{1}{Sc_{t,k}}\sum_k \frac{W_k}{W}\frac{d\overline{X_k}}{d\overline{T}}\Big|_{eq}\Delta h_{f,k}^0} \tag{4-7a}$$

$$B_q = \frac{T_\tau}{T_w} = \frac{\overline{q_w}}{\overline{\rho_w} C_p u_\tau T_w} \tag{4-7b}$$

and X_k is the molar fractions of species k, W_k is the atomic weight of species k, $W = \sum_k X_k W_k$ is the mean molecular weight of the mixture. When $B_q \to 0$ (isothermal case) and $\alpha \to Pr_t B_q$ (no chemistry), the Eq. (4–6) will tend to the classical logarithmic formulation.

Then using the T^+ calculated in Eq. (4–6), the wall heat flow can be explicitly expressed as:

$$q_w = -\frac{\rho C_P u^*}{T^+}(T_c - T_w) \tag{4-8}$$

Finally, Eq. (4–8) can be conveniently embedded into the previously mentioned numerical model using UDF.

Finally, an assumption needs to be further made, which is that the fluid in the near-wall region is at the chemical equilibrium state. This assumption is a compromise in order to compute Eq. (4–7), since the derivative term depends on not only the temperature but the pressure and mixture composition and these variables are almost impossible to be imported into the UDF in a non-equilibrium fluid. Subsequently, the mechanism and applicability of the coupled wall function to the specific GCH4/GO2 combustion chamber with film cooling investigated in this paper need to be discussed. According to the research of J. Wei on a multi-element combustion chamber without film [33], the heat flow values calculated from the coupled wall function are higher than general wall functions at a circumferential angle of 0°. This phenomenon is contrary to the expectation that the coupled wall function reduces the predicted value of heat flux, the reason is that the study object is confined to a two-dimensional situation and ignores the enormous influence of three-dimensional effects on the distribution of components.

For the simple 2D case, when the hot gas approaches the cooler wall, its chemical equilibrium will move to the direction of a lower total chemical enthalpy, and such movement in turn causes further exotherm of the gas, so that the chemical enthalpy of the mixture is negative along the *y*-direction, which will lead to an increase in the heat flux calculated by Eq. (4–5). However, in the case where film cooling is included, the temperature of film is low, which results in a lower gas temperature near the wall, and at the same time the substance used as coolant, methane, can itself be used as a fuel for exothermic chemical reactions, so the chemical enthalpy change due to the movement in chemical equilibrium is different, which is one of the effects of the film on the predicted wall heat flux using the coupled wall function.

For the three-dimensional case closed to the real combustion chamber, assuming the density of the gas mixture near the wall is constant, Eq. (4–8) can be rewritten in the form of column coordinates:

$$\sum_k \frac{d\overline{Y_k}}{dy} h^0_{f,k} = \frac{1}{\overline{\rho}} \sum_k \frac{d\overline{\rho Y_k}}{dr} h^0_{f,k} = \frac{1}{\overline{\rho}} \sum_k \frac{d\overline{\rho_k}}{dt} \frac{dt}{dr} h^0_{f,k} = \frac{\sum_k h^0_{f,k} \dot{\omega}_k}{\overline{\rho} V_r} = \frac{Q_C}{\overline{\rho} V_r} \tag{4-9}$$

from the Eq. (4–9), it can be seen that the direction of the radial velocity V_r will change the positive and negative sides of the equation, and then the direction of the enthalpy term. Thus, from a 3D perspective, the negative or positive radial velocity adjacent to the wall is highly relevant to the prediction of the wall heat flux. The injection of film along the wall changes the flow characteristics, and the radial velocity is different, which eventually leads to a different direction of action of chemical enthalpy term, then ultimately has an impact on the prediction of wall heat flux.

In addition to the effect on flow characteristics, we also should not limit our focus to the local heat flux at a particular angle or a particular region, but the net effect of the enthalpy term on the entire chamber wall. Due to the injection of the film, the mass fraction gradient of each component in the near wall region is also very different from the condition without film cooling, which changes the inner product of the enthalpy and the mass fraction gradient. This change means that the action direction of chemical enthalpy and the temperature gradient may be the same or opposite, so the chemical enthalpy term has a different effect on the predicted heat flux value.

In conclusion, in a combustion chamber with film cooling, the film affects the temperature gradient, radial velocity, chemical equilibrium movement and mass fraction of each component at the same time, and their influence on the wall heat flux is not independent from each other. Therefore, the prediction of wall heat flux in the combustion chamber with film cooling and the influence of various factors need to be further investigated.

5. Results and discussion

5.1. *Verification* ***of coupled wall function in a single element combustion chamber with film cooling***

Fig. 11 shows the pressure and temperature distribution curves with time from experiments. In Fig. 11, it is visible that the pressure gradually decreases as the sensor approaches the exit of the chamber, whereas the temperature gradually increases, which corresponds to the combustion pattern within the rocket combustion chamber. In addition, the experimental time of 4.2 *s*-5.9 *s* was chosen as the evaluation time mentioned in section 3, at which point the combustion reaches equilibrium, and the experimental parameters obtained at this time were chosen to validate the numerical model.

Afterwards, a numerical simulation case for validation is built based on the mentioned single element combustion chamber mesh. Fig. 12 shows the pressure distribution along the axial direction of the combustion chamber with enhanced wall function, coupled wall function, and the experimental values. It can be observed that the obtained pressure distributions using the enhanced wall function and the coupled wall function are very close, the error mainly comes from the inconsistent requirements on the first layer mesh thickness of the two wall functions. Since the *y*-plus is set to around 30 to meet the requires of the coupled wall function, and for comparison purpose the same mesh is used in the control case using the enhanced wall function, however, the accuracy of the calculation using the enhanced wall function increases as the wall *y*-plus decreases, and the best accuracy is obtained while *y*-plus approaches 1. Such results are also consistent with the corollary that the coupled wall function has no direct effect on the momentum equation. Furthermore, the pressure distribution obtained from the numerical simulations is in general agreement with the experimental data with an error<1%. Thus, it can be concluded that the RANS-based numerical framework proposed in this article is capable of simulating the turbulent characteristics of the entire combustion chamber.

The wall heat flux distribution along the axial direction is shown in Fig. 13. As can be seen from Fig. 13, even though the pressure tends to be the same throughout the chamber, the wall heat flux using enhanced wall function is about twice as high as the wall heat flow obtained from the experiment, and it can also be seen that the use of coupled wall function weakens this overprediction very well, especially in the fully developed section of the combustion chamber(x > 100 mm). At the same time, Fig. 13 indicates that the wall heat flux obtained using coupled wall function agrees well with the experimental values corrected by the inverse method. Even though there are slight errors in the section x > 145 mm to x < 220 mm, the errors are still within the range allowed by the inverse method (approx. 12%-16%).

Table 5 gives the area averages of the mass fraction gradients of the main components near the wall, which can be calculated by Eq. (5–1), and the third column of the table gives the corresponding enthalpies of each component. The second and third columns in Table 5 have an inner product value of approximately 1.6×10^8 J/kg, which is positive, indicating that the chemical enthalp term acts in the opposite direction to the temperature gradient term, so it reduces the predicated value of the wall heat flux, and this meets the initial expectation of using coupled wall function.

$$\overline{\nabla_r Y_k} = \frac{1}{A} \oiint \nabla Y_k \cdot \boldsymbol{n_r} ds \tag{5-1}$$

In conclusion, in a GCH4/GO2 combustion chamber with film cooling, there is still an overestimation of wall heat flow using regular wall functions, which is due to the fact that general wall treatments ignore the chemical reactions in the near-wall area. The overestimation is even more evident in a single injector combustion chamber, where the

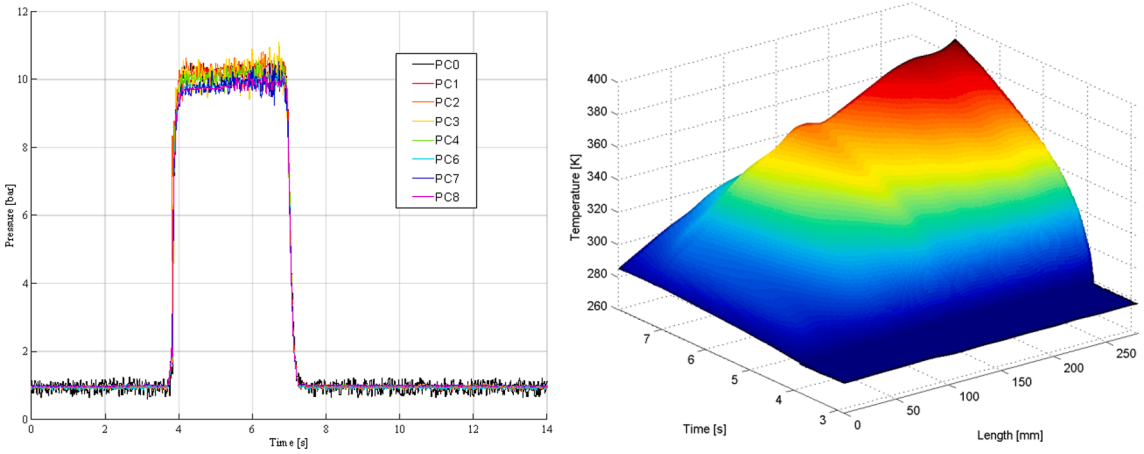

Fig. 11. Single element combution chamber pressure and temperature output curves with time.

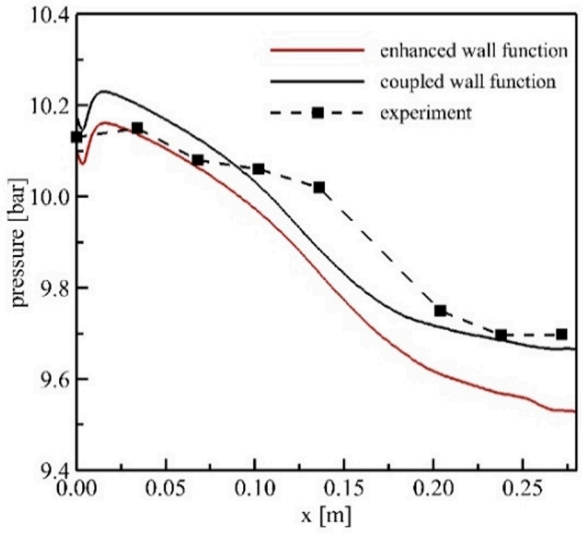

Fig. 12. Axial pressure distribution in the single-element chamber.

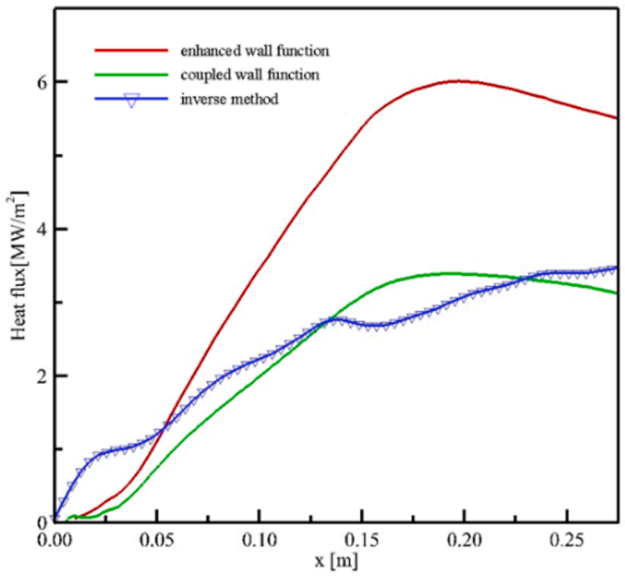

Fig. 13. Axial wall heat flux distribution in the single-element chamber.

Table 5
Aera averages of the mass fraction gradients of main components and their chemical enthalpies.

Species	Area averages of gradients	Chemical enthalpy $h^0_{f,k}[MJ/kg]$
CO2	−7.43	−8.94
CH4	39.69	−4.65
O2	0.39	0
H2O	−16.25	−13.4
CO	−15.37	−3.95

turbulent flow near the wall is particularly complex, and the wall heat transfer is mainly controlled by chemical reactions. However, by using coupled wall function, this overestimation was significantly improved and agreed well with the experimental results, thus it can be concluded that coupled wall function is able to predict the wall heat flux more accurately in a combustion chamber with film cooling. Furthermore, J. Wei et al. have verified that coupled wall function also performs well in RANS simulations of multi-element GCH4/GO2 combustion chamber without film cooling[32,33], so the coupled wall function is also applicable in wall heat transfer conditions dominated by both chemical reactions and complex turbulent flows. Combining the discussion of this subsection, it can be assumed that the numerical framework presented in this paper is able to accurately predict the wall heat flow in a GCH4/GO2 combustion chamber with film cooling, where chemical reaction and complex turbulence both contribute to the wall heat flux.

5.2. Prediction of wall heat transfer in a multi-element combustion chamber with film cooling

As the numerical framework is validated in a single-element chamber with film cooling, based on the mentioned mesh of the 7-element circular combustion chamber, another numerical case is established for predicting the heat transfer characteristics of the chamber wall. Fig. 14 shows the pressure distribution of a multi-element combustion chamber with film cooling using coupled wall function and enhanced wall function and compared with the pressure in a chamber without film. Based on this analysis, it appears that the pressure calculated by enhanced wall function and coupled wall function are almost identical as well, and this phenomenon confirms again that coupled wall function has little effect on the overall flow field. It is also evident that although the trend is the same, the pressure in the combustion chamber with film is slightly higher than in the chamber without film since additional methane is injected into the chamber as both coolant and fuel. In addition, in the part close to the injection plate($x < 20$ mm), a pressure rising due to the recircle zone created by the injected gas can be observed, while this kind of pressure variation is more obvious in a combustion chamber without

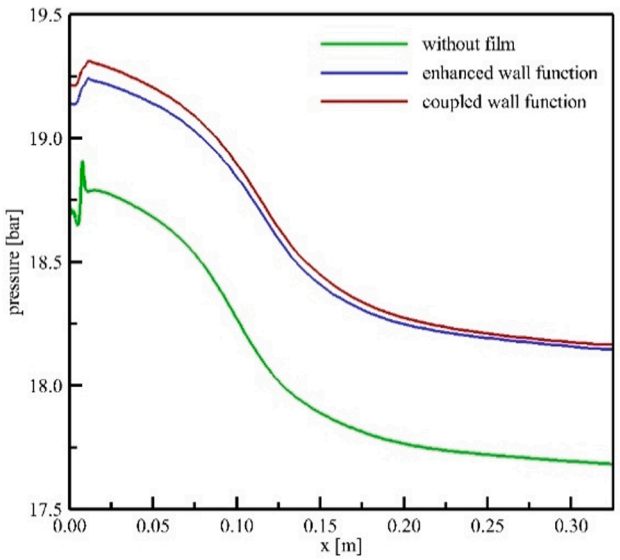

Fig. 14. Axial pressure distribution in the multi-element chamber.

film, the reason is that the injection of a high velocity film weakens the turbulence in the recircled zone, which consequently reflected in the pressure variation.

The calculated heat release rate is shown in Fig. 15. Fig. 15 demonstrates that the heat release rate of coupled wall function and enhanced wall function are almost identical, which again proves that wall functions have little effect on the mainstream flow and chemical reactions, and only act in the near-wall region. There are two peaks in the heat release rate curves, at about 15 mm and 110 mm from the injection plate respectively. The first peak value reaches 15 GW/m^3, in that region the chemical reaction area is small and the reaction is mainly controlled by the mixing rate. After this point, the mixing rate decreases due to the weakening of the recircled zone, results in a gradual decrease in the heat release rate. Afterwards, the heat release rate rises again to the second peak of 20 GW/m^3 due to the rapid expansion of the mixing zone and the increasing mixing area, after which the heat release rate progressively decreases until the combustion process is completed. Moreover, both peaks are higher compared to the simulation results in a chamber without film (8 GW/m^3 and 17 GW/m^3), because the injection

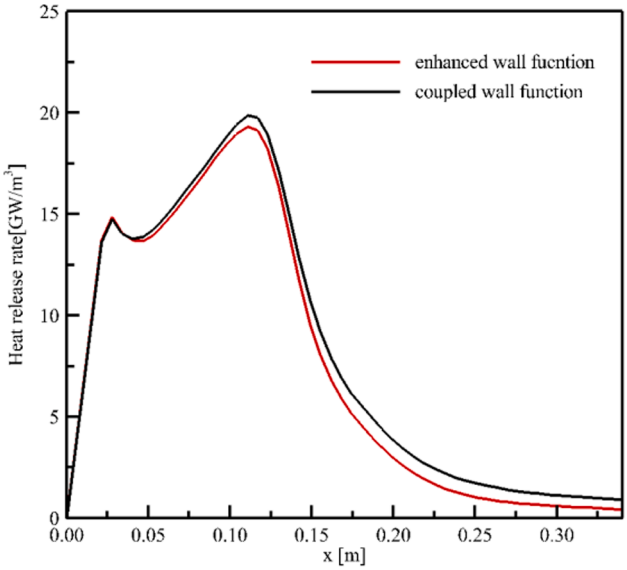

Fig. 15. Heat release rate of multi-element chamber.

of additional film can play a role as fuel and participate in chemical reactions at the front of the combustion chamber, which leads to more heat release, while the total heat release rate of the combustion increases as well due to the increase of the total fuel volume.

Fig. 16 shows the temperature contour in the central longitudinal section of the combustion chamber. Firstly, as can be seen, the mainstream temperature distribution is not significantly impacted by the change of wall function, and the temperature in a chamber with film is a little higher than it in a chamber without film, this is because extra methane is injected as film. Secondly, the temperature boundary layer is thicker due to the existence of film, resulting in a smaller temperature gradient near the wall, so the obtained heat flow value using the coupled wall function is correspondingly lower. Ultimately, in comparison with the case without film, the flame area near the wall of a chamber with film cooling does not exhibit a slimmer flame caused by gas compression. In the study of the combustion chamber without film cooling[33], this flame deformation in the front section of the chamber is caused by the restricted flame expansion near the wall, and the flame expansion is mainly controlled by the interior vortex structure. Since the *x*-component of the vortex is significantly larger than the other two directions, Fig. 17 shows the contours of only the *x*-component of vorticity at different cross-sections of the combustion chamber, where the positive values represent the clockwise vorticity. Due to the gradual weakening of the vortex, the effect of the near-wall vortex on the flame changes from stretching to restraining, which restricts and thins the flame expansion in the front of the combustion chamber whereas the rear section is virtually unaffected. In contrast, as shown in Fig. 17, the vorticity in the combustion chamber is lower and dissipates more rapidly due to the high-velocity film has been injected, while vortices in conditions using coupled wall function dissipate faster than enhanced wall function. Consequently, the near-wall vortex restrains flame expansion even more, so the flame near the wall in the combustion chamber with film cooling is not undeformed, but becomes slimmer due to the vortices.

Fig. 18 shows the heat flux distribution of the combustion chamber wall. From Fig. 18 it can be observed that the heat flux calculated using coupled wall function is much lower than enhanced wall function. Additionally, this result supports the previous study that chemical reactions near the wall are indeed to blame for excessive heat flow prediction when using general wall functions. However, compared with the results of the wall heat flux of the single element chamber with film cooling in the previous subsection, the discrepancy of calculated heat flux between using coupled wall function and enhanced wall function (50%-75%) is more than that in a chamber without film cooling (30%). As described in section 4, the coupled wall function affects wall heat flow prediction in several ways, particularly in a combustion chamber with film cooling, and the influences of these variables are coupled. In the next section, the reasons for such a low prediction are being discussed.

To begin with, the flow in a multi-element combustion chamber is more complicated than that of a single-element chamber, and the radial velocity at the wall can be positive or negative, thus changes the direction of Eq. (4–9) and the direction of the chemical enthalpy term, ultimately leads to different values of wall heat flux. The flow streamlines of several cross-sections of the combustion chamber are presented in Fig. 19. It is evident that the direction of chemical enthalpy term action varies considerably across the wall, which explains why the difference in wall heat flux prediction between coupled wall function and enhanced wall function jumps from around 50% in single element chambers to around 75% in multi-element chambers.

Secondly, in order to assess the overall effect of the chemical reaction on the wall heat flux, more attention should be paid to the net effect of the chemical enthalpy term across the entire chamber wall. Since the gradient in the vertical direction of the wall is much larger than the other two directions, only the *y*-component of the mass fraction gradient is considered. The area averaging of the entire wall is still calculated as

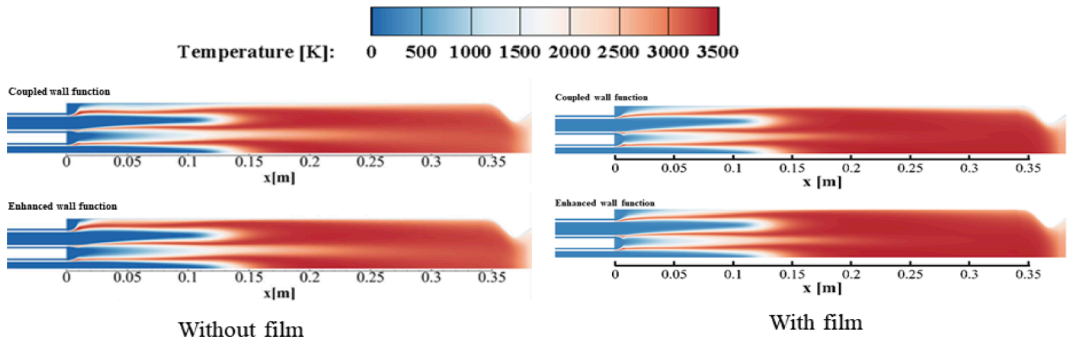

Fig. 16. Temperature contour in the longitudinal section of the multi-element chamber.

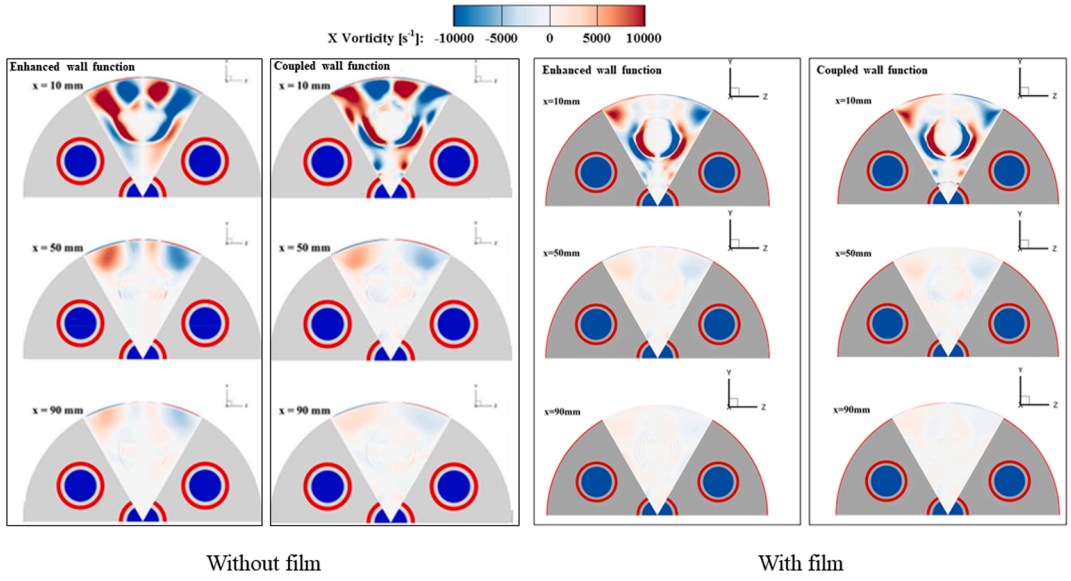

Fig. 17. Contours of the x-component vorticity for different cross-sections.

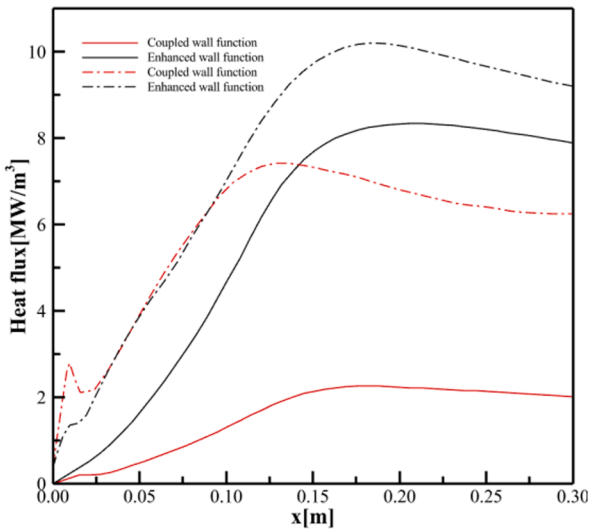

Fig. 18. Axial heat flux distribution on the wall of the multi-element chamber (— -with film; -●- -without film).

in Eq. (5–1) and the results of the mass fraction gradients of each main component near the wall are shown in Table 6.

The inner product of the second and third column of Table 6 gives a value of approximately 2.9×10^8 J/kg, which is still a positive value, indicating that the direction of chemical enthalpy term in a multi-element combustion chamber is opposite to the temperature gradient term acting direction, which results in a reduction of the predicted wall heat flux. Besides, it is also noted that the value of μ_t near the wall is of the order of 10^{-2}, which leads to an order of magnitude of the heat flux change due to the chemical enthalpy term of approximately 1.6×10^6 W in a single-element chamber and 2.9×10^6 W in a multi-element chamber with film cooling, both of them are higher than the value in a multi-element chamber without film cooling (4×10^5 W). This indicates that the injection of film influences the temperature of the gas near the wall and the mass fraction of each component, ultimately pushes the chemical reaction equilibrium near the entire chamber wall to the direction of an increase in the total chemical enthalpy, finally results in a greater discrepancy in the predicted wall heat flux than the case without film cooling.

Finally, it is also noticed that the three-dimensional effect is more pronounced in the multi-element combustion chamber, while the film also has a greater impact on the near-wall flow profile. It also makes the difference of wall heat flux between the case considering and not considering the chemical reactions near the wall greater than the single element combustion chamber with film cooling case.

6. Conclusion

An experimental test bench for a GCH4/GO2 combustion chamber using methane as a cooling film is built and a RANS-based numerical

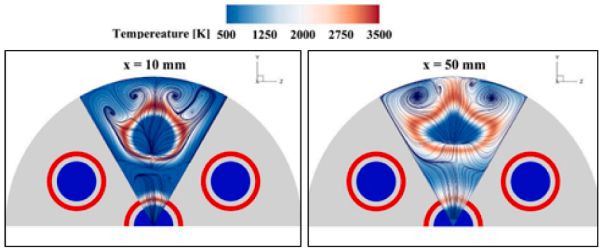

(a) Without film

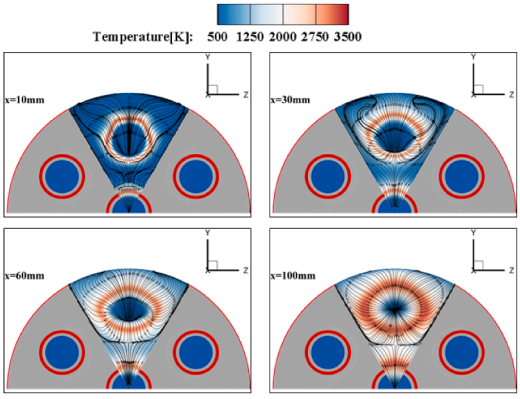

(b) With film

Fig. 19. Flow streamline of each cross-section of the multi-element chamber.

Table 6
Aera averages of the mass fraction gradients of main components and their chemical enthalpies.

Species	Area averages of gradients	Chemical enthalpy $h^0_{f,k}[MJ/kg]$
CO2	−4.76	−8.94
CH4	16.41	−4.65
O2	0.30	0
H2O	−19.74	−13.4
CO	−14.94	−3.95

framework is established. The experimental results have proved that the numerical frame established in this paper is able to calculate the combustion characteristics in the chamber and predict the wall heat flux more accurately. Then, based on the developed numerical framework, a multiple elements GCH4/GO2 combustion chamber with film cooling simulation is carried out.

The results of the single element chamber with film reveal that the wall heat flux calculated by the frame with enhanced wall function is about 50% higher than the experimental values. To correct this overprediction of wall heat flux, a coupled wall function is introduced through Fluent UDF, and the simulation results show that the mainstream characteristics of the combustion chamber are essentially unchanged, while the wall heat flux results are in good agreement with the experimental results. This indicates that the overestimation of the wall heat flow in a combustion chamber with film cooling is caused by the neglect of chemical reactions near the wall. Besides, it is also shown that the numerical framework based on the RANS method and coupled wall function can predict the flow and combustion process in the combustion chamber well and provide a more accurate prediction of wall heat flux in the case with film cooling.

Different from the single element square combustion chamber, multiple elements circular combustion chamber has more complex flows and more significant three-dimensional effects. Thus, it makes more sense to apply the numerical framework developed in this study to a multi-injector combustion chamber. The numerical simulation results of multi-element combustion chambers show that the pressure and heat release rate distribution of the combustion chamber using enhanced wall function and coupled wall function are almost identical, which suggests that the wall function only affects the wall area and has little effect on the mainstream. In addition, as the analysis of the vortex in the combustion chamber with film shows that the injection of film reduces the voracity near the chamber wall, resulting in a limited flame expansion in the high temperature zone near the wall and then made the overall flame in this zone become thinner. Finally, the wall heat flux calculated by using the coupled wall function is approximately 75% lower than using enhanced wall function, which again supports the view that chemical reactions were responsible for the overestimation of wall heat flow.

Furthermore, this paper also found that in the GCH4/GO2 rocket combustion chamber with film cooling, the discrepancy in predicted wall heat flux values between the case using coupled wall function and enhanced wall function was more significant than the case without film cooling. According to the chemical enthalpy analysis of the entire combustion chamber wall, it could be concluded that the injection of film changes the temperature and the mass fraction of each component near the wall, and their coupling influence ultimately causes the chemical reaction equilibrium to move to the direction of an increase of total enthalpy, which then leads to the enthalpy term in the couple wall function to increase compared to the temperature gradient term, eventually results in a lower predicted value of heat flux of the wall. Besides, in the multi-element combustion chamber, the three-dimensional flow characteristics could not be ignored and the injection of film affects the radial velocity direction at various parts of the wall, and their coupling effects causes the chemical reaction equilibrium movement, finally results in the prediction of the wall heat flux even lower.

To sum up, the numerical approach proposed in this paper can better predict the wall heat flux in a GCH4/GO2 combustion chamber with film cooling, and it is reasonable to assume that the numerical frame can also apply to more kinds of combustion chambers with film. And by using a reasonable numerical framework to predict the wall heat flux of a rocket engine combustion chamber with film, it is possible to improve the design of the rocket engine, protect the chamber wall better, and allocate fuel usage for the film coolant more rationally.

Declaration of Competing Interest

The authors declare that they have no known competing financial interests or personal relationships that could have appeared to influence the work reported in this paper.

Data availability

Data will be made available on request.

Acknowledgements

Jianing Liu (No.201706120033) is supported by China Scholarship Council when he conducted the work in this paper. The authors thank their colleagues for the support in the experiment and beneficial discussion, especially Mariella Celano, Nikolaos Perakis, Jingying Zuo, Qin Ma and Wenjing Yin.

Appendix A. Supplementary data

Supplementary data to this article can be found online at https://doi.org/10.1016/j.applthermaleng.2022.119544.

References

[1] S. Choi, T.Y. Kim, H.K. Kim, I.S. Jeung, J. Koo, O.C. Kwon, Combustion stability of gaseous CH4/O2 and H2/O2 coaxial jet flames in a single-element combustor, Energy. 132 (2017) 57–64.

[2] H. Burkhardt, M. Sippel, A. Herbertz, J. Klevanski, Kerosene vs. Methane: A Propellant Tradeoff for Reusable Liquid Booster Stages, J. Spacecraft Rockets. 41 (2004) 762-769.

[3] T. Neill, D. Judd, E. Veith, D. Rousar, Practical uses of liquid methane in rocket engine applications, Acta Astronaut. 65 (2009) 696–705.

[4] A.S. Gohardani, J. Stanojev, A. Demairé, K. Anflo, M. Persson, N. Wingborg, C. Nilsson, Green space propulsion: Opportunities and prospects, Prog. Aerosp. Sci. 71 (2014) 128–149.

[5] Y. Boué, P. Vinet, S. Magniant, T. Motomura, R. Blasi, J.-P. Dutheil, LOX/methane reusable rocket propulsion at reach with large scale demonstrators tested, Acta Astronaut. 152 (2018) 542–556.

[6] J. Applewhite, Energy Systems Division, NASA, Houston(TX, USA), 2011. Technical Report JSC-CN-23260.

[7] H. K. Kim, S. Choi, T. Y. Kim, O. C. Kwon, Studies on Flame Behaviors of GCH4/GO2 Coaxial Jets in a Model Combustor at Elevated Pressure, 52nd AIAA/SAE/ASEE Joint Propulsion Conference. (2016).

[8] J. Zhang, S. Zhang, C. Wang, X. Tan, Recent advances in film cooling enhancement: A review, Chin. J. Aeronaut. 33 (2020) 1119–1136.

[9] J.P. Feist, A.L. Heyes, S. Seefelt, Thermographic phosphor thermometry for film cooling studies in gas turbine combustors, Proc. Instit. Mech. Eng., Part A: J. Power Energy. 217 (2005) 193-200.

[10] J. Zuo, S. Zhang, D. Wei, L. Meng, J. Qin, W. Bao, O.J. Haidn, Effects of combustion on supersonic film cooling using gaseous hydrocarbon fuel as coolant, Aerosp. Sci. Technol. 106 (2020).

[11] P. Marquardt, M. Klaas, W. Schröder, Experimental Investigation of Isoenergetic Film-Cooling Flows with Shock Interaction, AIAA J. 57 (2019) 3910–3923.

[12] S. Choi, T.y. Kim, O.C. Kwon, Combustion Characteristics of Gaseous CH4/O2 Coaxial Jets in a Model combustor, in: 51st AIAA/SAE/ASEE Joint Propulsion Conference. (2015).

[13] W. Lin, J. Zhou, S. Liu, Z. Lin, An experimental study on CH4/O2 continuously rotating detonation wave in a hollow combustion chamber, Exp. Therm Fluid Sci. 62 (2015) 122–130.

[14] S. Silvestri, M. P. Celano, G. Schlieben, O. J. Haidn, Characterization of a Multi-Injector GOX/CH4 Combustion Chamber, 52nd AIAA/SAE/ASEE Joint Propulsion Conference. (2016).

[15] E.K. Quaye, J. Pan, Y. Zhang, Q. Lu, Y. Wang, A.A. Alubokin, Effects of influencing factors on premixed CH4-O2 combustion in a cylindrical porous media combustor, Chem. Eng. Process. - Process Intensif. 161 (2021).

[16] M. Son, K. Radhakrishnan, Y. Yoon, J. Koo, Numerical study on the combustion characteristics of a fuel-centered pintle injector for methane rocket engines, Acta Astronaut. 135 (2017) 139–149.

[17] Y. Daimon, H. Negishi, S. Silvestri, O.J. Haidn, Conjugated Combustion and Heat Transfer Simulation for a 7 element GOX/GCH4 Rocket Combustor, 2018 Joint Propulsion Conference. (2018).

[18] N. Perakis, O.J. Haidn, D. Eiringhaus, D. Rahn, S. Zhang, Y. Daimon, S. Karl, T. Horchler, Qualitative and Quantitative Comparison of RANS Simulation Results for a 7-Element GOX/GCH4 Rocket Combustor, 2018 Joint Propulsion Conference. (2018).

[19] A. Chemnitz, T. Sattelmayer, C. Roth, O. Haidn, Y. Daimon, R. Keller, P. Gerlinger, J. Zips, M. Pfitzner, Numerical Investigation of Reacting Flow in a Methane Rocket Combustor: Turbulence Modeling, J. Propul. Power 34 (2018) 864–877.

[20] J. Zips, C. Traxinger, M. Pfitzner, Time-resolved flow field and thermal loads in a single-element GOx/GCH4 rocket combustor, Int. J. Heat Mass Transf. 143 (2019).

[21] D. Maestro, B. Cuenot, L. Selle, Large Eddy Simulation of Combustion and Heat Transfer in a Single Element GCH4/GOx Rocket Combustor, Flow, Turbulence and Combustion. 103 (2019) 699–730.

[22] S. Yu, X. Liu, X.S. Bai, A.M. Elbaz, W.L. Roberts, LES/PDF modeling of swirl-stabilized non-premixed methane/air flames with local extinction and re-ignition, Combust. Flame 219 (2020) 102–119.

[23] Z. Huangwei, A. Giusti, E. Mastorakos, LES/CMC modelling of ignition and flame propagation in a non-premixed methane jet, Proceedings of the Combustion Institute. 37 (2019) 2125-2132.

[24] M. Calabro, Y. Daimon, H. Negishi, M. Koshi, D. Suslov, L. DeLuca, S. Frolov, L. Galfetti, O. Haidn, Numerical and experimental investigation of the methane film cooling in subscale combustion chamber, Progress in Propulsion Physics. (2016) 129-144.

[25] S. Kawai, J. Larsson, Wall-modeling in large eddy simulation: Length scales, grid resolution, and accuracy, Phys. Fluids 24 (2012).

[26] L. Ye, C.-L. Liu, H.-R. Zhu, J.-X. Luo, Experimental Investigation on Effect of Cross-Flow Reynolds Number on Film Cooling Effectiveness, AIAA Journal. 57 (2019) 4804–4818.

[27] X. Sun, G. Zhao, P. Jiang, W. Peng, J. Wang, Influence of hole geometry on film cooling effectiveness for a constant exit flow area, Appl. Therm. Eng. 130 (2018) 1404–1415.

[28] M.A. Keller, M.J. Kloker, H. Olivier, Influence of Cooling-Gas Properties on Film-Cooling Effectiveness in Supersonic Flow, J. Spacecraft Rockets. 52 (2015) 1443–1455.

[29] R. Hou, F. Wen, Y. Luo, X. Tang, S. Wang, Large eddy simulation of film cooling flow from round and trenched holes, Int. J. Heat Mass Transf. 144 (2019).

[30] G. Frank, M. Pfitzner, Investigation of the heat transfer coefficient in a transpiration film cooling with chemical reactions, Int. J. Heat Mass Transf. 113 (2017) 755–763.

[31] S. Andrej, P. Nikolaos, M. Palma, M.P. Celano, T. Martin, O. Haidn, CFD-analysis of the effect of a cooling film on flow and heat transfer characteristics in a GCH4/GOX rocket combustion chamber, Space Propulsion. (2018).

[32] J. Wei, M. Ye, S. Zhang, J. Qin, O.J. Haidn, Modeling of a 7-elements GOX/GCH4 combustion chamber using RANS with Eddy-Dissipation Concept model, Aerosp. Sci. Technol. (2020), https://doi.org/10.1016/j.ast.2020.105762.

[33] J. Wei, S. Zhang, X. Zhou, C. Cheng, J. Qin, O.J. Haidn, Effects of near wall flow and non-equilibrium reaction coupling on heat flux prediction inside a 7-elements GOX/GCH4 combustion chamber, Appl. Therm. Eng. 204 (2022), 118021.

[34] D. Muto, Y. Daimon, H. Negishi, T. Shimizu, Wall modeling of turbulent methane/oxygen reacting flows for predicting heat transfer, Int. J. Heat Fluid Flow 87 (2021).

[35] T. Kitano, H. Iida, R. Kurose, Effect of Chemical Reactions of H2/O2 Combustion Gas on Wall Heat Flux in a Turbulent Channel Flow, J. Heat Transfer 139 (2017).

[36] B. Betti, D. Bianchi, F. Nasuti, E. Martelli, Chemical Reaction Effects on Heat Loads of CH4/O2 and H2/O2 Rockets, AIAA Journal. 54 (2016) 1693–1703.

[37] J. Zuo, S. Zhang, J. Qin, W. Bao, N. Cui, X. Liu, Effects of cracking reaction on supersonic film cooling using gaseous hydrocarbon fuel as coolant, Appl. Therm. Eng. 171 (2020).

[38] O. Cabrit, F. Nicoud, Direct simulations for wall modeling of multicomponent reacting compressible turbulent flows, J. Physics of Fluids. 21 (5) (2009), 055108.

[39] M.P. Celano, S. Silvestri, C. Kirchberger, G. Schlieben, D.I. Suslov, O.J. Haidn, Gaseous Film Cooling Investigation in a Model Single Element GCH4-GOX Combustion Chamber, Trans. JSASS Aerospace Tech. 14 (2016) 129–137.

[40] M.P. Celano, C. Kirchberger, S. Silvestri, D. Suslov, O.J. Haidn, Model Assessment for Gaseous Film Cooling in a Subscale Single Element GCH4-GOX Combustion Chamber, Space Propulsion Conference. ID 3124835 (2016).

[41] N. Perakis, O.J. Haidn, Inverse heat transfer method applied to capacitively cooled rocket thrust chambers, Int. J. Heat Mass Transf. 131 (2019) 150–166.

[42] M.P. Celano, S. Silvestri, J. Pauw, N. Perakis, F. Schily, D. Suslov, O.J. Haidn, Heat flux evaluation methods for a single element heat-sink chamber. 6th European Conference for Aeronautics and Space Sciences (EUCASS), 2015.

[43] N. Perakis, M.P. Celano, O.J. Haidn, Heat flux and temperature evaluation in a rectangular multi-element GOX/GCH4 combustion chamber using an inverse heat conduction method. 7th European Conference for Aeronautics and Space Sciences (EUCASS), 2017.

[44] N. Perakis, J. Strauß, O.J. Haidn, Heat flux evaluation in a multi-element CH4/O2 rocket combustor using an inverse heat transfer method, Int. J. Heat Mass Transf. 142 (2019).

[45] S. Silvestri, C. Kirchberger, G. Schlieben, M.P. Celano, O. Haidn, Experimental and Numerical Investigation of a Multi-Injector GOX-GCH4 Combustion Chamber, Trans. Japan Soc. Aeronaut. Space Sci. Aerospace Technology Japan. 16 (2018) 374–381.

[46] L. Vervisch, R. Hauguel, P. Domingo, M. Rullaud, Three facets of turbulent combustion modelling: DNS of premixed V-flame, LES of lifted nonpremixed flame and RANS of jet-flame, J. Turbul. 5 (2004).

[47] F.F. Winter, N. Perakis, O.J. Haidn, Emission imaging and CFD simulation of a coaxial single-element GOX/GCH4 rocket combustor, 2018 Joint Propulsion Conference. (2018).

[48] A. Sternin, H. Ma, J. Liu, O. Haidn, M. Tajmar, Turbulence and Combustion and Film Prediction in Rocket Application via Parameter Adjustion, Model Variation and Deep Learning Method, Transregio 40-Summer Program Report. (2019).

[49] G. Dong, Y. Huan, Y.L. Chen, Study of effects of different chemical reaction mechanisms on computation results for methane jet turbulence diffusion flame, J. Fuel Chem. Technol. 28 (2000) 49–54.

A.2 Paper 2

Jianing Liu, Silong Zhang, Jianfei Wei, Oskar J. Haidn

Numerical Study of Film Cooling in Single-Element Injector Gaseous CH4/O2 Rocket Engine with Coupled Wall Function

Contribution: My primary contributions include the processing of experimental data, the modification and optimization of the numerical framework proposed in Paper 1, the execution of numerical simulations, the data analysis and discussion of the simulation results, and the writing and proofreading of the manuscript.

Numerical study of film cooling in single-element injector gaseous CH_4/O_2 rocket engine with coupled wall function

Cite as: AIP Advances 14, 035330 (2024); doi: 10.1063/5.0178273
Submitted: 26 September 2023 • Accepted: 12 February 2024 •
Published Online: 14 March 2024

Jianing Liu,[1] Silong Zhang,[2,a)] Jianfei Wei,[2] and Oskar J. Haidn[1]

AFFILIATIONS

[1] School of Engineering and Design, Department of Mechanical Engineering, Technical University of Munich, München, Germany
[2] School of Energy Science and Engineering, Harbin Institute of Technology, Harbin, China

[a)] Author to whom correspondence should be addressed: zhangsilong@hit.edu.cn

ABSTRACT

The investigation of film cooling in CH_4/O_2 rocket engines holds paramount importance in the advancement of rocket propulsion. However, the wall heat flux is always overestimated in numerical simulation processes. Hence, this article proposes a numerical framework that employs the Reynolds averaged Navier–Stokes method to simulate the single-element gaseous CH_4/gaseous O_2 combustion chamber, which is the basis for rocket engine simulations. The coupled wall function that considers chemical reaction effects is introduced to enhance the accuracy of wall heat flux prediction. The impact of utilizing a coupled wall treatment on the prediction of wall heat flux and its fundamental parameters are examined. In addition, a single-element combustion chamber experiment is performed to validate the simulation. The results demonstrate that the implementation of the coupled wall function hardly influences the main flow characteristics, whereas the wall heat flux calculated with general wall functions shows an overestimation, which can be reduced by the coupled wall function. Finally, the case with a coupled wall function can improve the cooling efficiency with greater accuracy and the cooling systems with optimized design. The proposed numerical framework and the findings of the study provide profound insights that can improve the design and optimization of rocket engines.

NOMENCLATURE

C_{mod}	Logarithmic law of velocity constant
C_p	Specific heat capacity, J/(kg K)
C_μ	Constant in the turbulent model, 0.09
h_f^0	Standard formation enthalpy, J/kg
k	Turbulent kinetic energy, J/kg
$\dot{m}$	Mass flow rate, g/s
p	Pressure, Pa
Pr	Prandtl number
q	Molecular heat flux vector, W/m^2
R_F	Film to total fuel ratio
ROF	Oxygen–fuel ratio
Sc	Schmidt number
t	Time, s
T	Temperature, K
u^+	Dimensionless wall velocity, u/u_τ
u_τ	Friction velocity, $\sqrt{\tau_w/\rho}$, m/s
Y	Mass fraction
y^+	Dimensionless wall distance
y_P	Distance from point P to the wall
η	Film cooling efficiency
κ	Kármán constant
λ	Thermal conductivity, W/(m K)
μ	Molecular viscosity, Pa s
ρ	Density, kg/m^3
τ	Shear stress, Pa

Subscripts

ad	Adiabatic
c	Center of the first layer of cells
CC	Combustion chamber
CH_4	Methane

film	With film
k	Species k
O_2	Oxygen
t	Turbulent
w	Wall

I. INTRODUCTION

In recent years, CH_4/O_2 rocket engines have attracted considerable attention in the aerospace propulsion field due to their high specific impulse compared to kerosene, superior storage capability compared to hydrogen, and highly effective cooling capacity.[1–5] A methane/oxygen rocket engine operating under high pressure experiences a combustion temperature exceeding 3500 K, high enough to destroy nearly all wall materials. Thus, the rocket engine cooling system is of utmost importance. The efficiency and even the reusability of the engines can also be improved by judicious placement of various cooling techniques. Among diverse cooling techniques, film cooling, which involves injecting a thin layer of coolant along hot gas-exposed surfaces to protect engine components, presents significant cooling efficiency with a straightforward mechanical design.[6–9]

The complex nature of rocket engines, which involve intricate fluid dynamics, combustion, and heat transfer processes, necessitates sophisticated simulation techniques to develop new engines, improve existing designs, and ensure safe and reliable operation. In particular, single-element rocket engine simulations are crucial since they allow researchers to examine specific components of the engine. By simulating the dynamics of a single-element injector, engineers can obtain valuable insights into the design of larger and more complex engines. Hence, it is essential to conduct research on single-element rocket engines and film cooling simulations to gain a deeper understanding of rocket engine performance and behavior. Previous studies have conducted numerous experimental[10,11] and numerical[12–14] research studies on subsonic film boundary layers. However, the existing studies primarily concentrate on the impact of geometry and injection parameters, with limited attention paid to the flow and chemical state of the boundary layer itself. Nevertheless, it is crucial to consider the properties of the boundary layer when designing a rocket engine combustion chamber and arranging its cooling system. Current research indicates that Direct Numerical Simulation (DNS) and Large-Eddy Simulation (LES) are capable of capturing the flow characteristics of the boundary layer accurately.[13,15,16] Nevertheless, Kawai and Larsson revealed that the viscous length scale of the layer is only around 1 μm,[17] resulting in the need for an extremely fine mesh near the wall for LES-based simulation and a consequent increase in computational cost, and the DNS method requires even a finer grid than LES. In addition, in studying the heat transfer properties, chemical reactions must also be considered, which leads to the inclusion of more equations. In addition to computational cost, controlling the convergence of DNS- and LES-based methods can also be challenging. Therefore, it is necessary to find a way to simulate a methane/oxygen chamber accurately at a low computational cost.

In essence, single-element gaseous CH_4/gaseous O_2 (GCH_4/GO_2) rocket engine simulations with film cooling form the basis for developing complex engine simulations. Despite this, current research on films in single-element chamber simulations is limited

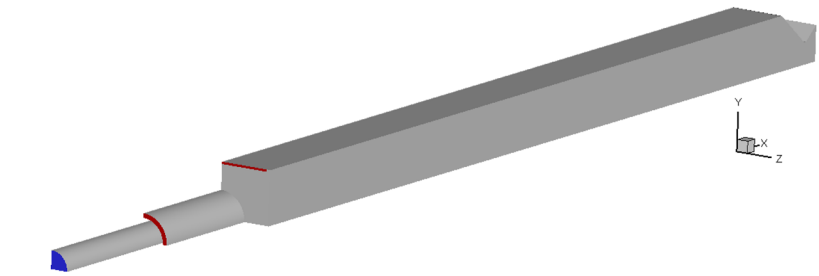

(a) Geometry

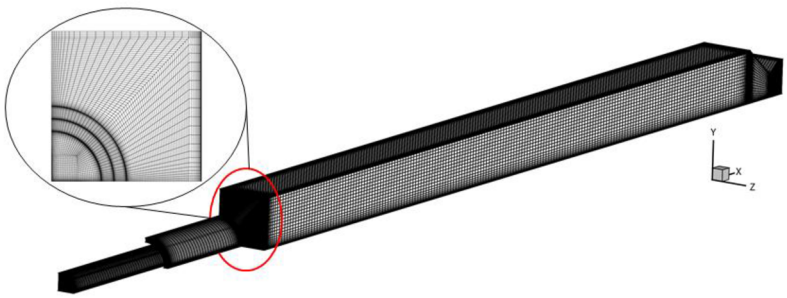

(b) Mesh

FIG. 1. Geometry and mesh of the numerical case.

in investigating wall heat transfer. In addition, the Reynolds Averaged Navier–Stokes (RANS) method is the least computationally expensive method to predict mainstream properties at small grid numbers while solving the grid scale problem using wall functions. Prior research has validated the efficacy of RANS-based simulations in accurately modeling the methane/oxygen combustion chambers. However, the wall heat flux is usually predicted higher than the experimental data when applying the RANS approach when simulating a chamber with film cooling.[18–21] Erroneous heat flux estimations can result in flawed cooling arrangements, thereby compromising not only the cooling effectiveness and the overall engine efficiency but also exposing the engine to the risk of severe damage.

To address the aforementioned overestimation problem and identify its causes, the authors have proposed a numerical framework in the previous work (see Ref. 22), which includes a coupled wall function proposed and modeled by Cabrit and Nicoud[23] and takes into account chemical reactions, undergoing preliminary validation in the GCH_4/GO_2 combustion chamber. Previous research by Wei *et al.* demonstrated that the disregard of chemical reactions within the boundary layer is a cause of heat flux overestimation[24] as commonly used wall treatments are based on non-reacting single-component flows that ignore chemical reaction influences. However, according to the related research, chemical reactions significantly affect wall heat flux,[25–28] and other numerical parameters such as turbulence Prandtl number (Pr_t), turbulence Schmidt number (Sc_t), and mesh sensitivity can also affect the calculated wall heat flux.[29–31] This paper investigates the impact of various numerical factors on wall heat flux when combined with a coupled wall function to determine the optimal numerical framework. In addition, to validate and optimize the numerical results, an experimental study is carried out on a single-element GCH_4/GO_2 combustion chamber. The optimized numerical model is used to simulate the corresponding chamber, and results are presented and discussed, including a discussion on film cooling efficiency based on simulation results. The conducted analyses will furnish normative guidance for forthcoming simulations about wall heat transfer of single-element combustion chambers and the implementation of film cooling techniques. In addition to that, these results also have the potential to improve the development of more efficient and reliable rocket engines.

II. NUMERICAL SETUP AND REFERENCE EXPERIMENT

A. Geometrical model and mesh

To gain convincing results from the numerical framework, the geometrical characteristics of the single-element GCH_4/GO_2 combustion chamber are adopted from the forthcoming test bench, as detailed in Sec. II B. As illustrated in Fig. 1(a), we have neglected the delivery pipeline as the primary emphasis of this study is placed on the flow and combustion process within the chamber. The retention of the nozzle aims to regulate the pressure within the chamber by ensuring supersonic outlet flow. Furthermore, we have reserved a certain length of the injection pipe for both the fuel injector (50 mm) and the oxygen injector (100 mm) to ensure the complete development of methane and oxygen flow. As depicted in Fig. 1(b), the mesh was established based on the geometry, and only a quarter of the chamber was retained to reduce computational costs. In addition, the mesh of the shear layer area was refined to increase the accuracy of the simulation.

B. Numerical setup and boundary conditions

In reference to prior investigations concerning methane/oxygen combustion simulations using the RANS method,[18,20,32,33] as it is a typical high Reynolds number flow process, the standard k-ε model is a cost-effective and accurate method for calculating turbulent mixing processes. Moreover, previous investigations by the authors[33] have illustrated the Eddy Dissipation Concept (EDC) model's efficacy in accounting for detailed chemical reaction mechanisms in turbulent reactions. This study employs the chemical reaction mechanism proposed by Dong *et al.*,[34] which comprises 14 species and 18 reactions. Table I summarizes the boundary conditions. The chamber wall temperature is gained from polynomial fitting of the experiment data, and since the nozzle part is not mainly investigated in this work, the temperature of the nozzle wall is set as consistent with the tail of the combustion chamber. Besides, since the injection plate is small compared to the chamber, it is reasonable to assume it as an adiabatic wall.

Concerning the wall treatment approach, general wall functions usually presume that the variable distribution is linear in the boundary layer. Nevertheless, to consider chemical reactions within the boundary layer, the coupled wall function is applied. This method preserves the original form of the momentum equation, but the energy equation incorporates the chemical enthalpy term. Subsequently, after a sequence of transformations and equivalent substitutions in the Fluent UDF, the wall heat flux of the coupled wall function can be presented as

$$q_w = -\frac{\rho C_P u^*}{T^+}(T_c - T_w), \tag{2.1}$$

where T^+ is the dimensionless wall temperature, which can be calculated as

$$T^+ = K(Pr) + \frac{\alpha}{B_q}u^+. \tag{2.2}$$

The constant denoted as $K(Pr)$ is only associated with the Prandtl number. The coefficient in front of u^+ can be expressed as

$$\frac{\alpha}{B_q} = \frac{C_P}{\frac{C_P}{Pr_t} + \frac{1}{Sc_t}\sum_k \frac{d\overline{Y_k}}{d\overline{T}} h^0_{f,k}}. \tag{2.3}$$

The presentation of the coupled wall function and detailed derivation can be found in Refs. 22 and 23.

TABLE I. Boundary conditions.

Boundary	Type	Specific
GOX inlet	Mass flow inlet	0.006 025 kg/s
GCH_4 inlet	Mass flow inlet	0.001 925 kg/s
Film inlet	Mass flow inlet	0.0011 kg/s
Injector wall and faceplate	Non-slip wall	Adiabatic
Chamber wall	Non-slip wall	Polynomial fitting
Nozzle wall	Non-slip wall	400 K

C. Mesh independence verification

To ensure that the mesh density does not affect the numerical results and to minimize computational costs, the verification of mesh independence is a crucial step and must be performed. Five groups of mesh with different densities are used, and the grid numbers range from 378 952 to 5 832 241. Each time the mesh is refined by adding a grid point between every two grid nodes, but the wall y^+ is maintained at around 30 as required by the wall function.

Figure 2 demonstrates the variation curves of several main combustion chamber parameters, such as average temperature, velocity, and wall heat flux, with the number of grids. As shown in Fig. 2, the calculated values from the first two groups with coarser grids differ significantly from those of the other groups, and upon exceeding a mesh count of 1.72×10^6, no significant changes are observed in the chamber parameters. Thus, to save calculation cost and guarantee calculation accuracy, a mesh with 1.72×10^6 grid numbers is used for the simulation in this paper.

D. Reference experiment

The reference experiment used for validating the numerical frame was carried out on the testbench at the Technical University of Munich (TUM),[35] which contains a heat-sink combustion chamber with a single injector, as shown in Fig. 3. 25 T-type thermocouples were installed uniformly on the cooled chamber wall, and extra thermocouples were set axially at distances of 1, 2, and 3 mm from the top wall in four groups since the temperature changes in the front part of the chamber are more intense and the film exerts a greater impact on the wall heat transfer in the front segment. Besides, on the bottom wall of the first segment, four thermocouples were also embedded to inspect the temperature changes of a wall without film. For the pressure measurement, nine pressure sensors were fixed at the sidewall uniformly to inspect the pressure decrease in the combustion chamber.

The film is injected along the upper wall of the chamber, and the thickness of the injector is 0.25 mm. The fuel and oxygen are injected

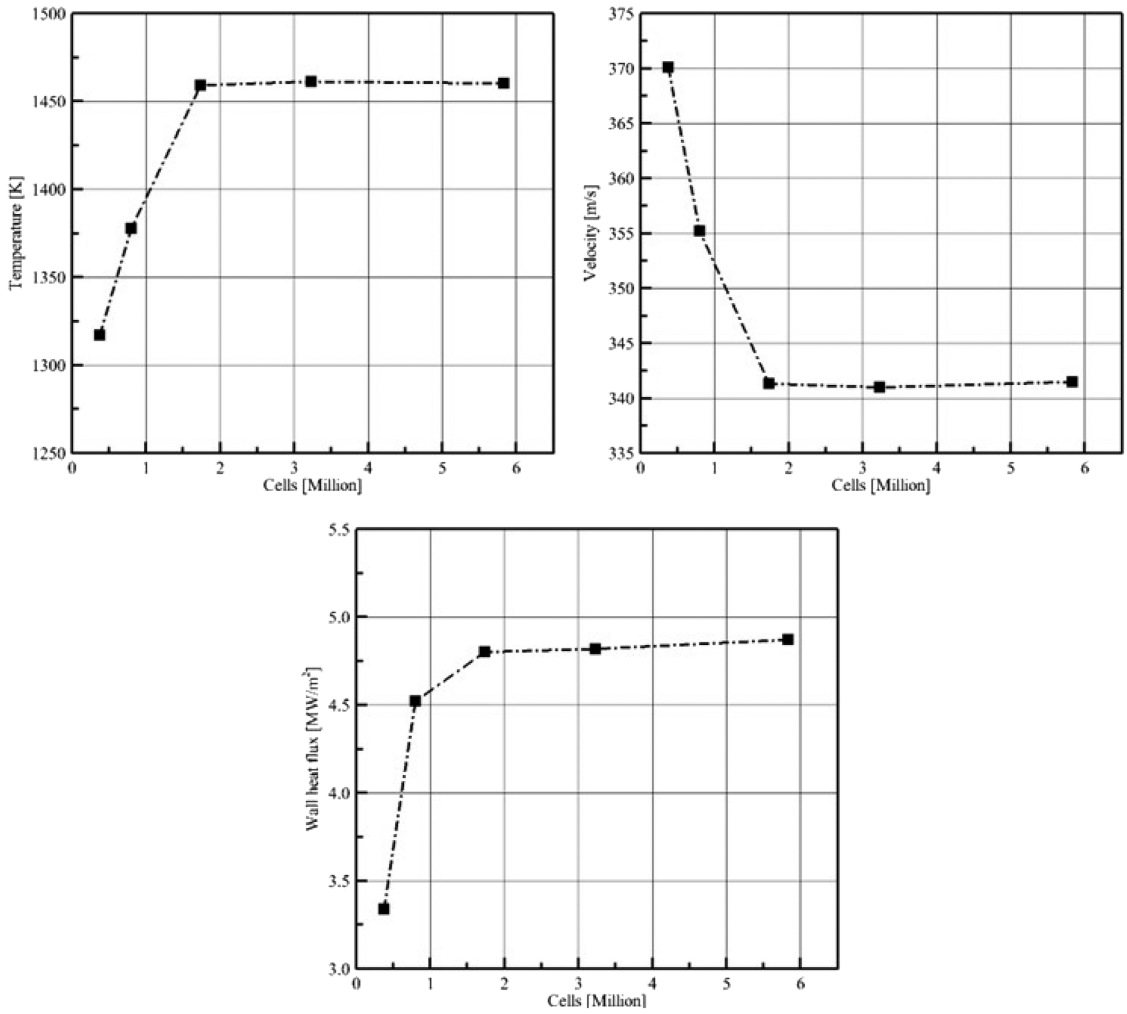

FIG. 2. Variation curves of chamber parameters with the number of grids.

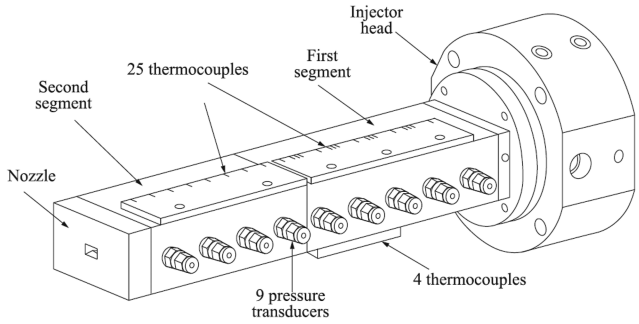

FIG. 3. Schematic diagram of the single-element chamber testbench.

coaxially into the combustion chamber. After a burning time of 3 s, the combustion is considered to reach the equilibrium state, and measurement data are extracted. Further parameters of the test-bench geometry and more experimental results can be found in Refs. 22 and 35. In addition, since the experimental results cannot directly obtain the heat flux, a series of data processing methods based on the experimental data and application of the inverse method are performed. The inverse method is a processing approach proposed by the author's research group.[36] It involves discretizing the near-wall region and utilizing the experimental measurement point values as the initial condition, leading to the iterative derivation of continuous parameters. Furthermore, this method exhibits the capability to mitigate discrepancies between the measurement point and the physical wall point where we are interested in.

III. RESULTS AND DISCUSSION

A. Parameter optimization

This section aims to explore the applicability of the coupled wall function in examining the impact of chemical reactions in the proximity of the wall on the wall heat flux. In addition, this study endeavors to provide a detailed analysis of the influence of numerical parameters on the wall heat flux. Finally, the optimized numerical factor will be summarized and applied for further simulations.

1. Effect of wall y-plus (y^+)

The dimensionless wall distance y-plus is the selection criterion for the near-wall problem solving method. Former studies have shown that y^+ has a great impact on the wall heat transfer characteristic simulations. In general, y^+ can be calculated by the following formula:

$$y^+ = \frac{\rho u_\tau y_P}{\mu}. \tag{3.1}$$

Figure 4 illustrates the chamber's upper wall heat flux calculated by different y-plus values. It can be noticed that when y^+ is less than 30, the wall heat flux decreases as y^+ increases, while if y^+ is greater than 30, the wall heat flux hardly changes with increasing y^+ anymore. This effect of y^+ on the heat flux is caused by its influence

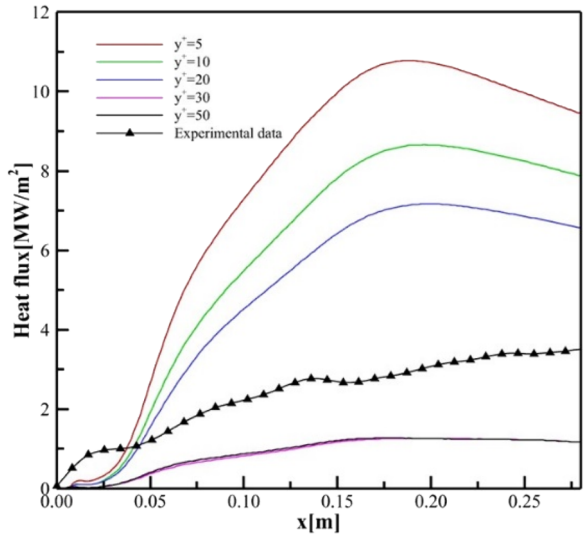

FIG. 4. Wall heat flux calculated with different y-plus values.

on u^+, as shown in Eq. (3.2), as the coupled wall function calculates u^+ as follows:

$$u^+ = \begin{cases} y^+ & \left(y^+ < 11.48\right), \\ \frac{1}{\kappa} \ln y^+ + C_{mod} & \left(y^+ \geq 11.48\right). \end{cases} \tag{3.2}$$

Figure 5 shows the image of Eq. (3.2). When y^+ is less than 30, u^+ increases sharply as y^+ increases, especially when y^+ is less than 11.48, and when y^+ is greater than 30, its effect on u^+ is significantly reduced. Therefore, while y^+ reached 30, increasing y^+ has a minor influence on wall heat flux but reduces the accuracy of

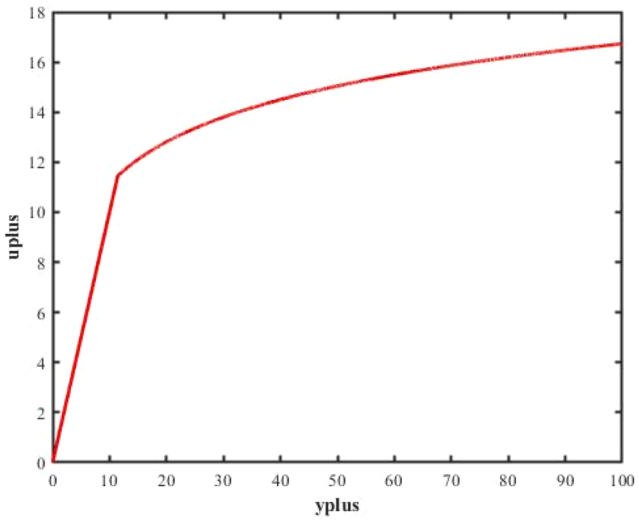

FIG. 5. u-plus vs y-plus curve.

calculating other parameters in the boundary layer. Figure 4 also displays the experimental wall heat flux data. The figure reveals that for a y^+ value ranging from 20 to 30, the calculated wall heat flux aligns most closely with the experimental results.

Nevertheless, the primary purpose of utilizing wall functions in RANS models is to circumvent the need for assuming a linear distribution and computing gradients within the boundary layer. Therefore, it is imperative to position the first layer grid center in the fully turbulent zone to satisfy the prerequisites of a turbulence model operating at high Reynolds numbers. Hence, it is reasonable to choose a y^+ value of ~30, and it enables the accurate calculation of other parameters within the boundary layer while maintaining numerical stability, and the differences between the simulated and experimental heat flux values that may arise from other variables will continue to be discussed in the following parts.

2. Effect of constant κ and C_{mod}

After choosing a value of 30 for y-plus, it can be seen that the von Kármán constant κ and the constant in the logarithmic law of velocity C_{mod}, in addition to y^+, also affect u^+, and thus, the calculated wall heat flux is according to Eq. (3.2). The classic values of $\kappa = 0.41$ and $C_{mod} = 5.5$, but some studies suggest that the value of κ must be assumed to be constant because it is not independent of the Reynolds number. Österlund *et al.* set the value of κ to 0.38 and C_{mod} to 4.1 and found that in this case, the log-law formulation no longer correlates with the Reynolds number.[37] Currently, it is difficult to determine which of these two choices of κ and C_{mod} constants is more accurate, but it is still possible to explore the application of different constant values chosen for the specific case of the single-element injector CH_4/O_2 combustion chambers.

Figure 6 shows the wall heat flux values obtained using two sets of constants. The wall heat flux computed using $\kappa = 0.41$ and $C_{mod} = 5.5$ is only slightly higher than the other one, and the reason can also be explained by the effect of the constant κ and C_{mod} on u^+ in Eq. (3.2). Changes in the values of κ and C_{mod} do not affect u^+ much, so the impact of these constants on the ultimate computed wall heat flux is also negligible. Specifically, in the initial half of the combustion chamber, there is no discernible difference between the two sets of constant values, while in the latter half, the disparity amounts to no more than 5%, which might be caused by the changing of the Reynolds number, so it is justifiable to disregard the influence of κ and C_{mod} on the wall heat flux calculation. Drawing on past numerical simulation experience, this paper selects $\kappa = 0.41$ and $C_{mod} = 5.5$ finally.

3. Effect of turbulent Prandtl number (Pr_t) and Schmidt number (Sc_t)

Aside from the above-mentioned factors, the turbulent Prandtl Number (Pr_t) and turbulent Schmidt Number (Sc_t), denoting the ratio between the turbulent transport rates of momentum and that of heat and mass transfer, respectively, also significantly affect the wall heat flux. According to Eq. (2.3), the Pr_t and Sc_t ultimately affect the calculated wall heat flux by influencing the coefficient $\frac{\alpha}{B_q}$ before u-plus. Regarding the range of Pr_t and Sc_t values, from the experimental data, the value of Pr_t has a range from 0.7 to 0.9,[38–40] and in the original coupled wall function derivation, the Lewis number ($Le = Sc/Pr$) was assumed to be equal to 1, which means $Pr_t = Sc_t$.

Figure 7 demonstrates the calculated heat flux changes with different turbulent Prandtl numbers and Schmidt numbers. Within the range of 0.7–0.9, an increase in both Pr_t and Sc_t leads to a decrease in wall heat flux, but the change is not significant. For every 0.05 increase in the value of Pr_t and Sc_t, the peak wall heat flux decreases by only around 5%, and in the vicinity of the injector plate where the film primarily acts, the differences in wall heat flux caused by the Pr_t and Sc_t changes are even smaller. Even so, in order to ensure that the computed wall heat flux closely corresponds to the experimental data, 0.7 has been chosen for both Pr_t and Sc_t.

In conclusion, the present study has successfully identified an optimal set of parameters for the combustion chamber of a single-element CH_4/O_2 engine, utilizing the coupled wall function for film simulation. The specific parameters are summarized in Table II,

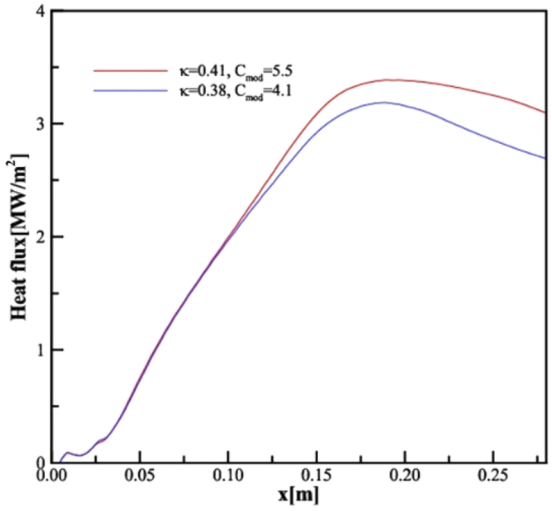

FIG. 6. Wall heat flux calculated with different κ and C_{mod} values.

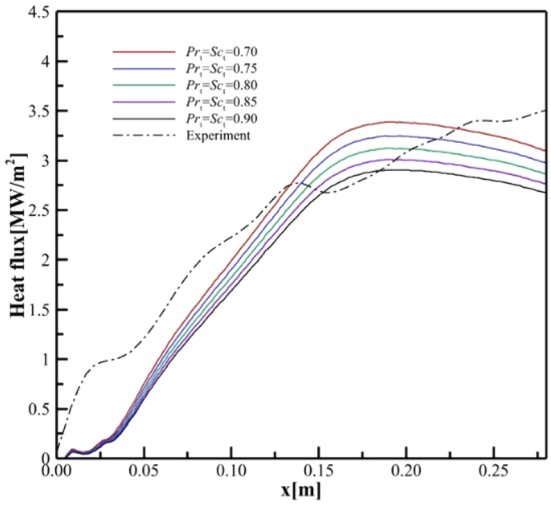

FIG. 7. Wall heat flux calculated with different Pr_t and Sc_t values.

TABLE II. Parameter settings of the coupled wall function.

y^+	κ	C_{mod}	Pr_t	Sc_t
30	0.41	5.5	0.7	0.7

thereby providing a comprehensive reference for researchers in the field of combustion modeling.

B. Numerical simulation results and discussion

Based on the parameters summarized in Table II in Subsection III A 3, a group of single-element injector combustion chamber simulations are carried out on the Ansys Fluent platform. The pressure distribution is illustrated in Fig. 8. Obviously, the pressure decreases as the flow progresses downstream. Furthermore, the pressure distribution obtained via the coupled wall function approach exhibits minimal deviation from the general wall functions, amounting to less than 1%, regardless of whether film cooling is considered. This finding is in line with our prior derivation of the coupled wall function, which asserts that it primarily accounts for the chemical reactions occurring in close proximity to the wall and exerts minimal influence on the main flow.[23] Finally, it is worth noting that the chamber pressure in the configuration incorporating film cooling is higher than that without film cooling. This is because the injected film serves not only as a coolant but also as an extra source of fuel. Moreover, as depicted in Fig. 8, the chamber pressure in the film-cooled chamber closely aligns with the experimental results. This outcome underscores the capability of the computational framework developed in this study to accurately simulate the flow behavior within a single-element combustion chamber with film cooling.

Figure 9 displays the analysis of the heat release rate in the single-element combustion chamber. The results suggest that the

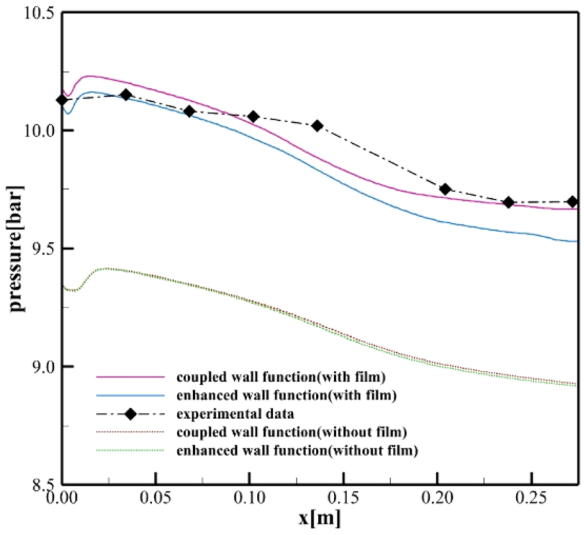

FIG. 8. Downstream direction pressure distribution.

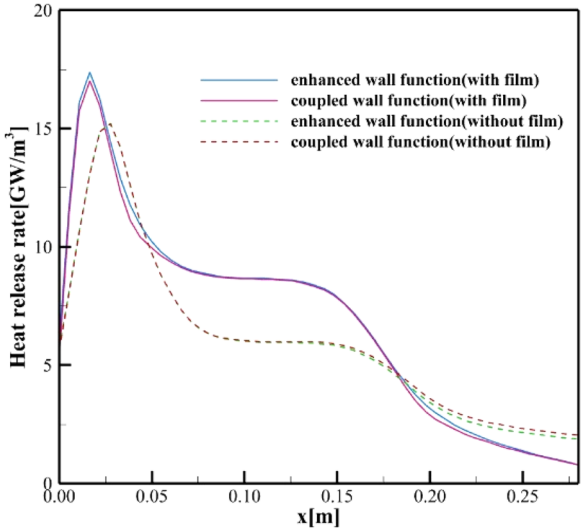

FIG. 9. Heat release rate of the combustion chamber.

implementation of the two different wall treatments does not have a substantial impact on the heat release rate, which further implies that the main flow remains unaffected. Due to the small chemical reaction area, the heat release rate reaches its maximum value at the beginning of the combustion chamber, which is dominated by mixing. The chamber with film injection shows a higher peak value (17 GW/m^3) than the chamber without film (15 GW/m^3) due to the enhanced mixing in this region. As the mixing rate decreases, there is a gradual decline in the heat release rate. However, in the middle section of the chamber, where the reaction area expands, the heat release rate remains constant. The chamber with film exhibits a higher heat release rate in this region because the film can be used as fuel in the reaction, leading to faster conversion from chemical to thermal energy. As the chemical reaction progresses toward completion, the heat release rate continues to decrease until the chamber tail. Interestingly, the heat release rate with film is lower than that of the chamber without film in this region, which may be attributed to the more intense chemical reactions in the middle section of the chamber, leading to reactant depletion at the chamber tail section.

The contour of temperature distribution in the chamber's central longitudinal section is presented in Fig. 10. By comparing the results with and without film cooling, the existence of film does weaken the high-temperature zone close to the chamber wall effectively, which indicates that film cooling is an excellent cooling method. In addition, it can still be noticed that in the chamber with or without film, the temperature distribution does not change much while using both kinds of wall functions because the main flow has not been affected much. Finally, the temperature contours also reflect that the flame expansion process is also consistent with the chemical reaction development about the heat release rate discussed earlier.

Other than the above-mentioned parameters, this paper pays more attention to the wall heat flux, which is also an important parameter in cooling studies. Primarily, taking the example of the chamber with film cooling using a general wall function, several

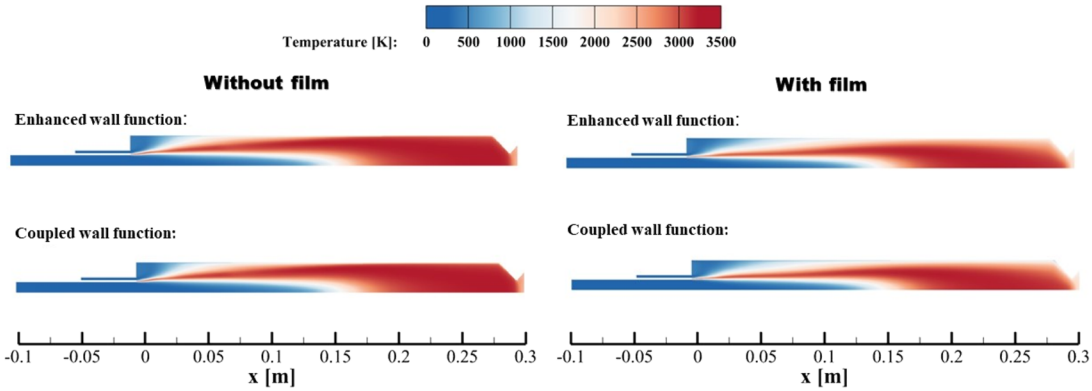

FIG. 10. Temperature distribution of the chamber central longitudinal section.

cross sections of the chamber upper wall heat flux distribution are depicted in Fig. 11. In the case of a square combustion chamber, the wall heat flux exhibits a parabolic distribution in the horizontal direction, with the exception of the boundary effect near the inner sidewalls, and other cases have similar results. Hence, the highest wall heat flux occurs along the midline of the combustion chamber, and the trend of the wall heat flux remains consistent in the downstream direction. Therefore, analyzing the heat flux distribution along the midline of the combustion chamber wall is considered the most representative approach.

Figure 12 presents the wall heat flux distribution downstream of the upper chamber wall midline. The figure demonstrates that the heat flux increases along the flow direction, as observed in Fig. 11. Another salient observation is that the cases with film cooling exhibit lower heat flux. Moreover, the comparison between the wall heat flux calculated using an enhanced wall function and coupled wall function reveals that the former overestimates the wall heat flux whereas the latter improves this overestimation and closely matches the experimental data. The present findings support the notion that the inaccuracy of general wall functions in predicting wall heat flux can be attributed to their inability to account for chemical reactions near the wall. The application of the coupled wall function, which considers these reactions, can lead to more precise simulations of the wall heat flux.

C. Study of cooling efficiency

Finally, it is necessary to carry on with the study of cooling efficiency and to investigate how the coupled wall function affects the cooling efficiency calculation. In a rocket engine combustion chamber, the efficiency of film cooling can be determined using the following equation, in general:

$$\eta = \frac{T_{ad} - T_{CC}}{T_{film} - T_{CC}}. \tag{3.3}$$

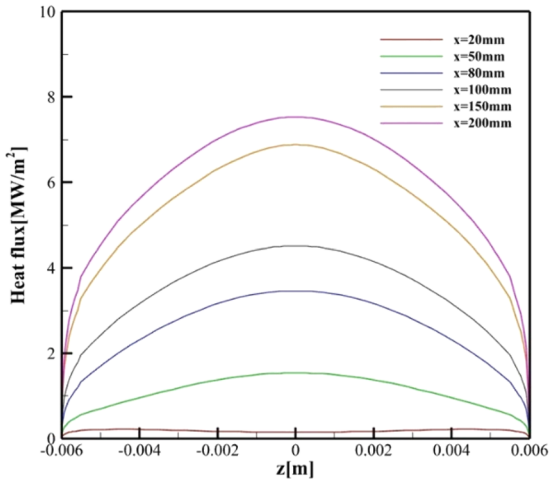

FIG. 11. Heat flux of different cross sections in the chamber with film.

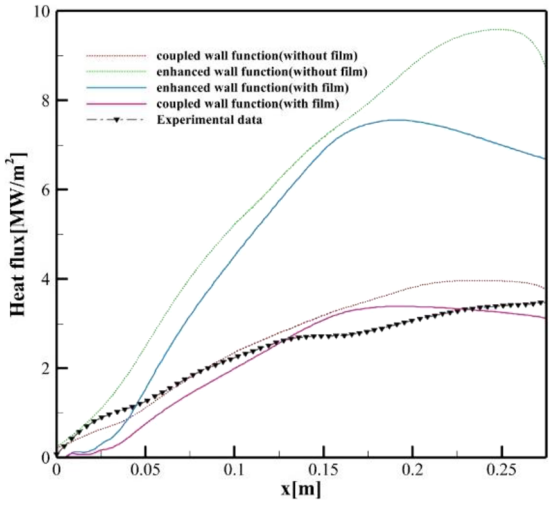

FIG. 12. Heat flux in the midline of the combustion chamber wall.

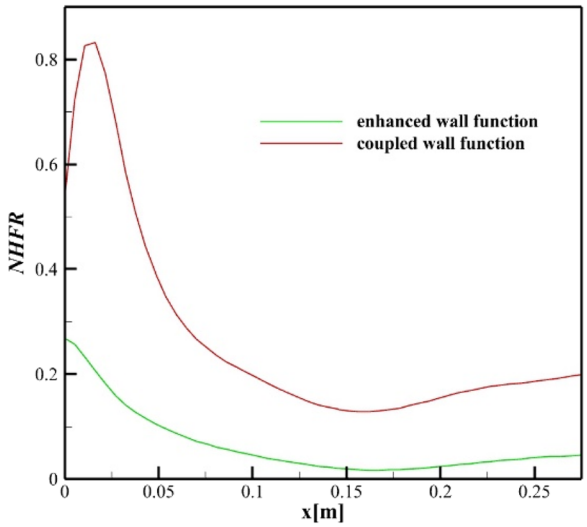

FIG. 13. NHFR distribution of the chamber wall in the downstream direction.

However, even though this cooling efficiency calculation method is widely used in cooling research, in the real rocket engine, the chamber wall is hard to reach adiabatic conditions. Accordingly, this study employs temperature as a wall boundary condition and employs the coupled wall function to improve the precision of the wall heat flux estimation. Therefore, using Eq. (3.3) to measure the cooling efficiency may not be appropriate. In contrast, it would be more suitable to utilize Net Heat Flux Reduction (NHFR) in this situation, as many relevant studies have shown.[41–43] The NHFR can be defined as follows:

$$NHFR = 1 - \frac{q_{film}}{\dot{q}_0} \cdot \left(\frac{P_{CC,0}}{P_{CC,film}} \right)^{0.8}, \tag{3.4}$$

where $\dot{q}_0$ is the heat flux without film injection and the term $\left(\frac{P_{CC,0}}{P_{CC,film}}\right)^{0.8}$ is a correction factor proposed by Bartz[44] to consider the effect of film injection on the combustion chamber pressure.

Figure 13 reveals the average NHFR distribution of the upper chamber wall in the downstream direction. Due to the effect of the recirculation zone, the film cooling efficiency first increases to a peak near the injection plate, then falls rapidly, and tends to a minimum value after x = 0.07–0.08 m, after which the cooling efficiency remains constant essentially. The reduction in cooling efficiency is a result of the gradual mixing of the film with the hot gas in the main flow. Therefore, in order to maintain higher cooling efficiency, it might be appropriate to set a film injection port every 80 mm on the chamber wall. Besides, the coupled wall function yields a higher NHFR than the enhanced wall function. Since it has been discussed that the coupled wall function provides a more precise estimation of the wall heat flux and the pressure remains unchanged with the use of different wall functions, the cooling efficiency calculated with the coupled wall function can be considered more accurate, according to Eq. (3.4). This finding is important because it is possible to reduce the coolant methane proportion in the design of rocket engines, thereby cutting the overall fuel load.

Figure 13 shows the NHFR distribution contour on the combustion wall upper wall. The same film cooling efficiency decay trend as shown in Fig. 13 has been shown more directly in Fig. 14. Besides, it can also be noticed that the NHFR near the injection plate calculated by the coupled wall function is overall marginally higher, which is also consistent with the above-mentioned result. Finally, as shown in Fig. 14, in square combustion chambers, the cooling efficiency is almost unchanged in the lateral direction, except for the reflux effect at the corners.

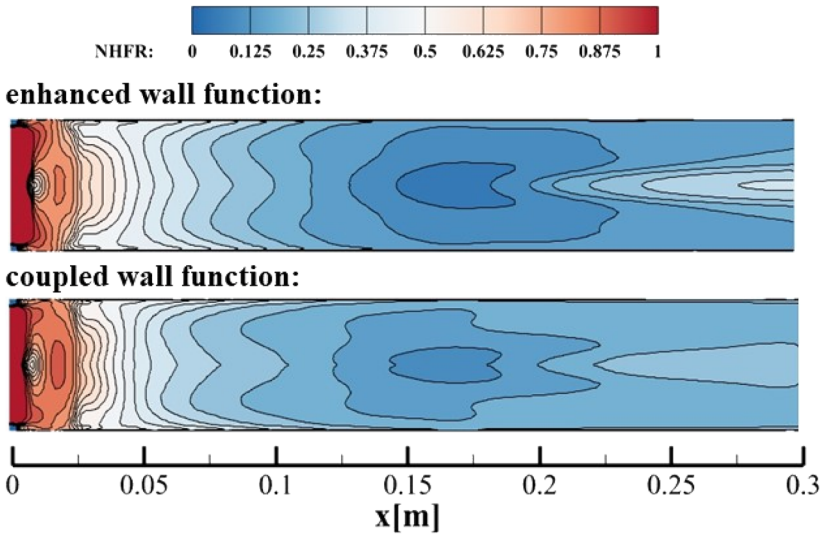

FIG. 14. NHFR distribution contour on the combustion chamber cooled-wall.

IV. CONCLUSION

A coupled wall function is incorporated into the framework based on the Ansys Fluent platform to improve the accuracy of wall heat flux prediction. In addition, simulation results are validated and parameters are optimized by conducting a corresponding experiment. As control groups, numerical simulations using a general wall function and without film cooling are carried out.

According to the parameter study, the wall heat flux decreases while the wall y-plus is below 30 and then remains constant after y-plus is above 30. It is also found that the values of κ and C_{mod} have a negligible effect on the film cooling acting area, and with the increase in the turbulent Prandtl number and Schmidt number in a range of 0.7–0.9, the wall heat flux increases as well. In summary, after a comparison of the wall heat flux values computed by various parameter configurations with the experimental results, the final parameter setup selected is that $y^+ = 30$, $\kappa = 0.41$, $C_{mod} = 5.5$ and $Pr_t = Sc_t = 0.7$.

Based on appropriate parameterization, several single-element combustion chamber simulations are carried out, which indicate utilizing coupled wall functions does not significantly affect the main flow characteristics, including pressure, heat release rate, and temperature, while the film injection can increase the overall pressure and weaken the high-temperature zone near the wall. In addition, film injection results in a higher heat release rate peak in the front chamber section, followed by higher values in the middle and a lower heat release rate at the end due to reactant decay. Wall heat flux has a parabolic distribution in the horizontal direction of the wall, with the highest values located on the midline of the chamber wall. Subsequently, downstream wall heat flux results suggest that film cooling can reduce wall heat flux, but general wall functions tend to overestimate it. However, the coupled wall function can significantly reduce this overestimation, with calculated wall heat flux values much closer to experimental data. Specifically, the inner product of the standard chemical enthalpies of the main components with their average mass fraction gradient within the boundary layer explains the quantitative reduction in the overestimated wall heat flux.

Finally, this study investigates the film cooling efficiency using the net heat flux reduction method instead of the traditional approach based on adiabatic wall temperature. This choice is motivated by the difficulty in achieving adiabatic conditions in real rocket combustion chambers. Furthermore, the main focus of this paper is to improve the precision of wall heat flux predictions. Based on the results, it can be seen that the cooling efficiency distribution is almost uniform in the horizontal direction. In addition, the impact of the coupled wall function on the net heat flux reduction distribution is observed to be negligible but results in a higher calculated cooling efficiency than the case with general wall functions, which means the methane fuel load can be cut down because it requires less methane use as a coolant to obtain the same cooling performance. Besides, the cooling efficiency decreases rapidly at a distance of 70–80 mm from the injection port, which indicates that it may be suitable to set injection ports every 70–80 mm along the chamber wall to maintain the high cooling efficiency and to protect the chamber wall.

To summarize, this paper proposes and utilizes a numerical framework to accurately simulate the combustion chamber of a single-element GCH_4/GO_2 rocket engine at a low computational cost. An optimized parameter setup and coupled wall function embedding significantly improve the wall heat flux, which is crucial for rocket engine wall protection research. Moreover, the study of film cooling efficiency provides more precise results and suggests proper film injection arrangements. A practical application of these findings can enhance the design of rocket propulsion systems and prevent excessive rocket engine temperatures.

ACKNOWLEDGMENTS

The work presented in this paper was supported by the China Scholarship Council for Jianing Liu (Grant No. 201706120033). Special thanks to Mariella Celano, Nikolaos Perakis, and Wenjing Yin for their contribution to this article.

AUTHOR DECLARATIONS

Conflict of Interest

The authors have no conflicts to disclose.

Author Contributions

Jianing Liu: Conceptualization (equal); Data curation (equal); Formal analysis (equal); Funding acquisition (equal); Investigation (equal); Methodology (equal); Resources (equal); Software (equal); Validation (equal); Visualization (equal); Writing – original draft (equal). **Silong Zhang**: Conceptualization (supporting); Funding acquisition (equal); Project administration (lead); Resources (equal); Supervision (lead); Writing – review & editing (equal). **Jianfei Wei**: Conceptualization (equal); Methodology (lead); Validation (supporting). **Oskar J. Haidn**: Data curation (supporting); Funding acquisition (supporting); Project administration (supporting); Resources (supporting); Supervision (equal); Writing – review & editing (equal).

DATA AVAILABILITY

The data that support the findings of this study are available from the corresponding author upon reasonable request.

REFERENCES

[1] S. Choi, T. Y. Kim, H. K. Kim, I.-S. Jeung, J. Koo, and O. C. Kwon, "Combustion stability of gaseous CH_4/O_2 and H_2/O_2 coaxial jet flames in a single-element combustor," Energy **132**, 57–64 (2017).

[2] T. Neill, D. Judd, E. Veith, and D. Rousar, "Practical uses of liquid methane in rocket engine applications," Acta Astronaut. **65**, 696–705 (2009).

[3] A. S. Gohardani, J. Stanojev, A. Demairé, K. Anflo, M. Persson, N. Wingborg, and C. Nilsson, "Green space propulsion: Opportunities and prospects," Prog. Aerosp. Sci. **71**, 128–149 (2014).

[4] R. Votta, F. Battista, V. Salvatore, M. Pizzarelli, G. Leccese, F. Nasuti, and S. Meyer, "Experimental investigation of transcritical methane flow in rocket engine cooling channel," Appl. Therm. Eng. **101**, 61–70 (2016).

[5] R. Saini, S. Prakash, A. De, and R. Yadav, "Investigation of NOx in piloted stabilized methane-air diffusion flames using finite-rate and infinitely-fast chemistry based combustion models," Therm. Sci. Eng. Prog. **5**, 144–157 (2018).

[6] P. Marquardt, M. Klaas, and W. Schröder, "Experimental investigation of isoenergetic film-cooling flows with shock interaction," AIAA J. **57**, 3910–3923 (2019).

[7]P. Concio, S. D'Alessandro, and J. Steelant, "Low-order modeling and validation of film cooling in liquid rocket combustion chambers," in 8th Space Propulsion, 2022.
[8]J. Zhang, S. Zhang, C. Wang, and X. Tan, "Recent advances in film cooling enhancement: A review," Chin. J. Aeronaut. **33**, 1119 (2020).
[9]J. Zuo, S. Zhang, D. Wei, L. Meng, J. Qin, W. Bao, and O. J. Haidn, "Effects of combustion on supersonic film cooling using gaseous hydrocarbon fuel as coolant," Aerosp. Sci. Technol. **106**, 106202 (2020).
[10]X. Sun, G. Zhao, P. Jiang, W. Peng, and J. Wang, "Influence of hole geometry on film cooling effectiveness for a constant exit flow area," Appl. Therm. Eng. **130**, 1404–1415 (2018).
[11]L. Ye, C.-l. Liu, H.-r. Zhu, and J.-x. Luo, "Experimental investigation on effect of cross-flow Reynolds number on film cooling effectiveness," AIAA J. **57**, 4804–4818 (2019).
[12]M. A. Keller, M. J. Kloker, and H. Olivier, "Influence of cooling-gas properties on film-cooling effectiveness in supersonic flow," J. Spacecr. Rockets **52**, 1443–1455 (2015).
[13]R. Hou, F. Wen, Y. Luo, X. Tang, and S. Wang, "Large eddy simulation of film cooling flow from round and trenched holes," Int. J. Heat Mass Transfer **144**, 118631 (2019).
[14]X. Ren, H. Chen, P. Li, Y. Gao, and S. Liu, "Numerical simulation of filling process of cryogenic propellants with inert gas purge," Therm. Sci. Eng. Prog. **29**, 101197 (2022).
[15]J. M. F. Peter and M. J. Kloker, "Direct numerical simulation of supersonic turbulent flow with film cooling by wall-parallel blowing," Phys. Fluids **34**, 025125 (2022).
[16]Y.-j. Sang, Y. Shan, J.-z. Zhang, and X.-m. Tan, "Numerical investigation of sweeping jet film cooling on a flat plate," Therm. Sci. Eng. Prog. **29**, 101230 (2022).
[17]S. Kawai and J. Larsson, "Wall-modeling in large eddy simulation: Length scales, grid resolution, and accuracy," Phys. Fluids **24**, 015105 (2012).
[18]A. Sternin, N. Perakis, M. Palma, M. P. Celano, T. Martin, and O. Haidn, "CFD-analysis of the effect of a cooling film on flow and heat transfer characteristics in a GCH_4/GOX rocket combustion chamber," in Space Propulsion, 2018.
[19]F. Di Matteo, M. Venanzi, M. De Rosa, and M. Onofri, "Modelling and simulation of film cooling in liquid rocket engine propulsion systems," in 48th AIAA/ASME/SAE/ASEE Joint Propulsion Conference and Exhibit, 2012.
[20]J. Wei, M. Ye, S. Zhang, J. Qin, and O. J. Haidn, "Modeling of a 7-elements GOX/GCH_4 combustion chamber using RANS with Eddy-Dissipation Concept model," Aerosp. Sci. Technol. **99**, 105762 (2020).
[21]K. A. Verma, K. M. Pandey, M. Ray, and K. K. Sharma, "The numerical analysis of combustion performance of a wedge shaped strut-based scramjet combustor," Therm. Sci. Eng. Prog. **20**, 100714 (2020).
[22]J. Liu, S. Zhang, J. Wei, and O. J. Haidn, "RANS based numerical simulation of a GCH_4/GO_2 rocket engine combustion chamber with film cooling and improvement of wall heat flux prediction," Appl. Therm. Eng. **219**, 119544 (2023).
[23]O. Cabrit and F. Nicoud, "Direct simulations for wall modeling of multicomponent reacting compressible turbulent flows," Phys. Fluids **21**, 21 (2009).
[24]J. Wei, S. Zhang, X. Zhou, C. Cheng, J. Qin, and O. J. Haidn, "Effects of near wall flow and non-equilibrium reaction coupling on heat flux prediction inside a 7-elements GOX/GCH4 combustion chamber," Appl. Therm. Eng. **204**, 118021 (2022).
[25]M. Son, K. Radhakrishnan, Y. Yoon, and J. Koo, "Numerical study on the combustion characteristics of a fuel-centered pintle injector for methane rocket engines," Acta Astronaut. **135**, 139–149 (2017).
[26]B. Betti, D. Bianchi, F. Nasuti, and E. Martelli, "Chemical reaction effects on heat loads of CH_4/O_2 and H_2/O_2 rockets," AIAA J. **54**, 1693–1703 (2016).
[27]J. Zuo, S. Zhang, J. Qin, W. Bao, N. Cui, and X. Liu, "Effects of cracking reaction on supersonic film cooling using gaseous hydrocarbon fuel as coolant," Appl. Therm. Eng. **171**, 115134 (2020).
[28]N. Perakis, O. J. Haidn, and M. Ihme, "Investigation of CO recombination in the boundary layer of CH_4/O_2 rocket engines," Proc. Combust. Inst. **38**, 6403–6411 (2021).
[29]Z. Zhang, Y. Mao, X. Su, and X. Yuan, "Inversion learning of turbulent thermal diffusion for film cooling," Phys. Fluids **34**, 035118 (2022).
[30]Y. Jiang, A. Murray, L. di Mare, and P. Ireland, "Mesh sensitivity of RANS simulations on film cooling flow," Int. J. Heat Mass Transfer **182**, 121825 (2022).
[31]X.-W. Sun, X.-L. Yang, and W. Liu, "Aero-optical and aero-heating effects of supersonic turbulent boundary layer with a tangential wall-injection film," Phys. Fluids **33**, 035118 (2021).
[32]S. Silvestri, C. Kirchberger, G. Schlieben, M. P. Celano, and O. Haidn, "Experimental and numerical investigation of a multi-injector GOX-GCH_4 combustion chamber," Trans. Jpn. Soc. Aeronaut. Space Sci., Aerosp. Technol. Jpn. **16**, 374–381 (2018).
[33]A. Sternin, H. Ma, J. Liu, O. Haidn, and M. Tajmar, "Turbulence and combustion and film prediction in rocket application via parameter adjustion, model variation and deep learning method," Transregio 40-Summer Program Report, 2019.
[34]G. Dong, Y. Huan, and Y. L. Chen, "Study of effects of different chemical reaction mechanisms on computation results for methane jet turbulence diffusion flame," J. Fuel Chem. Technol. **28**, 49–54 (2000).
[35]M. P. Celano, S. Silvestri, C. Kirchberger, G. Schlieben, D. I. Suslov, and O. J. Haidn, "Gaseous film cooling investigation in a model single element GCH_4-GOX combustion chamber," Trans. JSASS Aerosp. Technol. **14**, 129–137 (2016).
[36]N. Perakis and O. J. Haidn, "Inverse heat transfer method applied to capacitively cooled rocket thrust chambers," Int. J. Heat Mass Transfer **131**, 150–166 (2019).
[37]J. M. Österlund, A. V. Johansson, H. M. Nagib, and M. H. Hites, "A note on the overlap region in turbulent boundary layers," Phys. Fluids **12**, 1–4 (2000).
[38]D. M. McEligot and M. F. Taylor, "The turbulent Prandtl number in the near-wall region for low-Prandtl-number gas mixtures," Int. J. Heat Mass Transfer **39**, 1287–1295 (1996).
[39]S. W. Churchill, "A reinterpretation of the turbulent Prandtl number," Ind. Eng. Chem. Res. **41**, 6393–6401 (2002).
[40]A. Malhotra and S. S. Kang, "Turbulent Prandtl number in circular pipes," Int. J. Heat Mass Transfer **27**, 2158–2161 (1984).
[41]D. I. Suslov, R. Arnold, and O. Haidn, "Investigation of film cooling efficiency in a high pressure subscale LOX/H_2 combustion chamber," in 47th AIAA/ASME/SAE/ASEE Joint Propulsion Conference and Exhibit, 2011.
[42]J. L. Rutledge, P. I. King, and R. Rivir, "Time averaged net heat flux reduction for unsteady film cooling," J. Eng. Gas Turbines Power **132**, 121901 (2010).
[43]J. F. McCall and R. D. Branam, "Effects of radial curvature on net heat flux reduction in a film-cooled rocket," in *47th AIAA Aerospace Sciences Meeting Including The New Horizons Forum and Aerospace Exposition* **(AIAA,** 2009), Vol. 1586, pp. 1–11.
[44]D. R. Bartz, "A simple equation for rapid estimation of rocket nozzle convective heat transfer coefficients," J. Jet Propul. **27**, 49–51 (1957).

A.3 Paper 3

Jianing Liu, Silong Zhang, Jianfei Wei, Oskar J. Haidn

Velocity-Driven Optimization of Film Cooling in Methane/Oxygen Rocket Engines Using Coupled Wall Function

Contribution: My principal contributions encompass the proposition of novel velocity research methodologies, the refinement of the aforementioned numerical framework, the execution of numerical simulations, the meticulous analysis and discussion of findings, and the composition and validation of manuscripts.

Velocity-Driven Optimization of Film Cooling in Methane/Oxygen Rocket Engines Using Coupled Wall Function

Jianing Liu [a], Silong Zhang [b,*], Jianfei Wei [b], Oskar J. Haidn [a]

[a] School of Engineering and Design, Department Mechanical Engineering, Technical University of Munich

[b] School of Energy Science and Engineering, Harbin Institute of Technology

Abstract

This study investigates the application of coupled wall functions to the research of film cooling in methane/oxygen rocket engine combustion chambers. By manipulating film mass flow rate and inlet size, the influence of different film-mainstream velocity ratios on flow dynamics, combustion, wall heat transfer, and cooling efficiency within the combustion chamber is explored. Results indicate that as the ratio of film velocity to mainstream velocity (R_V) increases, the combustion chamber pressure initially decreases before increasing, with a corresponding trend observed in vortex intensity at the inlet section. Comparative analysis reveals that, while maintaining a constant mass flow rate, reducing the film inlet height results in lower pressures and weaker swirl strength. Furthermore, wall heat transfer decreases gradually with increasing R_V, with lower heat transfer observed in cases involving additional low-temperature methane injection. Notably, the introduction of coupled wall functions minimally impacts mainstream

flow and combustion. Analysis of Net Heat Flux Reduction (NHFR) indicates a rapid decrease in cooling efficiency in the front half of the combustion chamber, emphasizing the suitability of employing a film cooling inlet every one-fifth section in a methane/oxygen engine. Moreover, increasing the mass flow rate enhances cooling efficiency as R_V increases, while altering the inlet size yields nearly constant cooling efficiency. Therefore, maximizing film mass flow rate is deemed preferable for film cooling arrangements in a given rocket engine; however, comparative studies reveal a gradual reduction in engine specific impulse with increasing mass flow rate, underscoring the necessity for engine-specific determinations.

Keywords: Film cooling; Velocity ratio; Coupled wall function; NHFR; Rocket engine

Nomenclature

C_p	=	specific heat capacity, J/(kg·K)
F, G	=	functions
h	=	film inlet height, mm
$h_{f,k}^0$	=	standard formation enthalpy of the species k, J/kg
h_k	=	Total enthalpy of the species k, J/kg
h_s	=	specific sensible enthalpy J/kg
k	=	turbulent kinetic energy, J/kg
I_{sp}	=	specific impulse, s
$\dot{m}$	=	mass flow rate, g/s
p	=	pressure, Pa
q	=	heat flux, W/m^2
q_w	=	wall heat flux, W/m^2
T	=	temperature, K
T^+	=	dimensionless wall temperature
u^*	=	improved dimensionless wall velocity
V	=	Velocity, m/s
V_k	=	diffusion velocity of species k, m/s
Y_k	=	mass fraction of species k
y^+	=	dimensionless wall distance
ε	=	dissipation rate
ρ	=	density, kg/m^3
Subscripts		
cc	=	combustion chamber
k	=	species k
w	=	wall

1. Introduction

Liquid rocket propulsion systems utilizing methane and oxygen as propellants present several distinct advantages, foremost among them being their elevated specific impulse, facile storage characteristics, straightforward construction, and recyclability, as substantiated by prior research[1-3]. Moreover, scholarly investigations suggest that methane stands as the most promising fuel for potential synthetic extraction on exoplanets[4], thereby underscoring the significance of methane-based rocket engines in propelling humanity towards more extensive frontiers in space exploration. Typically, methane/oxygen rocket engines employ an amalgamation of cooling techniques to safeguard the integrity of the engine's structural components when subjected to the heightened temperatures prevailing within the combustion chamber[5].

Contemporary research on film cooling primarily revolves around investigating the influence of geometric parameters, such as the cross-sectional configuration of the film injector and the angle of injection, on the cooling effectiveness[5-8]. Furthermore, with respect to the characteristics inherent to film cooling, the principal body of research has been primarily oriented toward its application in external surface cooling applications, notably in contexts such as the cooling of turbine blades or airfoils[6, 9-11]. Nevertheless, there exists a dearth of comprehensive research about the implementation of film cooling within the confines of liquid rocket engines, with particular attention to comprehending the process of its intrinsic attributes and the intricate physicochemical interactions occurring between the film coolant and the main flow, as well as their impact on wall heat transfer and the overall effectiveness of the cooling mechanism.

The current investigation delves into the numerical exploration of combustion and wall heat transfer characteristics within a multi-element combustion chamber of a methane/oxygen rocket engine. To

simulate fluid flow and turbulence, three discrete computational fluid dynamics (CFD) methodologies are employed, namely, Reynolds-Averaged Navier-Stokes (RANS), Large Eddy Simulation (LES), and Direct Numerical Simulation (DNS). Typically, LES and DNS are harnessed for the purpose of obtaining intricate turbulence characteristics, particularly detailed information of vortices. Consequently, these methods often necessitate the use of finely resolved grids to accurately capture the minute-scale vortical structures[12, 13]. However, given that the primary emphasis of this investigation is to comprehend the overarching combustion characteristics within the combustion chamber, the adoption of the RANS-based approach suffices to adequately simulate the flow and turbulence dynamics within the chamber. Importantly, this choice offers the advantage of significantly reduced computational costs compared to LES and DNS methods, which are more computationally intensive.[14, 15].

In typical RANS simulations, the employment of wall functions is customary to avoid the computational burden associated with resolving the intricate features of the boundary layer. However, previous research findings indicate that the routine use of normal wall functions tends to result in an overestimation of wall heat flux in the context of methane/oxygen combustion chamber.[16-18]. In authors` previous work, ¡t has been determined that the overestimation arises due to the general wall functions' omission of chemical reactions occurring within the boundary layer.[18, 19]. It is also investigated that using coupled wall function proposed and modelled by Cabrit and Nicoud [20] can significantly reduce this overestimation and gain more accurate wall heat flux without influencing the mainstream flow characteristics. Hence, ¡n this study, a RANS computational framework integrated with a coupled wall function is employed to model the combustion and wall heat transfer phenomena within a methane/oxygen rocket combustion chamber.

Regarding the flow characteristics of the film, Zhou et al.[21], Xu et al.[22] and Xiang et

al.[23]found that with the film percentage increases, the cooling efficiency increases but the increment decreases. Zhang et al.[6, 24] and Zhu et al.[25] investigated different mass flow rate of film caused by different inlet areas while studying the geometric characteristics of film injection. In their studies, they suggest that an even higher film mass flow rate may increase the cooling performance, but it can also cause problems such as larger cascade enthalpy loss and film separation even reducing the overall engine effectiveness. Liu et al.[26] introduced that a higher Reynolds number (Re) improves the cooling efficiency. But higher vorticity caused by higher flow velocity may break up the film structure. Additionally, relying solely on mass flow rate as a solitary variable lacks objectivity, as the relative velocities between the main flow and the film play a crucial role in influencing turbulence within the boundary layer. This turbulence, when coupled with chemical reactions, significantly impacts wall heat transfer, and consequently, the overall effectiveness of the cooling process.

Apart from enhancing the accuracy of wall heat flux computations, this study delves into an examination of the impacts stemming from the characteristics of the film flow and the intricate interplay between the film and the mainstream flow on heat transfer and cooling efficacy. The joint influence of chemical reactions and flow interactions on wall heat transfer and cooling performance is concurrently investigated. Furthermore, the study of film cooling efficiency distribution and specific impulse offers valuable insights to inform the design process of methane/oxygen rocket engines in the future

2. Numerical Setups

This section introduces the numerical framework rooted in the RANS-based method. It encompasses the establishment of the geometric configuration and mesh, the selection of pertinent physical and numerical models, as well as the utilization of chemical models. Additionally, it provides

an overview of the coupled wall function approach and outlines the process of verifying mesh independence.

2.1 Geometry and Mesh Establishment

The geometry of the combustion chamber in this study is derived from the test bench established at the Technical University of Munich (TUM)[27], the primary modification involves the incorporation of a film injector located on the outer perimeter of the combustion chamber. To ensure the complete development of the propellant injection, certain sections of the injection pipelines have been retained. A detailed account of the reference experiment, which serves as a benchmark for validating the numerical framework, will be provided in the forthcoming section.

Figure 1 illustrates the schematic representation of the simulation domain. To economize computational resources, only one-sixth of the combustion chamber is retained due to its inherent symmetry. The oxygen inlet locations are denoted in blue, while the methane inlets are designated in red. Notably, methane serves a dual role as both a propellant and a film coolant, capitalizing on its favorable attributes of high thermal conductivity and low viscosity. Additionally, since methane also functions as a fuel, it actively participates in the combustion process. Hence, the chemical reactions occurring within the boundary layer become pivotal and cannot be ignored in film cooling investigations. The key geometric parameters are itemized in Table 1.

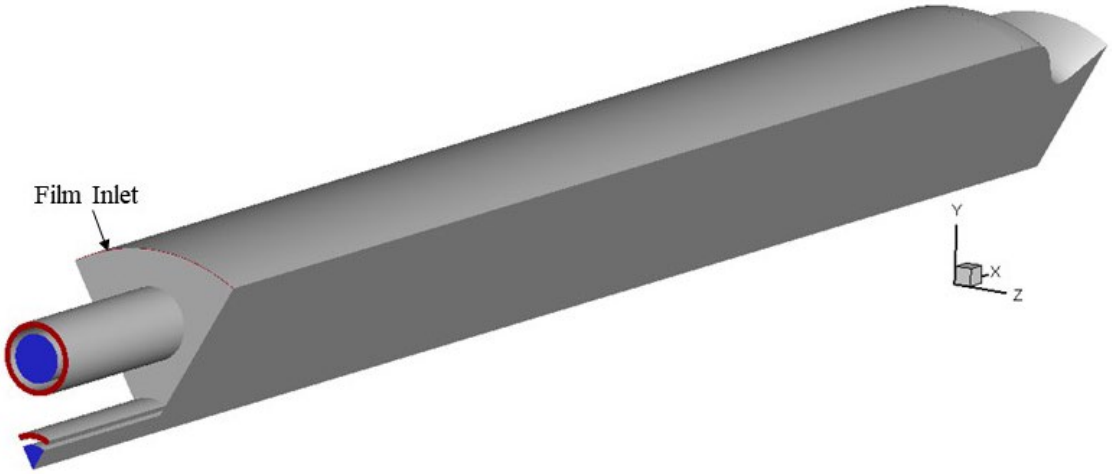

Figure 1 Geometry of seven-element combustion chamber

Figure 2 illustrates the grid structure established according to the previously mentioned geometry. To elevate the precision of the simulation, grid refinement is applied extensively within the boundary layer and shear layers. Additionally, refinement is also employed near the injection plate due to the heightened complexity associated with reflux areas and film performance in this region. The mesh architecture adopted in its entirety is hexahedral, and meticulous control is exercised over the grid expansion ratio, which is maintained at a value of 1.2. This approach is aimed at mitigating numerical disturbances and promoting convergence. In the proximity of the walls, the mesh is configured to align with the requirements of wall functions, ensuring that the *y*-plus (y^+) value remains around 30.

Table 2 Main geometric parameters of the combustion chamber

Parameter	Unit	Value
Chamber length	[mm]	341
Chamber diameter	[mm]	30
O2 injector diameter	[mm]	4
CH4 injector thickness	[mm]	1
Gap thickness between O2 and CH4 injector	[mm]	1
Nozzle length	[mm]	42

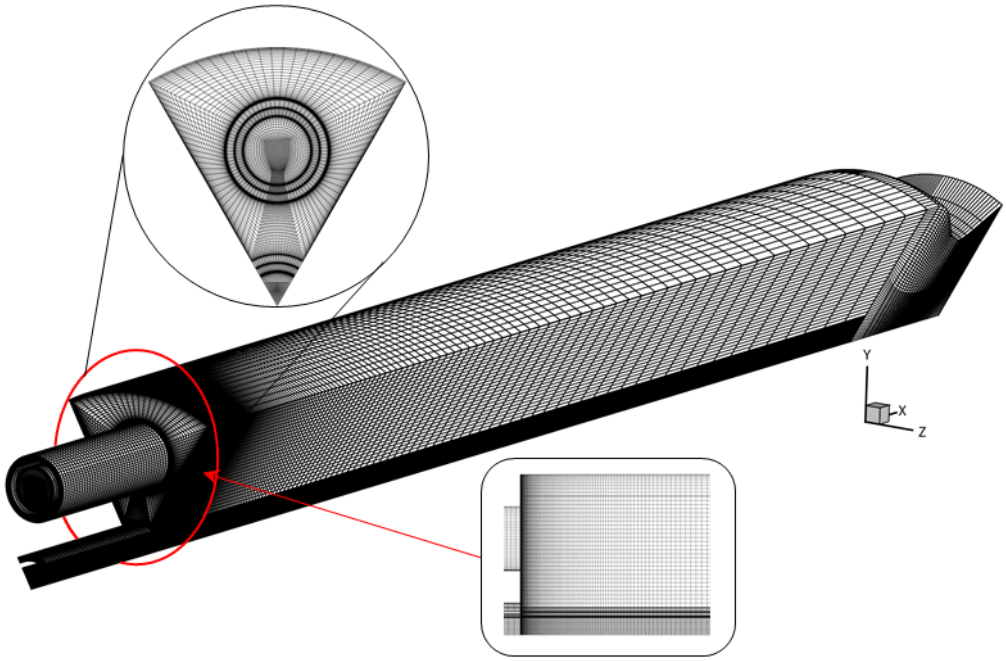

Figure 2 Mesh of seven-element combustion chamber

2.2 Numerical Model and Boundary Conditions

The RANS-based method characterizes turbulence effects through the use of a turbulence model that does not account for the transient fluctuations in flow. Consequently, this method demands fewer computational resources compared to Large Eddy Simulation (LES) and Direct Numerical Simulation (DNS), rendering it better suited for addressing large-scale and intricate engineering flow problems[28-30]. A very essential step of RANS-based simulation is the selection of viscous model, according to former studies, the standard $k-\varepsilon$ model can provide accurate prediction of the mixing and combustion processes within the methane/oxygen combustion chamber. [31-33].

Concerning chemical reactions, the Eddy Dissipation Concept (EDC) model is employed as the reaction model, primarily due to its suitability for treating combustion as a finite-rate process. Additionally, a chemical mechanism consisting of 14 species and 18 reactions, as proposed and validated

by Dong et al.[34]is incorporated into the simulation. In the context of turbulence simulation, prior studies recommend that the turbulent Prandtl Number (Pr_t) should fall within the range of 0.7 to 0.9[35, 36], and from the former experience of multi-element methane/oxygen combustion simulations of author` institute, it might be suitable to set the Pr_t to the value 0.85. This choice aligns with the initial assumption of the coupled wall function, which establishes the Lewis Number ($Le = Sc/Pr$) as equal to 1. Consequently, this implies that the turbulent Schmidt Number (Sc_t) also equals 0.85.

All boundary conditions utilized in the simulations presented in this paper have either been discretized or directly derived from corresponding experimental data. Inlet conditions are prescribed as mass flow inlets, while the outlet is defined as a pressure outlet boundary to closely mimic the experimental environment. Specific values for the inlet conditions, as well as inlet and outlet temperatures, are detailed in Table 2. Wall boundaries, including injector walls, the faceplate, chamber walls, and nozzle walls, are designated as non-slip walls. Symmetric faces are naturally set as symmetry boundaries. The injector walls and the faceplate are treated as adiabatic walls since they are not the primary focus of the study. The temperature of the combustion wall is derived through polynomial fitting and discretization based on experimental data, facilitating the investigation of heat transfer characteristics. Regarding the nozzle, as the film cooling effects are negligible in this region, the nozzle wall is assigned a uniform temperature of 412K, and it effectively serves as an extension of the chamber wall.

Table 2 Values of combustion chamber boundary conditions

Boundary	Values	Temperature
CH4 Inlet	0.0301kg/s	259.4K
O2 Inlet	0.001143kg/s	237.6K
Film Inlet	Changes based on research	237.6K
Outlet	1.01325bar	300K

2.3 Wall Treatment

In RANS simulations, it is common practice not to resolve the boundary layer all the way down to the wall due to computational constraints. Wall functions are usually employed to extend the predictions of the turbulence model from the outer flow regions into the near-wall region. This extension is critical for capturing the velocity and turbulent characteristics near the wall, which have a substantial impact on heat transfer and fluid dynamics.

The general wall function makes the simplifying assumption of linearly distributed physical quantities near the wall, which, while simple, comes with certain limitations. One of these limitations is the neglect of enthalpy changes in the near-wall region, resulting in the omission of chemical reactions in this area. Consequently, this oversight leads to an overestimation of the wall heat flux in the final calculations. To bridge this gap and address these limitations, the numerical framework utilized in this study integrates the coupled wall function devised by Nicoud and Cabrit. This approach replaces the energy equations (Eq. 2-1) in normal wall functions with the total enthalpy form (Eq. 2-2). However, the momentum equation retains its original form since momentum is minimally affected by chemical reactions.

$$\frac{\partial q_w}{\partial y} = G = 0 \tag{2-1}$$

$$\frac{\partial \overline{q_w}}{\partial y} = \frac{\partial}{\partial y}\left(\bar{\rho}\widetilde{v''h_s''} + \bar{\rho}\sum_k \widetilde{v''Y_k''}\, h_{f,k}^0 - \overline{\lambda\frac{dT}{dy}} + \bar{\rho}\sum_k (h_k\, Y_k\widetilde{V_{k,y}})\right) \tag{2-2}$$

To integrate the coupled wall function into the numerical model, several simplifications and transformations of Eq. 2-2 are required. Additionally, an intermediate dimensionless temperature variable, denoted as T+, is introduced since the gradient term cannot be directly invoked within the Fluent software. The ultimate calculation for wall heat transfer is then determined as follows:

$$q_w = -\frac{\rho C_P u^*}{T^+}(T_c - T_w) \tag{2-3}$$

where C_P is specific heat capacity, u^* is improved dimensionless wall velocity, T_c is the temperature located at the center of the cells in the first layer and T_w is wall temperature. The detailed derivation and simplification procedure of the coupled wall function can be found in Ref.[20] and Ref. [19]. In this way the chemistry reactions near the wall are taken into account.

2.4 Mesh Independence Verification

Verification of mesh independence in numerical simulations is a crucial step aimed at confirming the consistency and reliability of computational results across varying grid resolutions. This practice is pivotal within the realms of fluid dynamics and engineering computational simulations. In the simulations of this paper, the mesh of near wall area is changed since the film inlet sizes are different, but the involved grids are relatively less than overall grid numbers. Hence, the influence of the numbers of mesh in the near wall area are ignored, and the y^+ value is ensured to approximate 30, meeting the requirements for the coupled wall function.

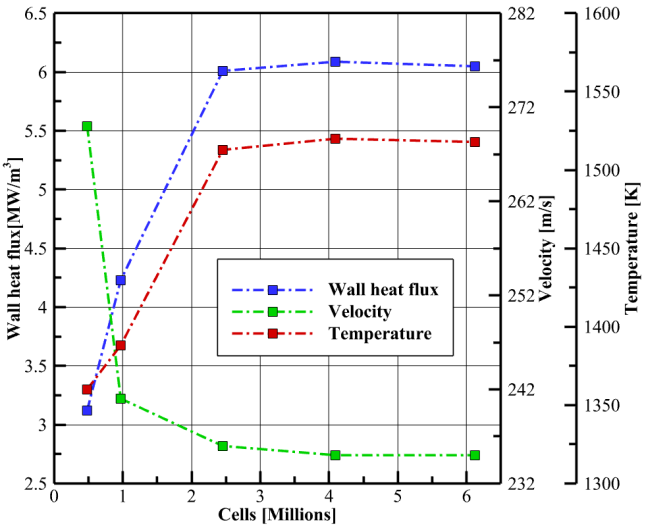

Figure 3 Parameters variation with the number of grids

To ascertain mesh independence, five sets of grid densities were tested, ranging from the coarsest

at 0.48 million to the finest at 6.12 million grid cells. During these simulations, three crucial parameters in fluid dynamic analysis—wall heat flux, velocity, and temperature were computed for each grid set. The trends in these parameters with respect to grid density are depicted in Figure 3. As observed in Figure 3, once the grid density surpasses 2.4 million, the key parameters exhibit minimal variation. Consequently, to uphold calculation accuracy while mitigating computational costs, a mesh comprising 2.46 million grid cells is employed for simulating the 7-element combustion chamber in subsequent sections.

3. Reference Experiments

The precision and dependability of the numerical framework have been verified through experiments conducted at the School of Engineering and Design, TUM. A single-element CH4/O2 combustion chamber experiment featuring film cooling[37] was carried out to assess the numerical model's performance in the boundary region with film cooling.

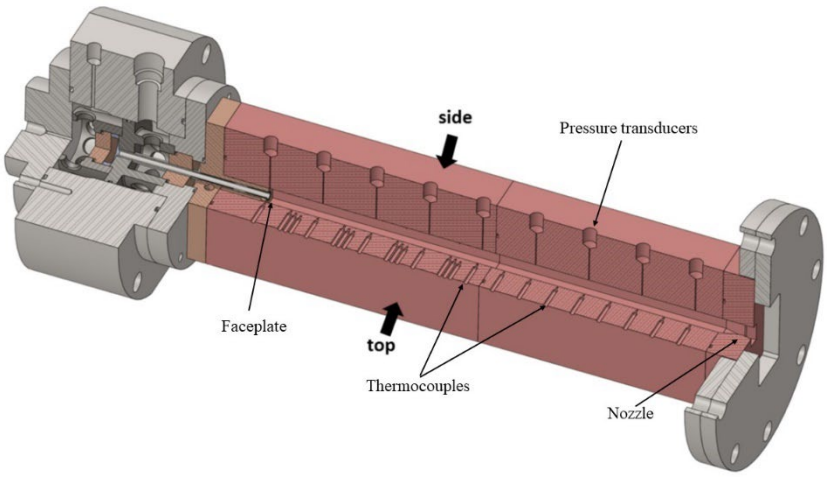

Figure 4 Single-element combustion chamber schematic

Figure 4 illustrates the schematic of the single-element chamber testbench, characterized by a heat sink chamber measuring 290mm in length and featuring an inner section with dimensions of 12mm by

12mm (square). A comparative analysis between the experimental and simulated outcomes is illustrated in Figure 5[19, 38]. The results indicate that the framework employing the coupled wall function outperforms normal wall functions, yielding more accurate predictions for chamber pressure and wall heat flux and these predictions align more closely with the experimental findings.

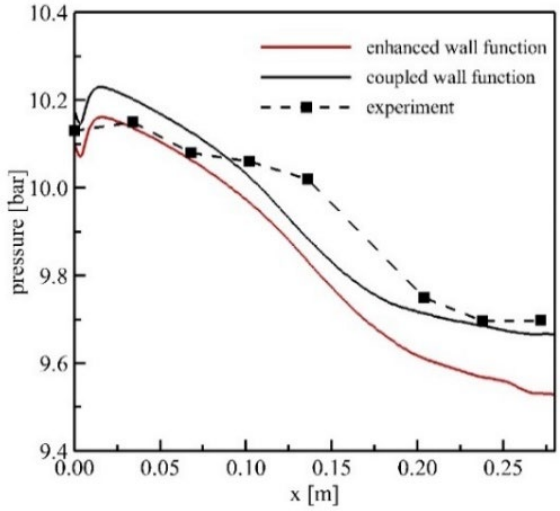

(a) Pressure distribution

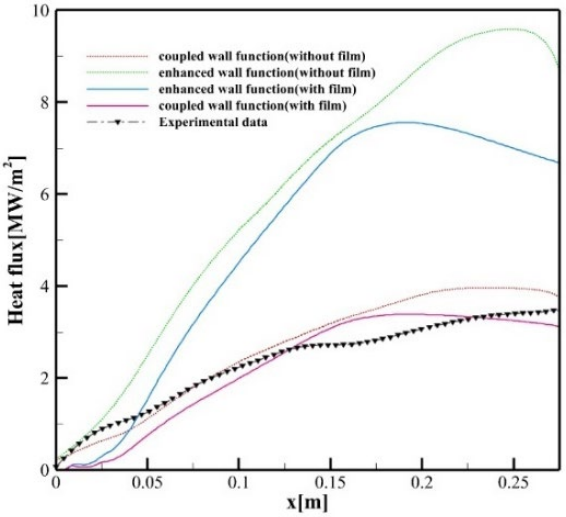

(b) Heat flux distribution

Figure 5 Experimental and simulated results of single injector combustion chamber

Given the increased complexity of flow within a multi-element combustion chamber compared to a single-element chamber, it becomes imperative to consider three-dimensional effects and the interactions among the injectors. Consequently, an experiment involving a seven-element CH4/O2 combustion

chamber has also been conducted[39]. Figure 6 presents a schematic depiction of the multi-element combustion chamber testbench. This chamber, like the single-element chamber, functions as a heat sink and possesses an overall length of 341mm, featuring an inner diameter of 30mm.

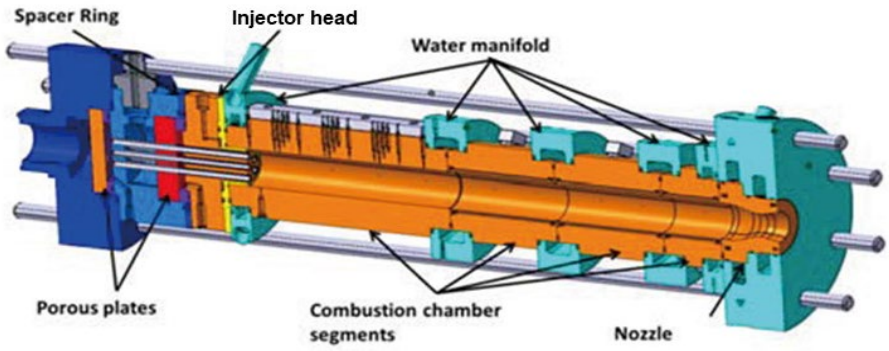

Figure 6 Seven-element combustion chamber schematic

A simulation utilizing the aforementioned testbench geometry has been executed, and the obtained results have been compared with the experimental data. The comparison of chamber pressure and wall heat flux is illustrated in Figure 7[40]. The pressure distribution appears to remain unaffected by the choice of wall functions and exhibits a good fit with the experimental data. Regarding the wall heat flux results, the utilization of the coupled wall function yields calculated heat flux values for each chamber segment that closely align with the experimental data.

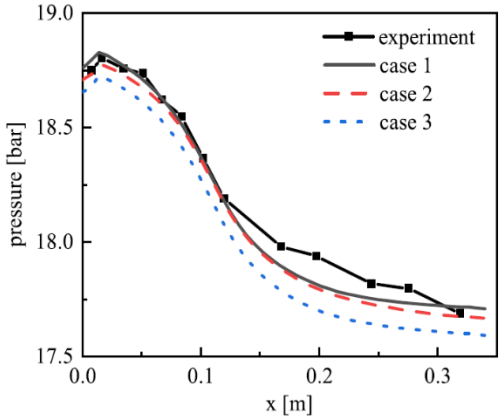

(a) Pressure distribution

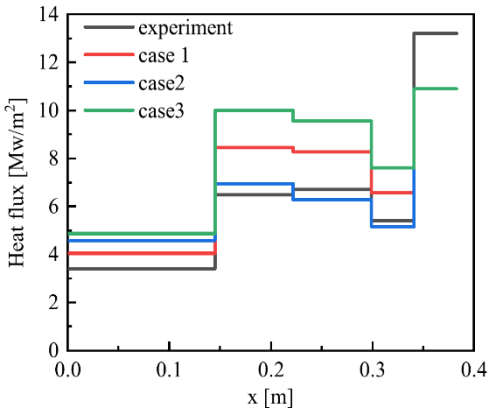

(b) Heat flux distribution

Figure 7 Experimental and simulated results of seven-element chamber (case 1: Enhanced wall treatment with y^+=1; case 2: Coupled wall treatment with y^+=30; case 3: Enhanced wall treatment with y^+=30)

In summary, prior research has substantiated the accuracy of the numerical model employed in this paper for predicting the flow and combustion processes within a CH4/O2 rocket engine combustion chamber. Furthermore, in comparison to standard wall treatments, the adoption of the coupled wall function has demonstrated its effectiveness in mitigating the issue of overestimated wall heat flux, which arises from neglecting the effects of chemical reactions in the near-wall region. Consequently, the aforementioned numerical framework is leveraged to simulate and explore the film cooling performance within the CH4/O2 rocket combustion chamber.

4. Results and Discussion

Owing to the impact of viscosity, the disparity in velocity causes the mixing zone within the shear layer to experience shear stresses from different directions between two turbulent flows, as shown in Figure 8. Consequently, the turbulence in the mixing zone becomes more intricate, exerting an impact on both specie distribution, heat transfer and the associated chemical reaction processes. Therefore, it is

imperative to investigate the influence of the velocity differential between the film and the main flow within the combustion chamber of the rocket engine, with a particular focus on its ramifications for combustion dynamics and heat transfer processes.

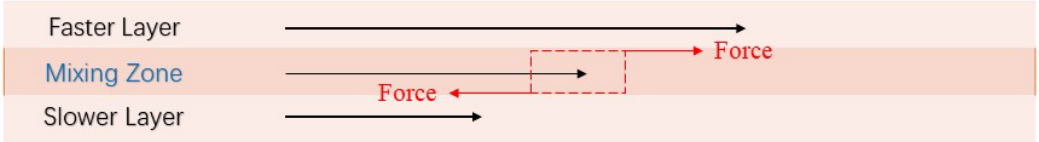

Figure 8 Force analysis diagram of the fluid mixing zone

In the first place, a dimensionless quantity R_V is defined to measure the relationship between the main flow and the film velocity. R_V can be defined as:

$$R_v = \frac{V_{film}}{V_{mainflow}} \tag{4-1}$$

where V_{film} is the velocity of film and $V_{mainflow}$ is the velocity of the main flow. In the pursuit of preserving the oxygen-fuel ratio, the mass flow rate at the methane and oxygen inlets were intentionally maintained at a constant level throughout this study, whereas the film inlet velocity is varied to obtain different R_V. Figure 9 demonstrates the average velocity distribution of the near-wall injector, a slight increase in fluid velocity is observed as the combustion progress downstream the chamber, and reaches the speed of sound at the nozzle throat then exhibits a further increment upon traversing through the nozzle. It is evident that the velocity undergoes minimal changes in the frontal section of the combustion chamber where the reaction has almost not started yet, and this is precisely the part where the film mainly performed. Consequently, the average velocity of the main flow within the initial 0.1 meters of the chamber (the red part in Figure 9), denoted as $V_{mainflow}$ in Eq. (4-1), was intercepted and computed to yield a value of $V_{mainflow}$ = 92.578 m/s.

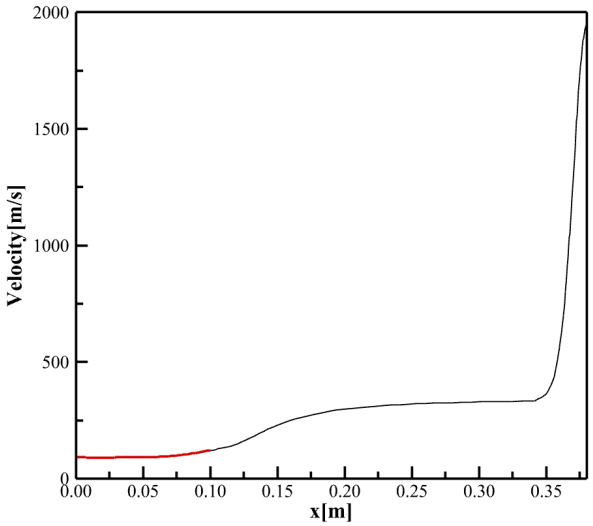

Figure 9 Velocity distribution of the main flow

Subsequently, it is clear that there are two distinct methods for controlling the injection velocity of the film: one involves manipulating the film`s inlet mass flow rate, while the other is adjusting the film inlet size (inlet height in this case). In this investigation, these two approaches were individually employed to achieve equivalent R_V values, and a set of cases was systematically designed to scrutinize their effects. The particulars of these cases are succinctly listed in Table 3.

Table 3 Case Summary list

Gr. / No.	Group A		Group B		R_V
	$\dot{m}\ (kg/s)$	$h_{film}(mm)$	$\dot{m}\ (kg/s)$	$h_{film}(mm)$	
0	0.001333	0.05	0.001333	0.05	1.276
1	0.000446	0.05	0.001333	0.15	0.427
2	0.000668	0.05	0.001333	0.10	0.639
3	0.000834	0.05	0.001333	0.08	0.798
4	0.001026	0.05	0.001333	0.065	0.982
5	0.001903	0.05	0.001333	0.035	1.822

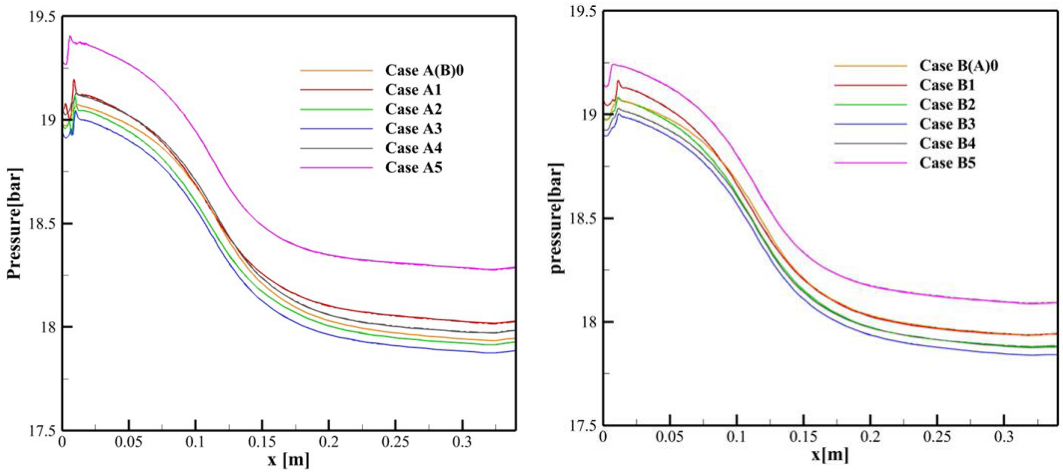

Figure 10 Chamber pressure distribution of two case groups
(— general wall function; -·-·- coupled wall function)

Figure 10 illustrates the distribution of chamber pressure. Initially, it is evident that the coupled wall function minimally affects the main flow, as its influence is confined to the energy equation within the boundary layer, without affecting the momentum equation; a similar trend is observed in the temperature and vorticity distributions, depicted separately in Figures 11 and 12. Subsequently, as the combustion chamber pressure is predominantly influenced by the injection of fuel and oxidizer, the overall pressure variation among different scenarios is relatively minor. Nonetheless, it is noteworthy that with lower film injection speeds, an initial slight decrease in pressure is observed as film velocity increases. This phenomenon is attributable to the low speed and temperature of the film, resulting in chemical reactions near the wall primarily being governed by turbulence intensity. Furthermore, the entry of low-temperature gas into the combustion chamber leads to a reduction in gas temperature near the wall, and the combined effects of chemical reactions and cooling mitigate pressure. As film velocity gradually aligns with mainstream velocity, turbulence diminishes, allowing for the gradual formation of a complete air film near the wall, leading to a weakening of the chemical interaction between methane and the mainstream. Consequently, the combustion chamber pressure experiences a slight increase.

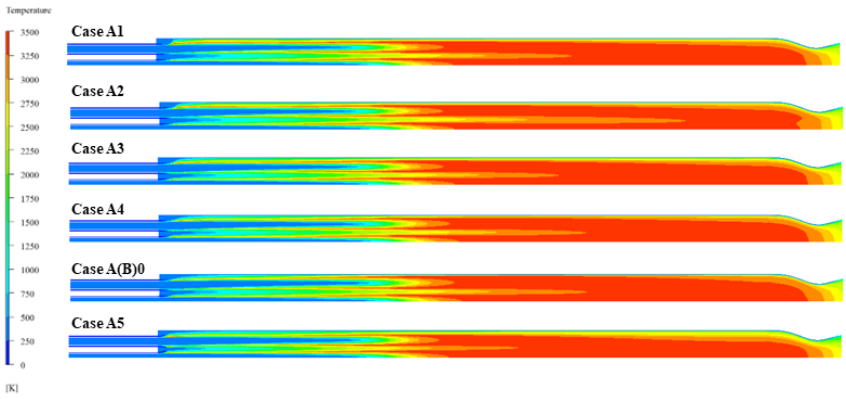

(a) Case group A with general wall function

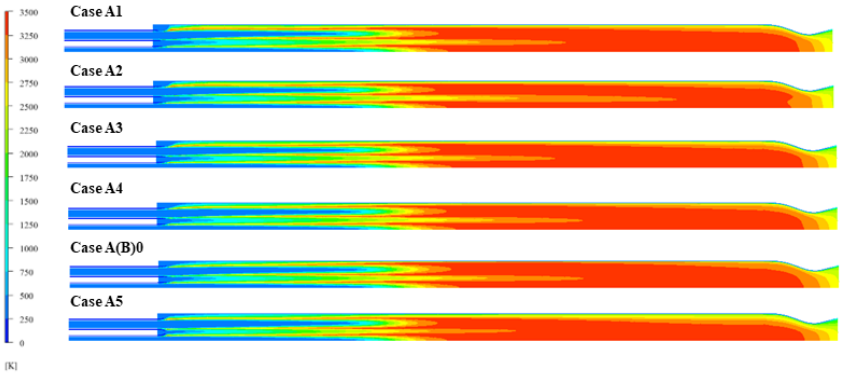

(b) Case group A with coupled wall function

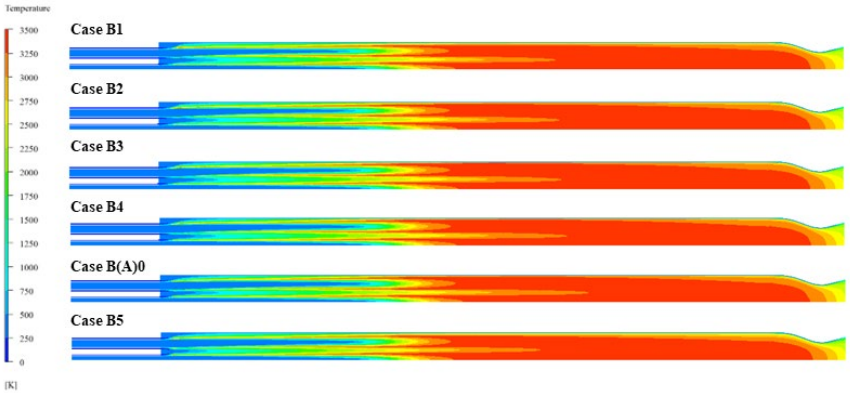

(c) Case group B with general wall function

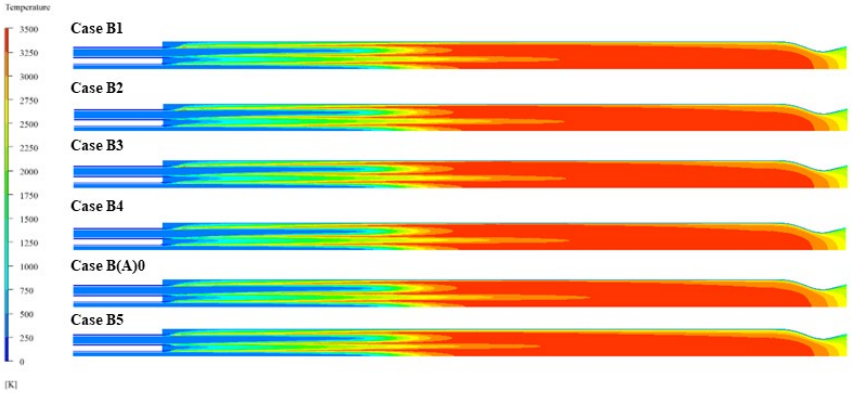

(d) Case group B with coupled wall function

Figure 11 Temperature distribution in the longitudinal section of the chamber center

The diminishing trend of this chemical reaction is also apparent in Figure 11. Upon observation, it is noted that with increasing film speed, the thickness of the temperature boundary layer gradually increases. Furthermore, an intriguing phenomenon is observed in the pressure distribution depicted in Figure 10. When increasing the film intake speed by augmenting the film volume (Case group A), it is observed that after the film speed exceeds 1, there is a slight reduction in pressure. This phenomenon can be attributed to the formation of a rich combustion zone near the wall due to the additional methane injection, leading to a shift in chemical equilibrium towards the product. If the cooling effect fails to sufficiently counterbalance the pressure drop induced by this phenomenon, a slight reduction in pressure occurs. Additionally, the pressure distribution reveals that the overall pressure of case group B is marginally lower than that of group A, this is also easy to understand because there is additional fuel injection in group A. Furthermore, the temperature contour also indicates that the mainstream temperature in group A is elevated.

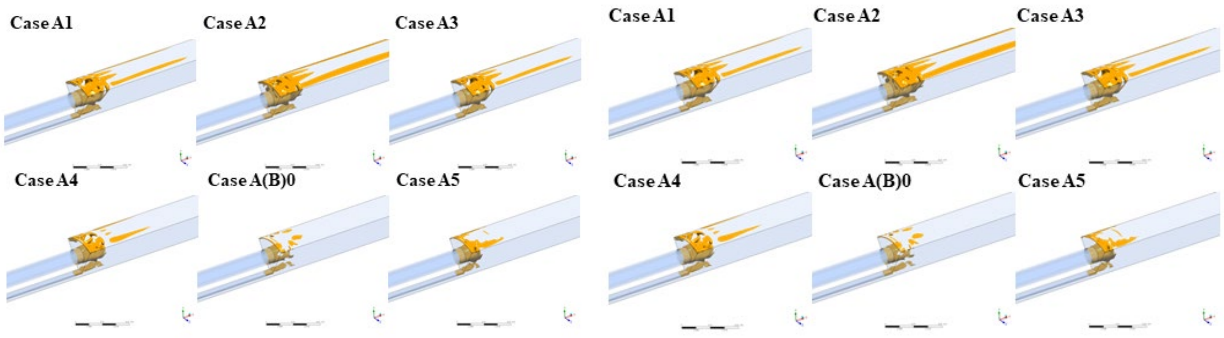

Figure 12 Swirl strength near the combustion chamber inlet

(left: general wall function; right: coupled wall function)

Figure 12 vividly illustrates the intricate swirl strength proximate to the inlet of group A's chamber,

effectively portraying the underlying vorticity of the flow. As previously elucidated, wall functions exert minimal influence on the flow characteristics. Furthermore, with the escalation of film entry velocity, a notable decline in swirl strength near the entrance ensues. This phenomenon is readily explicable. As the film's intake speed accelerates, it entrains the mainstream gas, leading to downstream flow within the combustion chamber and consequently diminishing the vorticity proximate to the inlet. Nevertheless, it is noteworthy that an excessively high R_V (greater than 1), results in a slight increase in vorticity. This phenomenon arises due to viscosity, wherein the mainstream gas recaptures the high-speed film. Figure 13 delineates a comparative analysis of swirl strength between two distinct methodologies for regulating film inlet velocity. Apparently, cases in group A induce greater vorticity proximate to the combustion chamber inlet, attributable to the introduction of a higher volume of low-temperature gas compared to the other group operating at similar flow velocities. The higher viscosity of low-temperature methane in comparison to mainstream gas results in a stronger entrainment effect within group A's combustion chamber, consequently leading to augmented swirl strength.

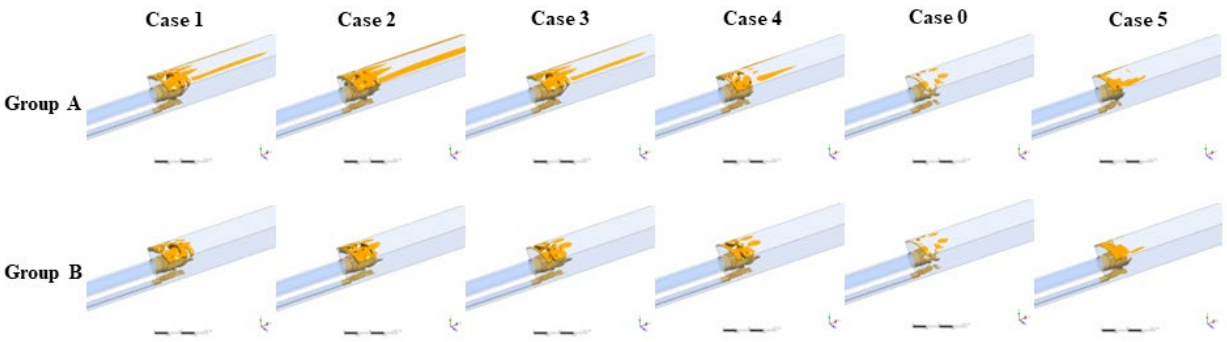

Figure 13 Comparison of swirl strength near the chamber entrance between two case groups

Figure 14 illustrates the distribution of heat flux on the combustion chamber wall. Firstly, it is evident that employing coupled wall functions effectively mitigates the issue of overestimating wall heat flux, thereby attributing this overestimation to the disregard of chemical reactions within the boundary

layer. As highlighted in the author's preceding research, this disparity can be elucidated by the chemical enthalpy term[19, 38]. Secondly, observation from Figure 14 reveals that in the initial segment of the combustion chamber, with the augmentation of film velocity, a coherent film progressively develops, consequently resulting in a gradual decline in wall heat flux. Moreover, in the absence of accounting for chemical reactions within the boundary layer, wall heat transfer predominantly hinges upon turbulence, thereby precipitating a scenario analogous to pressure distribution within group A. Upon surpassing an R_V value of 1, there is a marginal increment in wall heat flux. Such an occurrence is obviated when employing the coupled wall function. Ultimately, it becomes evident that wall heat flux in group B marginally surpasses that of group A. This discrepancy arises due to the introduction of a greater volume of low-temperature gas into the chamber within group A.

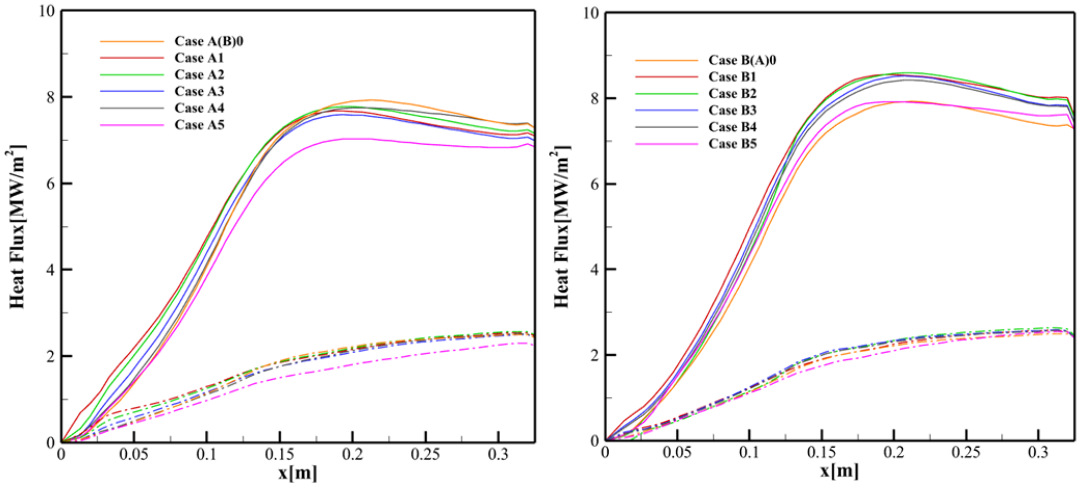

Figure 14 Heal flux on the combustion chamber wall
(— general wall function; -·-·- coupled wall function)

Regarding film cooling efficiency, which is conventionally defined by the subsequent formula:

$$\eta = \frac{T_{ad} - T_{CC}}{T_{film} - T_{CC}} \tag{4-2}$$

where η is film cooling efficiency, T_{ad} is adiabatic wall temperature, T_{CC} is combustion chamber temperature and T_{film} is wall temperature with film cooling. Nevertheless, this study investigates wall heat flux under a specified wall temperature, acknowledging the challenge of realizing the adiabatic

condition as stipulated in Equation (4-2) within practical contexts. Thus, akin to numerous other numerical simulation investigations concerning film cooling[41-43], the Net Heat Flux Reduction (NHFR) method is employed as a metric for assessing film cooling efficiency. Concurrently, Bartz's method[44] was referenced for pressure correction, yielding the following ultimate formulation:

$$NHFR = 1 - \frac{q_{film}}{q_0} \cdot \left(\frac{P_{CC,0}}{P_{CC,film}}\right)^{0.8} \tag{4-3}$$

where q_{film} is the heat flux with film, q_0 is the heat flux without film, $P_{CC,0}$ is the chamber pressure without film and $P_{CC,film}$ is the chamber pressure with film.

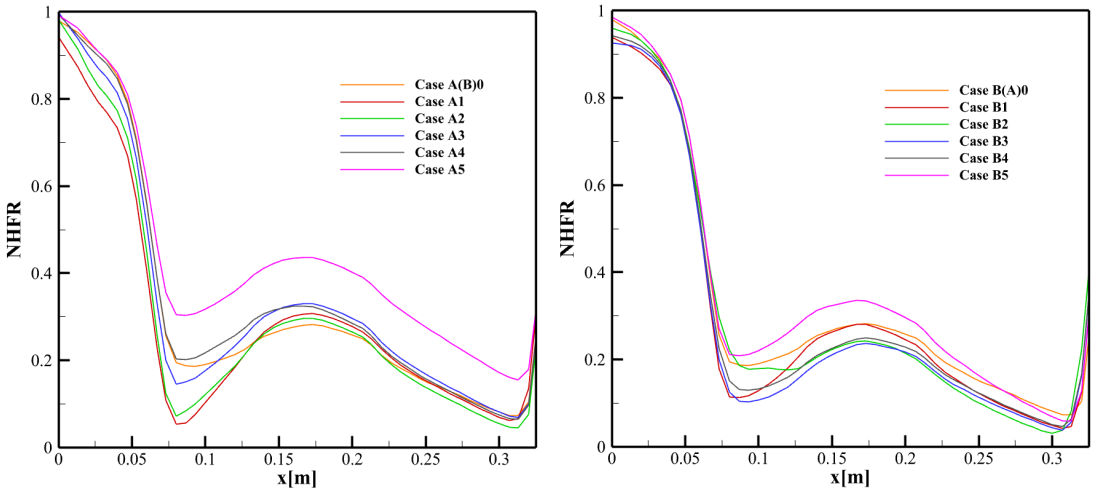

Figure 15 NHFR distribution of the chamber wall with coupled wall function

Figure 15 illustrates the non-dimensional heat flux ratio (NHFR) distribution along the combustion chamber wall employing a coupled wall function. As depicted, the cooling efficacy diminishes gradually due to the interaction between the air film and the mainstream, reaching its nadir at x=0.07. Consequently, it is discernible that within the methane-oxygen multi-nozzle rocket engine's combustion chamber, siting a film inlet at approximately each one-fifth of the total chamber length facilitates effective film cooling. Furthermore, subsequent to reaching its minimum, the NHFR exhibits a slight upward trajectory followed by attenuation. This phenomenon arises from variations in the distribution of high-temperature

zones between chambers with and without a gas film. However, given our primary focus on the region where the air film is operative at the front of the combustion chamber, we shall refrain from delving extensively into these fluctuations.

Furthermore, it can also be seen from Figure 15, upon examining the NHFR distribution within group B, it becomes apparent that the disparities in cooling efficiencies resulting from modulating air film speed via alterations in air film inlet size are negligible. Conversely, with regard to augmenting speed through elevating the mass flow rate of the air film, a progressive increase in cooling efficiency is observed in the entrance segment of the combustion chamber as the R_V gradually escalates. This phenomenon ensues as a greater volume of low-temperature gas infiltrates the combustion chamber, thereby promoting the gradual establishment of a comprehensive air film. Consequently, the cooling efficiency exhibits a commensurate rise. Hence, within a given rocket engine's combustion chamber, maximizing coolant mass flow rate appears to be imperative for enhancing cooling efficiency.

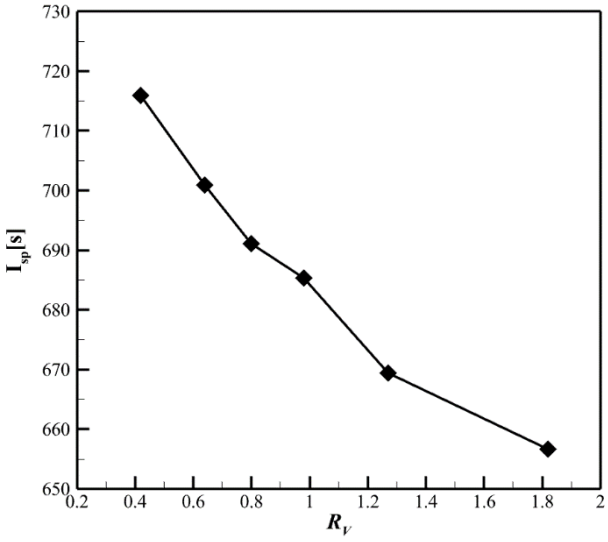

Figure 16 Specific impulse at different R_V

Prudent consideration must be exercised regarding the indiscriminate escalation of film coolant mass flow rates solely for the purpose of enhancing cooling effectiveness, as it necessitates a

comprehensive evaluation of the consequent effect on the overall efficiency of the rocket engine due to methane injection. Illustrated in Figure 16 are the variations in specific impulse across different R_V utilizing the coupled wall function. It becomes evident that with an increase in R_V, there is a notable decrement in engine specific impulse. This phenomenon can be attributed to the observation that while supplementary methane injection augments the engine's thrust, its augmentation rate does not match the pace of escalation in fuel mass flow, thereby resulting in an attenuated overall engine specific impulse. Hence, in the process of engine design, alongside deliberations on cooling efficiency, due consideration must be accorded to the repercussions of introducing supplementary coolant on the engine's comprehensive performance.

5. Conclusion

The present study innovatively applies previously validated coupled wall functions to investigate the film cooling of methane/oxygen rocket engine combustion chambers. By manipulating the mass flow rate and inlet size of the film, the study explores the influence of different film-mainstream velocity ratios on flow dynamics, combustion, wall heat transfer, and cooling efficiency within the combustion chamber. Results indicate that as the ratio of film velocity to mainstream velocity (R_V) increases, the combustion chamber pressure initially decreases before increasing. Concurrently, the vorticity at the inlet section of the combustion chamber exhibits a similar trend. Furthermore, contrasting the results obtained by varying film velocity through different methods reveals that, with a constant mass flow rate, reducing the film inlet height yields lower pressures and weaker swirl strength. Additionally, analysis of swirl strength and temperature distribution contours within the combustion chamber indicates that, when controlling film velocity by altering the mass flow rate at the inlet, as R_V increases, the temperature boundary layer

thickens gradually, with the coupling of vortices and chemical reactions causing a slight pressure reduction after R_V exceeds 1, followed by a subsequent increase. This pressure variation similarly affects wall heat transfer as computed using the general wall function, whereas results obtained utilizing the coupled wall function, which accounts for chemical reactions within the boundary layer, do not exhibit this behavior. Investigation into wall heat transfer further reveals a gradual decrease with increasing R_V, with lower wall heat transfer observed in cases involving additional low-temperature methane injection. Subsequently, consistent with prior research, the introduction of coupled wall functions minimally impacts mainstream flow and combustion, suggesting that the overestimation inherent to wall functions can be mitigated by accounting for chemical reactions in close proximity to the wall. Finally, analysis of Net Heat Flux Reduction (NHFR) indicates a rapid decline in cooling efficiency in the front half of the combustion chamber, reaching a minimum at one-fifth of its length, suggesting that employing a film cooling inlet every one-fifth section in a methane/oxygen engine is optimal. Moreover, increasing the mass flow rate enhances cooling efficiency as R_V increases, whereas altering the inlet size yields nearly constant cooling efficiency. Therefore, maximizing film mass flow rate is deemed preferable for film cooling arrangements in a given rocket engine; however, comparative studies reveal a gradual reduction in engine specific impulse with increasing mass flow rate, underscoring the imprudence of indiscriminate mass flow rate escalation and the necessity for engine-specific determinations.

Declaration of Competing Interest

No known competing interests have to be declared.

Acknowledgements

Jianing Liu (Scholarship number:201706120033) received support from the China Scholarship

Council during the conduct of this paper. The authors express gratitude to their colleagues for their support during the experiments and discussions, particularly Mariella Celano, Nikolaos Perakis and Wenjing Yin.

References

[1] G.P. Sutton, History of Liquid Propellant Rocket Engines, American Institute of Aeronautics and Astronautics2006.
[2] M. Pizzarelli, F. Battista, Oxygen–methane rocket thrust chambers: Review of heat transfer experimental studies, Acta Astronautica, 209 (2023) 48-66.
[3] A.S. Gohardani, J. Stanojev, A. Demairé, K. Anflo, M. Persson, N. Wingborg, C. Nilsson, Green space propulsion: Opportunities and prospects, Progress in Aerospace Sciences, 71 (2014) 128-149.
[4] S.W. Sheehan, Electrochemical methane production from CO(2) for orbital and interplanetary refueling, iScience, 24 (2021) 102230.
[5] N.A. Adams, W. Schroeder, R. Radespiel, O.J. Haidn, T. Sattelmayer, C. Stemmer, B. Weigand, Future Space-Transport-System Components under High Thermal and Mechanical Loads, Springer2021.
[6] J. Zhang, S. Zhang, C. Wang, X. Tan, Recent advances in film cooling enhancement: A review, Chinese Journal of Aeronautics, 33 (2020) 1119-1136.
[7] S. Soller, R. Behr, F. Grauer, K. Claramunt, C. Dinescu, Experimental and Numerical Invesitgation of Liquid Film Cooling in Small Rocket Engines, 7th European Conference for Aerospace Sciences, EUCASS, 2019, pp. 1-19.
[8] X. Ma, B. Sun, T. Wang, D. Liu, Experimental investigation of the gas film cooling efficiency of the cylindrical holes near the injector region, International Journal of Thermal Sciences, 165 (2021).
[9] J.-X. Wang, W. Guo, K. Xiong, S.-N. Wang, Review of aerospace-oriented spray cooling technology, Progress in Aerospace Sciences, 116 (2020).
[10] J. Wang, L. Li, J. Li, F. Wu, C. Du, Numerical investigation on flow and heat transfer characteristics of vortex cooling in an actual film-cooled leading edge, Applied Thermal Engineering, 185 (2021).
[11] J. Yao, P. Su, J. He, J. Wu, J. Lei, Y. Fang, Experimental and numerical investigations on double-jet film-cooling with different mainstream incidence angles, Applied Thermal Engineering, 166 (2020).
[12] R. Hou, F. Wen, Y. Luo, X. Tang, S. Wang, Large eddy simulation of film cooling flow from round and trenched holes, International Journal of Heat and Mass Transfer, 144 (2019).
[13] N. Christopher, J. Peter, M. Kloker, J.-P. Hickey, DNS of Turbulent Flat-Plate Flow with Transpiration Cooling, (2019).
[14] S.I. Baek, J. Ahn, Large Eddy Simulation of Film Cooling Involving Compound Angle Holes: Comparative Study of LES and RANS, Processes, 9 (2021).
[15] M. Calabro, Y. Daimon, H. Negishi, M. Koshi, D. Suslov, L. DeLuca, S. Frolov, L. Galfetti, O. Haidn, Numerical and experimental investigation of the methane film cooling in subscale combustion chamber, Progress in Propulsion Physics, 2016, pp. 129-144.
[16] A. Sternin, N. Perakis, M.P. Celano, M. Tajmar, O.J. Haidn, CFD-analysis of the effect of a cooling film on flow and heat transfer characteristics in a GCH4/GOX rocket combustion chamber, Space Propulsion, 275 (2018) 1-13.

[17] K.A. Verma, K.M. Pandey, M. Ray, K.K. Sharma, The numerical analysis of combustion performance of a wedge shaped strut-based scramjet combustor, Thermal Science and Engineering Progress, 20 (2020).
[18] J. Wei, M. Ye, S. Zhang, J. Qin, O.J. Haidn, Modeling of a 7-elements GOX/GCH4 combustion chamber using RANS with Eddy-Dissipation Concept model, Aerospace Science and Technology, 99 (2020).
[19] J. Liu, S. Zhang, J. Wei, O.J. Haidn, RANS based numerical simulation of a GCH4/GO2 rocket engine combustion chamber with film cooling and improvement of wall heat flux prediction, Applied Thermal Engineering, 219 (2023).
[20] O. Cabrit, F. Nicoud, Direct simulations for wall modeling of multicomponent reacting compressible turbulent flows, Physics of Fluids, (2009).
[21] C. Zhou, N. Yu, J. Ren, G. Cai, The influence law of the film percentage and injection on gas film cooling effect of the liquid oxygen/methane attitude control engine, Applied Thermal Engineering, 220 (2023).
[22] J. Xu, T. Jing, Y. Li, F. Qin, S. Zhu, Numerical Simulation on Flow and Heat Transfer Characteristics of Film/Regenerative Compound Cooling Process, 2021 12th International Conference on Mechanical and Aerospace Engineering (ICMAE), 2021, pp. 77-83.
[23] J. Xiang, B. Sun, T. Wang, J. Yuan, Effects of angled film-cooling on cooling performance in a GO2/GH2 subscale thrust chamber, Applied Thermal Engineering, 166 (2020).
[24] J.-z. Zhang, X.-d. Zhu, Y. Huang, C.-h. Wang, Investigation on film cooling performance from a row of round-to-slot holes on flat plate, International Journal of Thermal Sciences, 118 (2017) 207-225.
[25] X.-d. Zhu, J.-z. Zhang, X.-m. Tan, Numerical assessment of round-to-slot film cooling performances on a turbine blade under engine representative conditions, International Communications in Heat and Mass Transfer, 100 (2019) 98-110.
[26] C.-l. Liu, G. Xie, H.-r. Zhu, J.-x. Luo, Effect of internal coolant crossflow on the film cooling performance of converging slot hole, International Journal of Thermal Sciences, 154 (2020).
[27] S. Silvestri, M.P. Celano, G. Schlieben, O.J. Haidn, Characterization of a Multi-Injector GOX/CH4 Combustion Chamber, 52nd AIAA/SAE/ASEE Joint Propulsion Conference, 2016.
[28] L. Vervisch, R. Hauguel, P. Domingo, M. Rullaud, Three facets of turbulent combustion modelling: DNS of premixed V-flame, LES of lifted nonpremixed flame and RANS of jet-flame, Journal of Turbulence, 5 (2004).
[29] RANS/LES/DES/DNS: The Future Prospects of Turbulence Modeling, Journal of Fluids Engineering, 127 (2005) 829-830.
[30] M. Germano, From RANS to DNS: towards a bridging model, Direct and Large-Eddy Simulation III: Proceedings of the Isaac Newton Institute Symposium/ERCOFTAC Workshop held in Cambridge, UK, 12–14 May 1999, Springer, 1999, pp. 225-236.
[31] F.F. Winter, N. Perakis, O.J. Haidn, Emission imaging and CFD simulation of a coaxial single-element GOX/GCH4 rocket combustor, 2018 Joint Propulsion Conference, 2018.
[32] K.L. Harrison, D.G. Bogard, Comparison of RANS Turbulence Models for Prediction of Film Cooling Performance, Volume 4: Heat Transfer, Parts A and B, 2008, pp. 1187-1196.
[33] A. Sternin, H. Ma, J. Liu, O.J. Haidn, M. Tajmar, Turbulence, Combustion and Film Prediction in Rocket Application via Parameter Adjustion, Model Variation and Deep Learning Method, Transregio 40-Annual ReportGermany, 2019, pp. 119-136.
[34] G. Dong, Y. Huan, Y.L. Chen, Study of effects of different chemical reaction mechanisms on

computation results for methane jet turbulence diffusion flame, J. Fuel Chem. Technol., 28 (2000) 49-54.
[35] D. McEligot, M. Taylor, The turbulent Prandtl number in the near-wall region for low-Prandtl-number gas mixtures, International Journal of Heat and Mass Transfer, 39 (1996) 1287-1295.
[36] S.W. Churchill, A reinterpretation of the turbulent Prandtl number, Industrial & engineering chemistry research, 41 (2002) 6393-6401.
[37] M.P. Celano, S. Silvestri, C. Kirchberger, G. Schlieben, D.I. Suslov, O.J. Haidn, Gaseous Film Cooling Investigation in a Model Single Element GCH4-GOX Combustion Chamber, Transactions of the Japan society for aeronautical and space sciences, aerospace technology Japan, 14 (2016) 129-137.
[38] J. Liu, S. Zhang, J. Wei, O.J. Haidn, Numerical study of film cooling in single-element injector gaseous CH4/O2 rocket engine with coupled wall function, AIP Advances, 14 (2024).
[39] S. Silvestri, C. Kirchberger, G. Schlieben, M.P. Celano, O. Haidn, Experimental and Numerical Investigation of a Multi-Injector GOX-GCH4 Combustion Chamber, Transactions of the Japan Society for Aeronautical and Space Sciences, Aerospace Technology Japan, 16 (2018) 374-381.
[40] J. Wei, S. Zhang, X. Zhou, C. Cheng, J. Qin, O.J. Haidn, Effects of near wall flow and non-equilibrium reaction coupling on heat flux prediction inside a 7-elements GOX/GCH4 combustion chamber, Applied Thermal Engineering, 204 (2022).
[41] D. Suslov, R. Arnold, O. Haidn, Investigation of film cooling efficiency in a high pressure subscale lox/h2 combustion chamber, 47th AIAA/ASME/SAE/ASEE Joint Propulsion Conference & Exhibit, 2011, pp. 5778.
[42] J. McCall, R. Branam, Effects of radial curvature on net heat flux reduction in a film-cooled rocket, 47th AIAA Aerospace Sciences Meeting including The New Horizons Forum and Aerospace Exposition, 2009, pp. 1586.
[43] J.L. Rutledge, P.I. King, R. Rivir, Time Averaged Net Heat Flux Reduction for Unsteady Film Cooling, (2010).
[44] D.R. Bartz, A simple equation for rapid estimation of rocket nozzle convective heat transfer coefficients, J. Jet Propul., 27 (1957) 49-51.